AN ABSTRACT OF THE THESIS OF

John P. Lemmon for the degree of Doctor of Philosophy in Chemistry presented on October 5, 1994. Title: The Synthesis and Characterization of Components for Solid-State Lithium Cells: Amorphous Polyether-Salt Complexes, Planar-Sheet Graphite Fluorides, and Layered Organic/Inorganic Nanocomposites.

Abstract approved: _____

Michael M. Lerner

The amorphous polymer poly[(oxymethylene)oligo(oxyethylene)] (PEM), $[OCH_2(OCH_2CH_2)_m]_n$ (m=8-10), is prepared by the oxy-methylene linkage of poly(ethylene gylcol), $H(OCH_2CH_2)_mOH$ (m=8-10). Sodium salt complexes (PEM_xNaAn, An = ClO_4^- and I^-, x = 8 - 150) are prepared and characterized by variable temperature impedance spectroscopy, differential scanning calorimetry (DSC) and ^{23}Na nuclear magnetic resonance (NMR). Bulk conductivities at ambient temperature are between 10^{-4}-10^{-5} Scm^{-1} and a broad conductivity maximum is obtained at low salt concentrations. Glass transition temperatures are determined for each complex and at higher salt concentration, x > 25, the complexes remain amorphous between 190 and 295 K. ^{23}Na NMR on complexes with x = 50, 25, and 8 show two components distinguished by relaxation rates. Mole fraction, molal concentration and T_2^* are determined over the temperature range of 208 - 358 K.

Planar-sheet graphite fluorides, C_xF, are prepared at ambient temperature by the reaction of graphite with the transition fluorometallates K_2MnF_6 and K_2NiF_6 in anhydrous HF (AHF). For each reagent, the net reactions are identified by stoichiometry and X-ray diffraction of the solid products. The graphite fluorides synthesized at the oxidation limit are close in composition to C_6F and C_2F for the Mn^{4+} and Ni^{4+} fluorometallates, respectively. Reaction products of graphite with Na_3FeF_6 or CoF_3/KF in AHF are also reported.

Single-phase nanocomposites of MoS_2, TiS_2 and MoO_3 containing poly(ethylene oxide) (PEO) or PEM are prepared by an exfoliation/adsorption method. The nanocomposites are characterized by powder X-ray diffraction, DSC and electronic conductivity measurements by the four-probe method. X-ray diffraction indicates an expansion of 8 Å in the interlayer spacing, consistent with the incorporation of a polymer double layer within the inorganic galleries. Reaction stoichiometries and elemental analysis are consistent with the following compositions: $Li_{0.12}(PEO)_yMoS_2$ (y = 1.0-1.3), $Li_{0.02}Na_{0.25}(PEO)_{0.8}TiS_2 \cdot 0.1NMF$, and $Li_{0.2\text{-}0.3}(PEO)_{0.9}MoO_3 \cdot H20$ for single phase products. Electronic measurements between 77 and 274 K for the Mo and Ti nanocomposites imply a conductivity between 10^{-4} - 10^{-5} Scm^{-1} and 10^{-2} - 10^{-3} Scm^{-1} respectively, with little temperature dependence.

The Synthesis and Characterization of Components for Solid-State Lithium Cells: Amorphous Polyether-Salt Complexes, Planar-Sheet Graphite Fluorides, and Layered Organic/Inorganic Nanocomposites

by

John P. Lemmon

A THESIS

submitted to

Oregon State University

in partial fulfillment of
the requirements for the
degree of

Doctor of Philosophy

Completed October 5, 1994
Commencement June 1995

Doctor of Philosophy thesis of John P. Lemmon presented on October 5, 1994

APPROVED:

Redacted for Privacy

Major Professor, representing Inorganic Chemistry

Redacted for Privacy

Chair of Department of Chemistry

Redacted for Privacy

Dean of Graduate School

I understand that my thesis will become part of the permanent collection of Oregon State University libraries. My signature below authorizes release of my thesis to any reader upon request.

Redacted for Privacy

John P. Lemmon, Author

ACKNOWLEDGMENT

I would like to thank Dr. Michael Lerner for his support and guidance in both my research and the preparation of this thesis. He has been a mentor and teacher and I have enjoyed working with him and learning from him. He has always challenged me to excel, and I am grateful. Financial support for my research was provided by the National Science Foundation, Allied Signal Inc., and the N. L.Tartar Foundation. I would also like to acknowledge the members of the Lerner group, Steve Sloop, Zhengwei Zhang, Rick Nafshun, Jinghe Wu, Chris Oriakhi, and Denny Givens for their friendship, suggestions and distractions. Finally, I wish to thank my wife Teresa for her constant encouragement and faith in me, and my parents for all their support.

CONTRIBUTION OF AUTHORS

Dr. Michael M. Lerner was involved in the design, analysis, and writing of each manuscript. Rodger L. Kohnert collected the ^{23}Na NMR data and Jinghe Wu conducted the research on MoO_3.

TABLE OF CONTENTS

Page

TABLE OF CONTENTS (Continued)

TABLE OF CONTENTS (Continued)

TABLE OF CONTENTS (Continued)

LIST OF FIGURES

LIST OF FIGURES (Continued)

LIST OF FIGURES (Continued)

LIST OF TABLES

The Synthesis and Characterization of Components for Solid-State Lithium Cells: Amorphous Polyether-Salt Complexes, Planar-Sheet Graphite Fluorides, and Layered Organic/Inorganic Nanocomposites.

Chapter 1
INTRODUCTION

1.1 General Introduction

This thesis examines the synthesis and characterization of materials with potential applications as components in solid-state alkali electrochemical cells. Alkali metals, especially lithium, have been widely studied for use as an anode. To date, several primary (irreversible) lithium cells with organic liquid electrolytes, such as Li/C_xF, Li/CuO, Li/MnO_2 and $Li/AgV_2O_{5.5}$ have been developed and commercialized. Advantages of such cells include; high output voltages (up to 4 V depending on the cathode), superior performance per weight compared to other conventional cells, and consistent discharge characteristics (1).

Currently, secondary (reversible) cells based on Ni-Cd or Pb-Acid dominate the rechargeable, portable power-source market. These cells have an output voltage between 1-2 volts, perform well over a wide temperature range, and can be cycled several hundred times. However, both impose environmental and health hazards by employing toxic heavy metals, and in the case of the Pb-Acid cell, a corrosive electrolyte. Other drawbacks include the potential for cell rupture when the cells are rapidly charged or discharged. Secondary lithium

cells are predicted to possess similar advantageous characteristics as mentioned for primary lithium cells. Such cells would avoid the use of toxic heavy metals and offer a theoretical advantage over other commercial cells in terms of energy density and shelf life. However, the development of secondary lithium cells utilizing a liquid organic electrolyte, has been hindered in part by safety problems and dendritic growth of lithium on the anode upon cycling. (One major safety concern involves the volatilization of the organic electrolyte, and subsequent cell rupture, incurred upon sudden heating in the case of a short-circuit.) The development of secondary lithium cells employing solid inorganic electrolytes offers an attractive solution to problems associated with organic liquid electrolytes. However, the performance of such cells has in part been hampered by high resistance at the electrode/electrolyte interfaces (2).

Much current lithium cell research remains focused around basic research; the development of new materials for use as anodes, cathodes, and electrolytes. The materials science poses many challenges as each component requires specific chemical, physical, and electrochemical properties. Thus, the materials chemist will play a vital role in the design and synthesis of such components.

1.1.1 Anode Materials

Although materials of this nature were not studied for this thesis, the synthesis of new anodic materials plays an important role in lithium cell

research. Until recently, lithium or lithium based alloys, such as LiAl, were most commonly used for both primary and secondary cell applications. However, as previously mentioned, they are susceptible to dendritic growth upon cycling in secondary cells containing liquid organic electrolytes.

An attractive solution to alleviate dendritic growth that has recently been studied involves replacing the lithium metal anode with an intercalation compound. Typically, a form of lithium intercalated carbon such as LiC_6 (Li/graphite) or LiC_{12} (Li/carbon black) is employed. Cells utilizing such materials are commonly referred to as "rocking chair-type" or "lithium ion" cells (3). Their principle advantage lies in the use of existing organic liquid electrolyte and anion technology. Problems associated with lithium plating morphology and cycling efficiency can also be avoided. However, the irreversible consumption of Li^+ (up to 25%) during the initial charge cycle, along with the reduction of the organic liquid electrolyte by the anode, LiC_x, remain important issues in their development (4, 5).

1.1.2 Electrolytes

As previously mentioned, the use of an organic liquid electrolyte in lithium anode and "lithium ion" type cells can lead to cell failure. The development of such cells depends on the formation of electrolytes, prepared by dissolving salts such as $LiBF_4$, $LiPF_6$, and $LiClO_4$ in organic liquids, which are chemically stable

and produce conductive solutions. However, this combination of properties has been difficult to achieve (6).

In general, the ionic conductivities of inorganic solid electrolytes at ambient temperature are much lower than that of liquid electrolytes, Table 1.I. The utilization of such electrolytes has also been hampered by the failure to maintain the interfacial electrode/electrolyte contact during cycling. (Although the commercialization of a primary solid-electrolyte cell based on lithium iodide has been successful (7).) Many of the materials in Table 1.I are inappropriate for common cell applications, although some may find use in high temperature cells where there is a significant increase in conductivity.

The utilization of lithium ion solvating polymers, such as poly(ethylene oxide) (PEO), as an electrolyte in lithium cells was first proposed by Armand in the early 1980s. Previously, the interaction between a salt and PEO was studied in the early 1950s (9), and measurements of ionic conductivity in polymer salt complexes were carried out in the mid 1970s (10). Although the ionic conductivity of polymer electrolytes is 2 to 3 orders of magnitude below desirable levels, they can be processed into very thin films of large surface area thereby decreasing the bulk resistance. Also, their flexible nature accommodates volume changes incurred during cell cycling without degradation of the interfacial contacts. These properties, combined with their low chemical reactivity, make polymer electrolytes leading candidates for use in an all solid-state lithium secondary cell. Further introduction into the structure and models of ion conduction in polymer electrolytes is presented in section 1.2. A detailed

study of the polymer electrolyte poly[(oxymethylene)oligo(oxyethylene)] (PEM) containing sodium salts is presented in chapters 2 and 3.

1.1.3 Cathode Materials

Many materials have been examined for use as cathodes in lithium primary batteries. These include; liquids such as $SOCl_2$, metal oxides (MoO_3, V_2O_5, MnO_2, CuO,), metal sulfides (FeS, CuS,), and graphite fluorides ($(C_xF)_n$). The application of graphite fluorides as a cathodic material in lithium cells is particularly attractive due to their high temperature and chemical stability. Also, the $Li/(C_xF)_n$ cell is among the highest in gravimetric energy density. The development and commercialization of a primary $Li/(C_xF)_n$ battery utilizing $(C_xF)_n$ as the cathode was first accomplished in the early 1970s. Further realization for the use of $(C_xF)_n$ as a cathode material was demonstrated in 1982 by the development of a $Li/(C_xF)_n$ dry cell (Matsushita Co., Japan). Current research of graphite fluorides as cathodic materials includes the use of thin-film polymer electrolytes in the formation of an all-solid-state cell (11). Further introduction to graphite and graphite fluoride synthesis is presented in section 1.3. A study on the synthesis of planar-sheet graphite fluorides is presented in chapter 4.

Several mixed conductors have been suggested as cathode materials for secondary lithium cells. These materials are typically lithium intercalation compounds such as layered transition metal dichalcogenides and oxides (12). The reversible intercalation reaction involves the interstitial introduction and

conduction of lithium ions into the host lattice with little or no structural modification to the host during cycling (13). A secondary lithium cell utilizing TiS_2 and a thin film polymer electrolyte is shown in Figure 1.1. The improvement of ion diffusion in such materials has been realized by the formation of organic/inorganic nanocomposites. This involves the placement of electroactive polymers, such as PEO, into the van der Waals space of layered mixed conductors. Further introduction to such nanocomposites is presented in section 1.4. The synthesis and characterization of nanocomposites of polyethers and MoS_2, TiS_2 and MoO_3 are presented in chapters 5 and 6.

1.2 Introduction to Polymer Electrolytes

Polymer electrolytes are formed by polar macromolecular solids with electron donor atoms (Lewis base) or groups which are capable of coordinating a metal ion (Lewis acid) of an ionic salt. The stability of the resulting polymer-salt complex is determined by the dielectric constant of the polymer and the lattice energy of the salt. Consequently, salts containing small alkali cations (Li, Na) are used to form stable polymer complexes. These salts typically have large, chemically stable anions, such as $SO_3CF_3^-$, ClO_4^-, I^-, and BF_4^-, which are suitable for solvation by the polymer. The relative energy associated with the solvation of the cation and the anion by the polymer, which is the driving force for complex formation, must exceed the lattice energy of salt formation. The

Hard-Soft Acid-Base principle (HSAB) has been used to account for and predict the stability of complexes formed between such Lewis acids and bases (14).

The ionic conductivity of an electrolyte can be expressed in the general terms shown in equation 1.1:

$$\sigma = \sum_i n_i z_i \mu_i \qquad [1.1]$$

where z_i is the ionic charge, n_i is the number of charge carriers, and u_i is the ionic mobility. In polymer electrolytes, the mechanism responsible for ion transport has been related to the segmental motion of the polymer backbone. The temperature dependence of conductivity in polymer electrolytes is best described by the Vogel-Tamman-Fulcher (VTF) equation,

$$\sigma = A/T \exp(-B/T-T_o) \qquad [1.2]$$

where A is a constant proportional to the number of charge carriers, B is a pseudo activation energy, and T_0 is the temperature at which the configurational entropy of the polymer becomes zero (which can be related to the glass transition temperature (T_g) of the polymer). The VTF equation is an adaptation of the William-Landel-Ferry relation, which describes physical properties associated with flow behavior of polymers, such as viscosity and dielectric relaxation time as a function of temperature (15). The segmental motion of the polymer backbone depends on thermal activation above T_g, thus ion mobility is increased at ambient temperatures for low T_g polymers, resulting in enhanced conduction. One method investigated to increase segmental motion in polymer salt-complexes involves the use of highly flexible, low T_g polymer backbones such as, $(P{=}N{-})_n$ and $(-SiO-)_n$ (16, 17). These polymer backbones themselves

are not able to complex salts significantly, therefore they are derivatized by grafting coordinating organic chains. Table 1.II lists thermal transitions and room temperature conductivities of several polymer electrolytes.

Many linear polymers crystallize to form spherical lamellar crystals called spherulites. Relatively large boundary regions form between spherulites due to chain end entanglements and slow diffusion kinetics associated with macromolecules. These boundary regions remain amorphous and comprise 10 - 50% of the volume in many commercial polymers. Such polymers are referred to as semi-crystalline and ionic conduction has been shown to take place in these amorphous regions of polymer electrolytes (18). A significant increase in ionic conductivity is therefore typically observed above the melting transition temperature of semi-crystalline polymers, where the polymer is entirely amorphous. Enhancing the properties associated with the conducting amorphous regions, while retaining desirable structural properties associated with crystalline or semi-crystalline materials has been one goal in polymer electrolyte research (19).

The formation of a completely amorphous polymer electrolyte at ambient temperature, can lead to increased conductivity. Current synthetic strategies, designed to suppress crystallization of the polymer involve modification of the polymer structure to inhibit chain regularity. These methods include the formation of branched or comb-shaped co-polymers, block co-polymers, and polymer networks which can be formed by chemical or irradiated crosslinks. Another method to enhance ambient conductivity involves the use of large

anions such as the imide, $N(SO_2CF_3)_2^-$. The lithium salt of this imide exhibits a plasticizing effect on semi-crystalline polymer electrolytes and results in substantially increased ambient conductivities. Low-molecular-weight solvents with high dielectric constants such as ethylene carbonate (EC), propylene carbonate (PC), and N-methyl pyrrolidone (NMP) have been used as plasticizing agents in polymer electrolytes (20). These platicizing solvents can also complex cations and can lead to liquid-like properties such as molecular diffusion and volatility. Because of these properties, electrolytes of this nature are not truly solid-state materials and are related to gel electrolytes (14).

Chapter 2 in this thesis describes the synthesis and characterization of the amorphous polymer electrolyte poly[(oxymethylene)oligo(oxyethylene)] (PEM). PEM, $[OCH_2(OCH_2CH_2)_m]_n$ (m=8-10), is a block co-polymer similar in structure to the polymer electrolyte poly(ethylene oxide), $(CH_2CH_2O)_n$ (PEO), which has been widely studied for application as a solid electrolyte in alkali metal cells. The effect of Na ion concentration on the ionic conductivity of the corresponding sodium salt complexes PEM_xNaClO_4 and PEM_xNaI (x = 8 - 150) is also presented. In chapter 3, further investigation of the sodium ion mobility within the polymer matrix, utilizing ^{23}Na NMR and differential scanning calorimetry, is discussed. Observed trends are presented in terms of mobile charge carriers and crosslink sites.

1.3 Introduction to Graphite Fluorides

Graphite has an infinite two-dimensional array of sp^2 hybridized carbon atoms in hexagonal rings, forming planar sheets. The *ab* (intralayer) plane of these sheets consist of C-C σ bonding enhanced by π overlap from the remaining p_z orbital. Bonding in the *c* (interlayer) direction arises from weak van der Waals interactions between the sheets. Oxidation or reduction of the carbon sheets by either chemical or electrochemical methods is accompanied by the intercalation of the appropriately-charged guest ion between the carbon layers, resulting in the formation of a graphite intercalation compound (GIC). Intercalation of graphite usually proceeds in stages as shown in Figure 1.2 The extent of intercalation is highly dependent on the relative oxidizing or reducing strength of the reactants (or potential applied in the case of electrochemical synthesis). Many changes in physical, chemical and electrochemical properties can be attributed to the addition or removal of electrons from the carbon anti-bonding or bonding orbitals, respectively upon the formation of a GIC (21).

Graphite fluorides were first prepared in the early 1930s with the synthesis of the polycarbon fluoride $(CF_{0.92})_n$, which was obtained by the reaction of elemental fluorine with graphite at 400-500 °C (22). However, the harsh synthetic conditions (high temperatures, use of fluorine) required for their fabrication have been a major obstacle in the widespread manufacturing of such materials.

In 1947, C_4F was formed by the reaction of a mixture of fluorine-hydrogen fluoride with graphite (23). This more facile approach has lead to graphite fluorides C_xF ($2 < x < 6$) prepared at ambient temperatures by the reaction of graphite with elemental fluorine in the presence of liquid anhydrous HF (24). More recently, a highly oxidized C_xF ($x < 2$) has been synthesized at room temperature by the fluorination of 2nd, and 3rd stage $C_x^+AsF_6^-$ salts in liquid anhydrous HF (25). Although compounds synthesized by the low temperature method are iso-stoichiometric with materials formed at high temperatures, their structure is different. The low-temperature products contain semi-ionic C - F bonds and retains the planarity of the original graphite, the high-temperature products contain covalent C - F bonds, and puckered sp^3 hybridized sheets. C_2F synthesized by the low temperature method has demonstrated equal if not superior performance characteristics as cathode materials in lithium cells relative to the high-temperature analog (26).

Chapter 4 deals with the synthesis of planar-sheet graphite fluorides in anhydrous HF $(C_xF)_n$ ($x = 2 - 6$), using fluorometallate salts of transition metals as oxidants. The extent of oxidation is determined by the carbon / transition metal ratio. The first chemical route to highly-oxidized graphite fluorides at ambient temperature without the use of elemental fluorine is described. A strategy for synthesis of planar-sheet graphite fluorides in polar organic solvents is also presented.

1.4 Introduction to Organic/Inorganic Nanocomposites

Nanoscale synthesis can be described as the process of controlling the structure of materials to the dimensions of one to several atoms. The formation of such materials can lead to novel properties or combinations of properties. The development of synthetic methods to control and attain such materials has been of fundamental interest to material chemists. One area of particular interest focuses on host(inorganic)-guest(organic) interactions confined to two-dimensional networks, resulting in the formation of nanocomposites (27, 28, 29).

Several different types of two-dimensional inorganic host materials have been studied, these include; clays, layered oxides, layered dichalcogenides, and phosphates to name a few. The organic guest molecules can range from small molecules to polymers (insulating or electroactive). The structure of such nanocomposites typically consists of the interlamellar region of the layered inorganic host occupied with the organic guest (although nanocomposites containing single-sheets of inorganic dispersed in a organic matrix have been studied). The breadth of the interlamellar space in these nanocomposites can range from 3 Å, for small molecules, to 50 Å for macromolecules.

Various techniques to synthesize such materials have been developed. These include; vapor deposition (CVD, sputtering, etc.), Langmiur-Blodgett methods, intercalation, and self assembly from colloidal solutions. Intercalation and self-assembly methods are attractive because they can be employed on a large scale and allow for the formation of materials that may not have volatile

precursors or be otherwise difficult to prepare via CVD or sputtering. In the preparation of complexed cations or oligomer-containing organic/inorganic nanocomposites intercalation and self-assembly have been utilized. One self-assembly method employed includes the co-condensation of an anionic inorganic species with a cationic surfactant under basic conditions (30). While intercalation involves the reduction or oxidization of the layered inorganic host accompanied by the simultaneous incorporation of cations (or anions) between the layers. These ions can also be accompanied by a solvating neutral molecule, such as an organic solvent or oligomer.

Intercalation is an impractical method in the preparation of self-assembled polymer-containing organic/inorganic nanocomposites. This is due to the reaction mechanism, which relies on the diffusion of species into and out of the interlamellar space, and is thereby a kinetically restricted process. Thus far two prevalent procedures have been utilized to incorporate organic macromolecules between inorganic layers. The first procedure, termed exfoliation-adsorption, involves the exfoliation of a layered inorganic host into single sheets in colloidal suspension. This is followed by the adsorption of a guest organic polymer onto the individual inorganic sheets and the resulting nanocomposite is then precipitated or centrifuged out of solution. The second procedure consists of the intercalation of organic monomers into the van der Waals gap of the inorganic host, followed by the *in situ* polymerization of the organic molecules. This may be accomplished by the use of initiators contained within the inorganic sheets (31, 32, 33), or the addition of an external reagent (34, 35).

Currently, one area of nanocomposite research consists of the development of materials toward electrochemical applications, such as a cathodes in secondary cells. One approach involves the incorporation of electroactive polymers in the van der Waals gap of layered electrode materials. Two advantages a nanocomposite of this type may display over present secondary electrodes are {1} faster ion conduction in the van der Waals gap during charging and discharging, and {2} reduced electrode/electrolyte interfacial resistance. The formation of such nanocomposites can be accomplished by the exfoliation/adsorption technique.

Chapter 5 investigates the formation and characterization of organic/inorganic layered nanocomposites, using the exfoliation/adsorption method, with the composition of $Li_x(PEO)_yMoS_2$. Chapter 6 describes the synthesis and characterization $Li_xNa_z(PEO)_yTiS_2$ and $Li_x(PEO)_yMoO_3$ nanocomposites. The host structures for these nanocomposites ($LiMoS_2$, Li_xTiS_2, and Li_xMO_3) have been widely studied as cathodic electrode materials in primary and secondary Li cells.

1.5 General apparatus and procedures

1.5.1 Stainless steel vacuum line

Manipulation of anhydrous hydrogen fluoride (AHF) (Matheson) and F_2 was carried out on a stainless steel vacuum line equipped with high-pressure

Autoclave Engineering SW - 4074 (valve type) valves and Whitey 1KS4 valves with Kel-F tipped stems as previously described (36). The vacuum line was fitted with a Kel-F trap (approx 20 ml volume) into which AHF could be dynamically condensed (Figure 1.3). A mechanical pump, protected by a glass trap held at 77 K, was attached to the line. Unreacted volatile fluorides were destroyed by a soda-lime tower placed before the cold trap. Pressure was monitored by a Helicoid gauge (0 - 1500 torr) and Varian thermocouple gauge (0 - 2000 microns). Connection of reaction vessels to the line were made via 316 stainless steel Swagelok compression fittings equipped with Teflon ferrules. The line was periodically passivated with F_2.

1.5.1.1 Handling of AHF

In a dry atmosphere, 1 - 2 ml of SbF_5 were placed into the Kel-F trap fitted with Whitey valves at both the inlet and outlet ends of the stainless steel head (Figure 1.3). The inlet of the trap was connected to the metal vacuum line while the outlet was connected to a cylinder of AHF. The trap was held at 77 K while HF was condensed in under dynamic vacuum. After collection, the trap was slowly warmed to room temperature. Any water present as an impurity reacts to form the slightly volatile hydronium salt $H_3O^+SbF_6^-$. Very dry AHF may therefore be transferred into reaction vessels when the temperature is held at 0°C.

1.5.1.2 Reaction apparatus used with AHF

Reactions utilizing AHF were carried out in 3/8" FEP Teflon tubing in which one end was heat sealed and the other capped with a Whitey valve via a Swagelok fitting equipped with Teflon ferrules. In some cases a 316 stainless steel T was added to allow for multiple Teflon reaction tubes (Figure 1.4). The apparatus was loaded with involatile reactants in a dry atmosphere and attached to the metal vacuum line via a Swagelok fitting with Teflon ferrules.

1.5.2 Glass vacuum line

Glass vacuum lines were equipped with ground glass stopcocks sealed with high vacuum grease. A mechanical pump was attached to the line and protected by a glass trap held at 77 K. The pressure was monitored by a Varian thermocouple gauge (0 - 2000 microns). Samples were handled in glass drying tubes equipped with a removable top which sealed to the bottom portion via a 50 mm o-ring joint. The top portion was furnished with a 15 mm O-ring joint for connection to the glass vacuum line and a Teflon stopcock with which the tube could be sealed once removed from the line.

1.5.3 Schlenck methods and glassware

Air/moisture sensitive materials, solvents, and reactions were manipulated using standard Schlenk line techniques (37). Nitrogen was dried by

flowing the gas through a tower consisting of P_2O_5 (Aldrich) and $CaSO_4$ (Aldrich). Involatile materials were loaded into Schlenck flasks under a dry atmosphere while solvents and other liquid reactants were transferred via stainless steel needles and disposable plastic syringes. Glassware was constructed from round bottom flasks modified with a side arm which included a Teflon stopcock for connection to the Schlenk line. The flasks were capped with a 15 mm O-ring joint seal and glass top.

1.5.4 Dry-box

Air-sensitive solids and involatile liqiuds were handled and stored in a Vacuum Atmospheres Corp. Dri-Lab (North Hollywood CA) filled with a dry argon atmosphere. Air-sensitive volatiles were stored in a nitrogen purge box (Forma Scientific Inc.) containing dry nitrogen.

1.5.5 Solvent and reagent purification

Acetonitrile (Aldrich, 99%) and hexane (Aldrich, reagent grade) were distilled under a dry nitrogen atmosphere over CaH_2. N-methyl formamide (Aldrich, 99%) was distilled under reduced pressure over KOH and stored under nitrogen. Dichloromethane (Mallinckrodt, HPLC grade) was stirred over molecular sieves (4A) and stored under nitrogen. To remove volatile impurities, graphite (SP1 Union Carbide, spectroscopic powder, average particle size 100 um) was repeatedly flamed to red heat in a quartz tube while subjected to a

dynamic vacuum. NaI (Mallinckrodt, analytical grade) was recrystallized from ethanol/water and dried under vacuum at 70 °C for several days. $NaClO_4$ (EM, reagent grade) was dried under vacuum at 70 °C for several days. All purified reagents were stored in an dry argon atmosphere. The purity of all crystalline reagents was checked by X-ray powder diffraction prior to use.

1.6 Characterization techniques

1.6.1 X-ray powder diffraction

X-ray powder diffraction data was obtained with a Norelco Debye-Scherrer camera (36 cm circumference) using Ni-filtered CuK_α radiation. Air-sensitive samples were loaded in 0.5 mm quartz capillaries (Charles Supper Co.) in a dry box and the capillaries were plugged with halocarbon grease and sealed with a microtorch. Typically, samples were rotated and exposed to X-rays for 24 hours. A Siemens D5000 powder diffractometer with a modified sample holder designed to contain an inert atmosphere was also used to collect diffraction data on air sensitive or air-stable samples.

A Enraf-Nonius Guinier camera utilizing $CuK_{\alpha 1}$ radiation and employing SP1 graphite as an external standard was used for some sample evaluation. Products could be loaded in capillaries as described above or by spreading a small amount (spatula tip) of sample onto transparent tape (3M). Samples were rotated and exposed to X-rays for up to 12 hours.

1.6.2 Elemental analysis

Atomic absorption spectroscopy data for Fe, Li, or Na content in samples were obtained on a Buck Scientific 200 analyzer or a Varian Techtron AA6 atomic absorption spectrophotometer. Standard analytical procedure was used for instrument settings and standard preparation (33). Sample preparation will be described in the appropriate chapters. Elemental analyses for C, H and N were performed by Desert Analytical (Tucson, AZ).

1.6.3 Transmission Infrared spectroscopy

IR spectra were collected on a Nicolet 510P FTIR (64 scans averaged, resolution = 2 cm^{-1}). Samples for IR spectroscopy were cast onto polyethylene films and dried under vacuum. The FTIR sample chamber was purged continuously with dry air.

1.6.4 Nuclear Magnetic Resonance spectroscopy (NMR)

^{13}C (1000 averaged scans) and ^{1}H (32 averaged scans) NMR data were obtained using a Bruker FT 300-MHz spectrometer. The polymer samples were loaded in NMR tubes in a dry atmosphere and dissolved in deuterated dichloromethane (Aldrich) with TMS as an internal standard.

^{23}Na NMR data were collected using an Bruker FT 400-MHz spectrometer with a 5-mm broad band probe. Neat samples of the polymer-salt complexes

were loaded into tubes under an inert atmosphere. An inversion-recovery (INVREC) pulse sequence at 105.8 MHz with variable delays was utilized to examine samples at various temperatures.

1.6.5 Thermal analysis

Differential Scanning Calorimetry (DSC) and simultaneous Differential Thermal Analysis/Thermogravametric Analysis (DTA/TGA) data were obtained on a Netzsch, Inc., STA 419C scanning calorimeter. Samples (10 - 25 mg) were loaded into aluminum pans in a dry atmosphere and made airtight by wrapping with Teflon tape. The sample chamber was evacuated prior to use and backfilled with dry He. In the case of sub-ambient temperatures, samples were stabilized by slow cooling to 190 K and allowed to equilibrate. Scanning rates were in the range of 2 to 10K/min.

1.6.6 Gel permeation chromatography (GPC)

GPC was performed on a Hewlett-Packard 1050 HPLC system using an ultrahydrogel linear column (Waters Chromatography) and Waters 410 RI detector. The column was calibrated using poly(ethylene oxide) standards (American Polymer Standards Corp.). Standards and samples were eluted at 0.85 mL/min in deionized water containing 0.05% NaN_3.

1.6.7 Electrical measurements

Variable-temperature impedance spectra were collected using a computer-controlled Solartron 1260 impedance analyzer and Sun ECO1 environmental chamber. Impedance measurements were acquired in the frequency range 15 MHz to 1Hz, applying a 1-V sine wave. Samples annealed as pellets were loaded in a dry Ar atmosphere in airtight Kel-F cells (Figure 1.5). Electrode arrangement will be described in the appropriate chapter.

Cyclic voltammetry (scan rates 10-20 mV/s) of thin film PEM sodium salt complexes (Figure 1.6), and charge/discharge measurements of $A_x(poly)_yMS_2$ (M=Ti or Mo) nanocomposites, were obtained on a computer controlled PAR362 potentiostat/galvanostat. Conductivity measurements of nanocomposites were made using the four probe method on pressed pellets under a blanket of nitrogen.

1.7 References

1. Linden, D. *Handbook of Batteries and Fuel Cells*; Linden, D., Ed.; Mc Graw Hill: New York, 1984.

2. Malachesky P. A. *Handbook of Batteries and Fuel Cells*; Linden, D., Ed.; Mc Graw Hill: New York, 1984.

3. Dahn, J. R.; Von Sachen, U.; Juzkow, M. W.; Al-Janaby, H. *J. Electrochem. Soc.* **1991**, *138*, 2207.

4. Guyomard, D.; Tarason, J. *Adv. Mater.* **1994**, *6*, 408.

5. *Lithium Batteries, New Developments and Perspectives*, Industrial Chemistry Library; Pistoia G., Ed.; Elsevier: Netherlands, 1994.

6. Takehara Z. Seventh International Meeting on Lithium Batteries, Extended Abstracts. Boston, 1994.

7. Owens, B. B.; Skarstad, P. M.; Unterker, D. F. *Handbook of Batteries and Fuel Cells*; Linden, D., Ed.; Mc Graw Hill: New York, 1984.

8. Armand, M. B.; Duclot, M.; *Fast Ion Conduction in Solids*, Mundy, J. N.; Shenoy, G. K., Eds., New York, 1979.

9. Doscher, T. M.; Myers, G. C.; Atkins, D. C. *J. Colloid Sci.* **1951**, *6*, 223.

10. Fenton, B. E.; Parker, J. M.; Wright, P. V. *Polymer* **1973**, *14*, 589.

11. Yazami, R.; Hamwi, A. *Solid State Ionics* **1990**, *40*, 982.

12. Whittingham, M. S. *Prog. Solid State Chem.* **1978**, *12*, 41.

13. Whittingham, M. S.; Huggins, R. A. J. *Chem. Phys.* **1971**, *54*, 414.

14. Grey, F. M. *Solid Polymer Electrolytes, Fundamentals and Technological Applications*, VCH: New York, 1991.

15. Ratner, M. *Polymer Electrolyte Reviews - 1*; MacCallum, J. R., Vincent, C. A., Eds.; Elsevier: New York, 1987.

16. Blonsky, P. M.; Shriver, D. F.; Austin, P.; Allcock, H. R. *J. Am. Chem. Soc.* **1984**, *106*, 6854.

17. Nagaoka, K.; Naruse, H.; Shinohara, I.; Watanabe, M. *J. Poly. Sci. Poly. Lett.* **1984**, *22*, 659.

18. Berthier, C.; Gorecki, W.; Minier, M. *Solid State Ionics* **1983**, *11*, 91.

19. Armand, M. B. *Polymer Electrolyte Reviews - 1*; MacCallum, J. R., Vincent, C. A., Eds.; Elsevier: New York, 1987.

20. Abraham, K. M. *Applications of Electroactive Polymers,* Scrosati, B., Ed.; Chapman and Hall: New York, 1993.

21. Bartlett, N.; Mc Quillan, B. W. In *Intercalation Chemistry*; Whittingham M. S.; Jacobson, A. J., Eds; Academic Press: New York, 1982.

22. Ruff, O.; Bretschneider, O.; Ebert, F. *Z. Anorg. Allg. Chem.* **1934**, *217*, 1.

23. Rüdorff, W.; Rüdorff, G. *Anorg. Allg. Chem.* **1947**, *253*, 281.

24. Mallouk, T.; Bartlett, N. *J. Chem. Soc., Chem. Comm.* **1983**, 103.

25. Hagiwara, R.; Lerner, M.; Barlett, N. *J. Chem. Soc., Chem. Comm.* **1989**, 573.

26. Hagiwara, R.; Lerner, M.; Barlett, N. J. *Electrochem Soc.* **1988**, *135*, 2393.

27. Stucky, G. D. *Prog. Inorg. Chem.* **1992**, *40*, 99-177.

28. Ozin, G. A. *Adv. Mater.* **1992,** *4*, 613.

29. Stein, A.; Keller, S. W.; Mallouk, T. E. *Science* **1993**, *259*, 1558.

30. Schüth, F.; Stucky, G.; *et al. Nature* **1994**, *368*, 317.

31. Kanatzidis, M. G.; Wu, C.; Marcy, H. O.; Kannewurf, C. R. *J. Am. Chem. Soc.* **1989**, *111*, 4139.

32. Kanatzidis, M. G.; Wu, C.; Marcy, H. O.; De Groot, D. C.; Kannewurf, C. R. *Chem. Mater.* **1990**, *2*, 222.

33. Mehrota, V.; Giannelis, E. P. *Solid State Comm.* **1991**, *77*, 155.

34. Bissessur, R.; DeGroot, D. C.; Schindler, J. L.; Kannewurf, C. R.; Kanatzidis, M. G. *J. Chem. Soc. Chem. Comm.* **1993**, 687.

35. Chang, T. C.; Ho, S. Y.; Chao, K. J.; *J. Chin. Chem. Soc.* **1992**, *39*, 209.

36. Lerner, M. Ph.D. Thesis 1988, University of California at Berkeley.

37. Shriver D. F. *The Manipulation of Air-Sensitive Compounds*; Mc Graw Hill: New York, 1969.

1.8 Figures

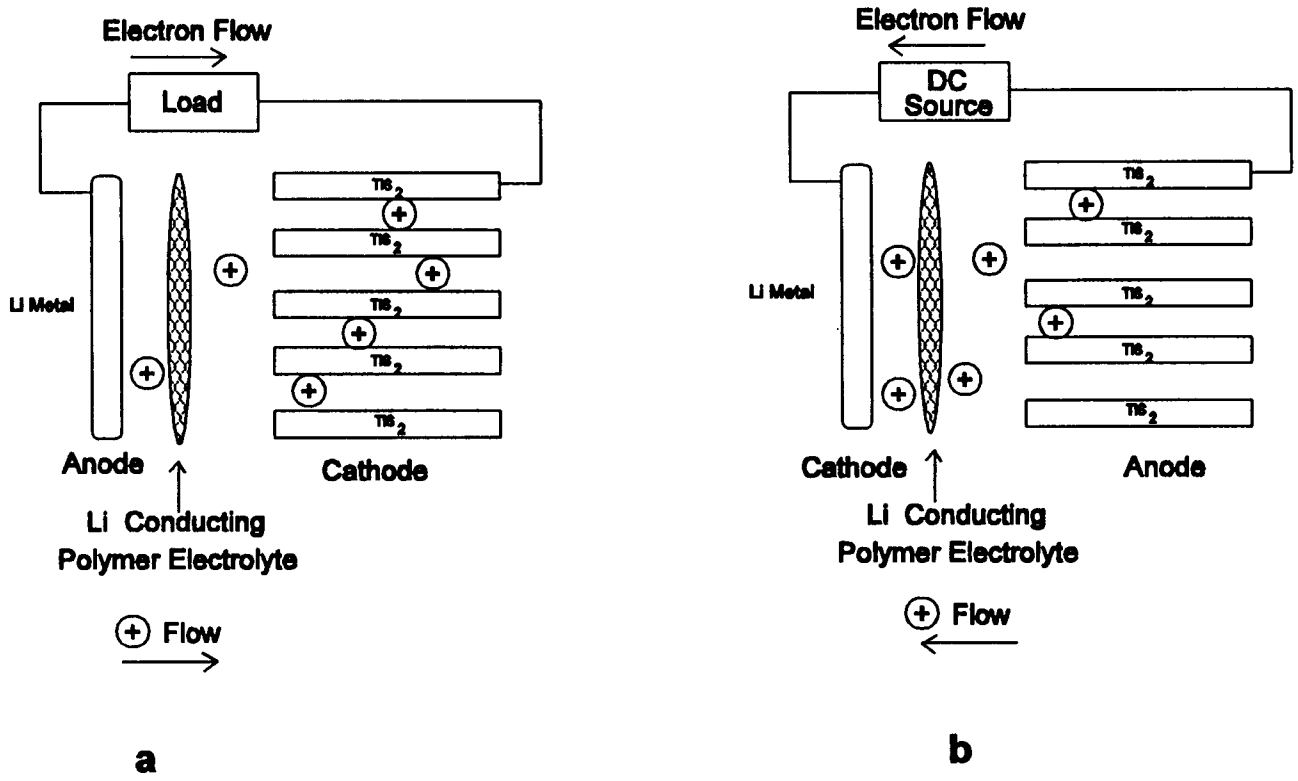

Figure 1.1 Simplified solid state battery, (a) discharging, (b) charging.

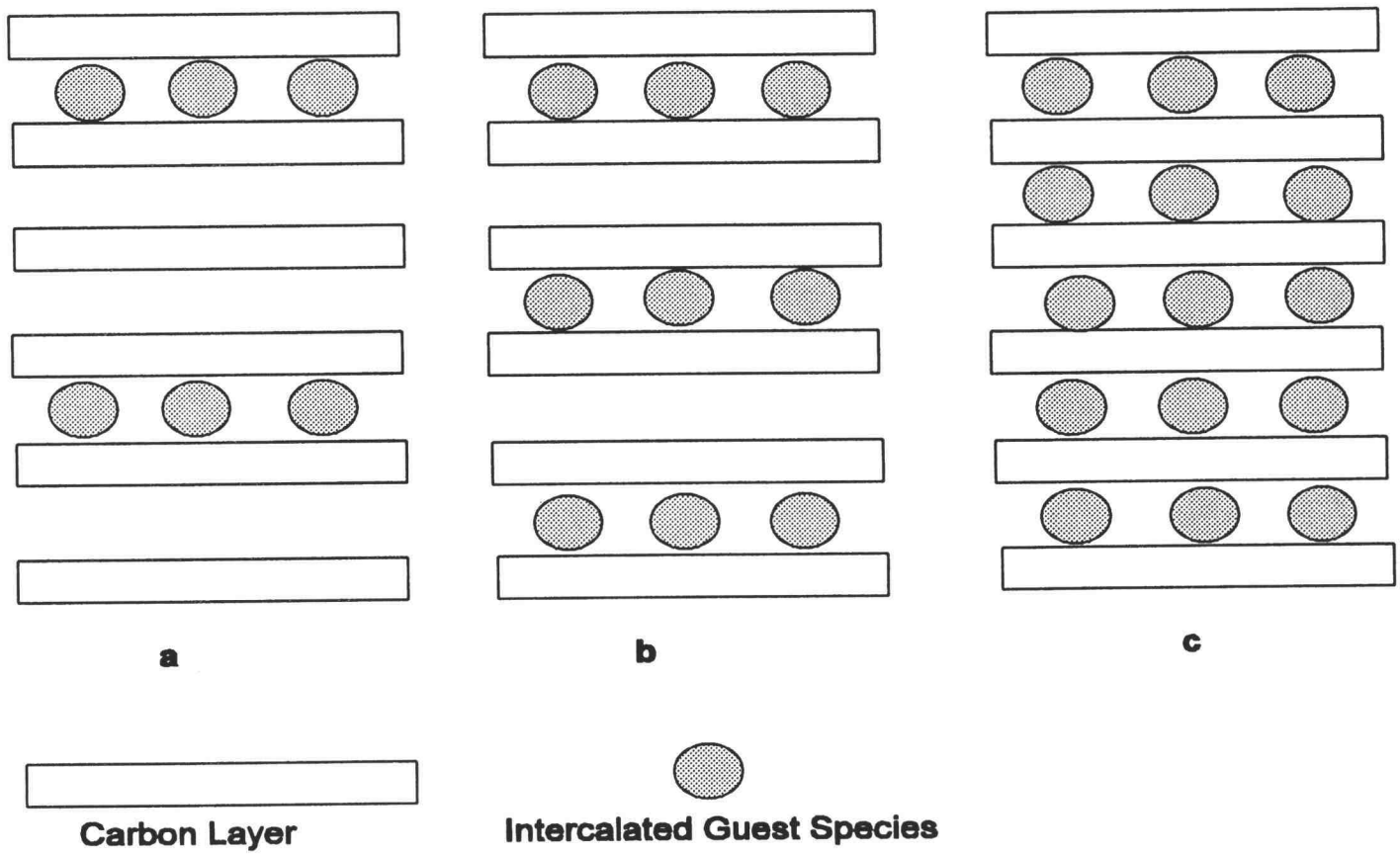

Figure 1.2 Staging in graphite intercalation compounds, (a) third, (b) second, (c) first (21).

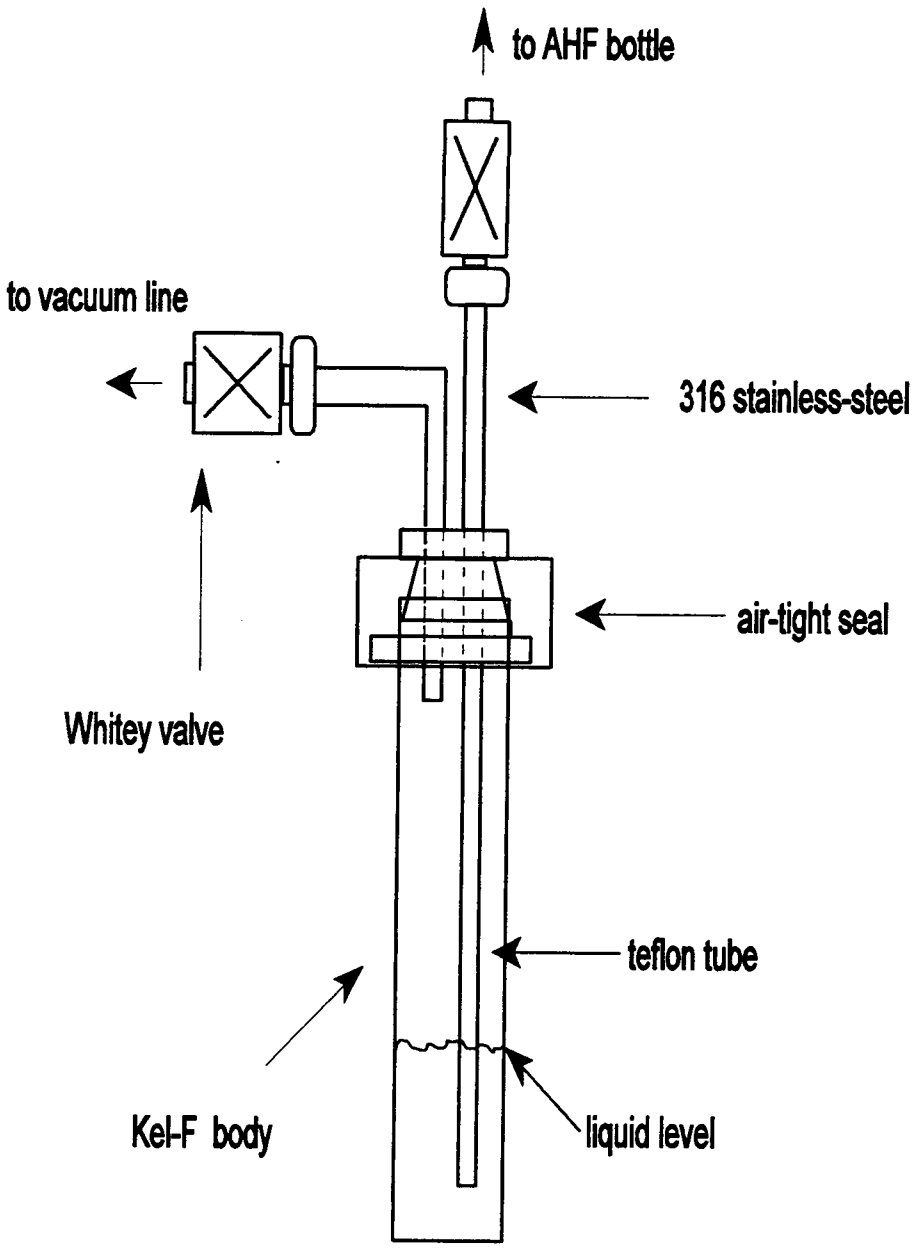

Figure 1.3 Cross section for the AHF trap employed on the metal vacuum line.

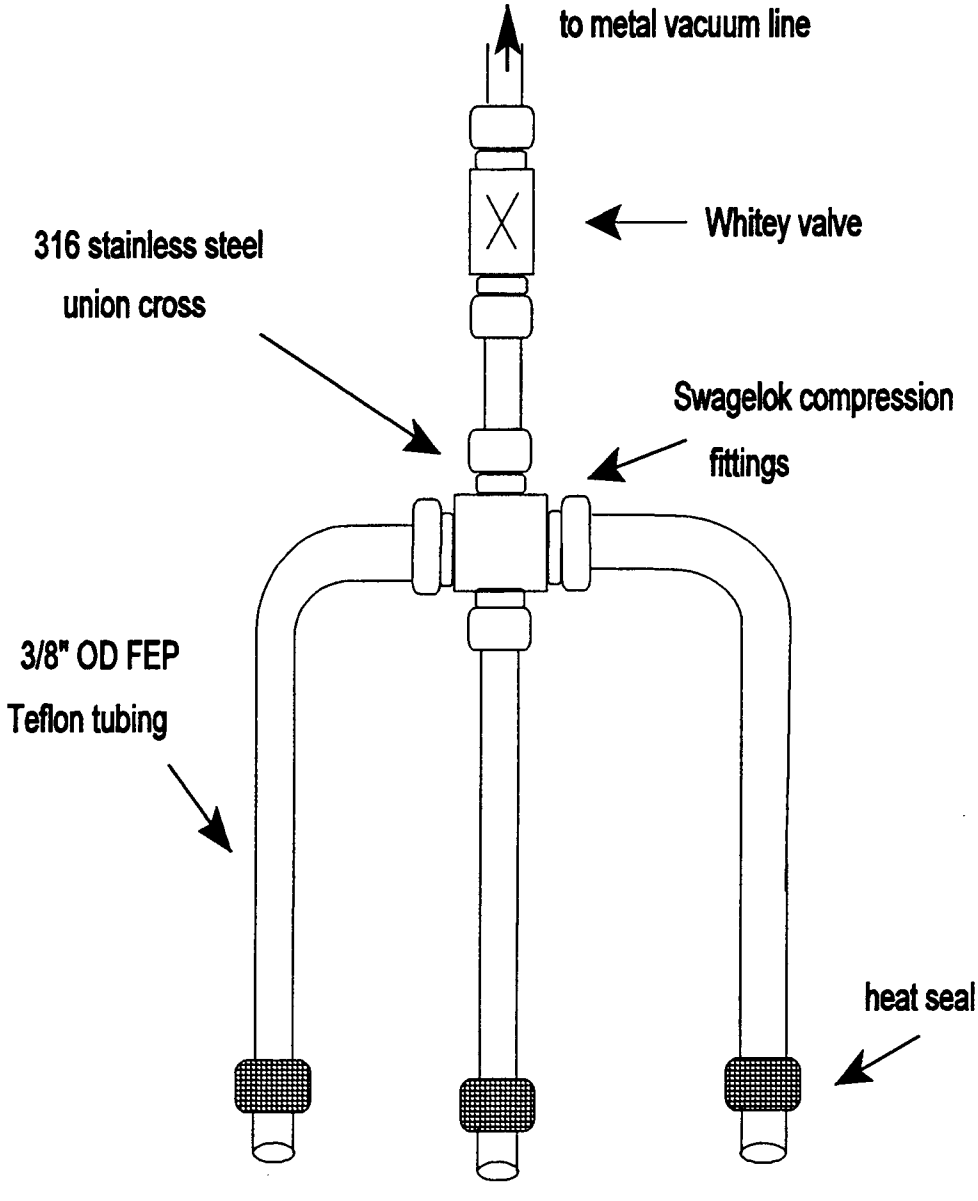

Figure 1.4 Apparatus employed when a predetermined stoichiometry of reactants was loaded into the same tube for reactions in an AHF medium.

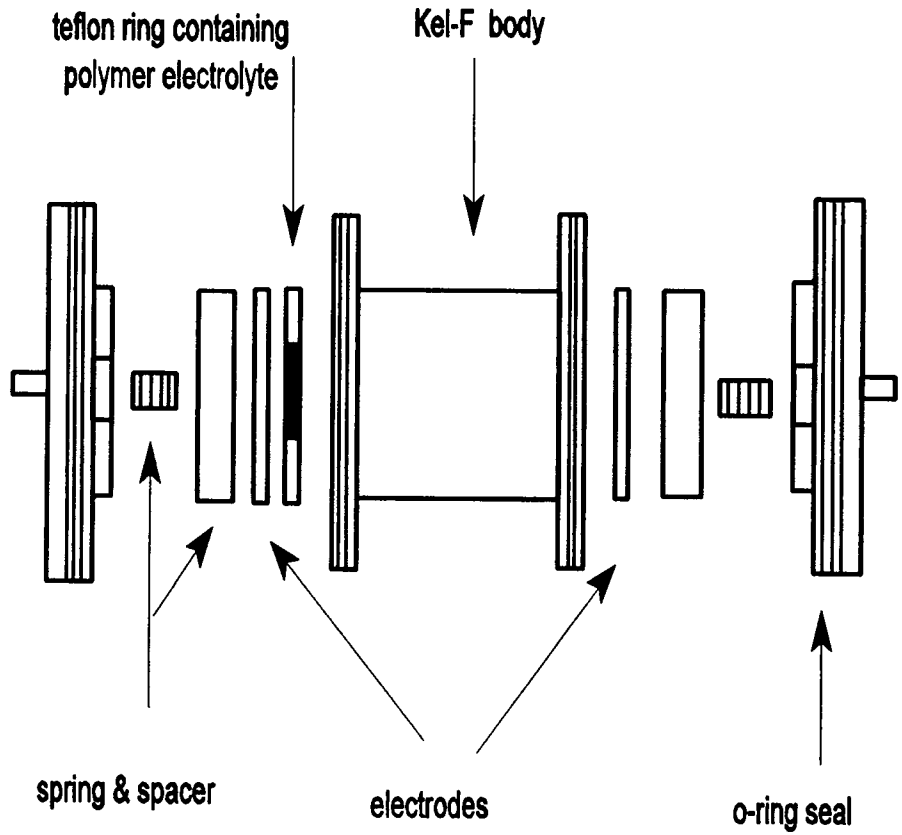

Figure 1.5 Air-tight impedance spectroscopy measurement cell. Sodium, lithium or stainless steel electrodes can be employed.

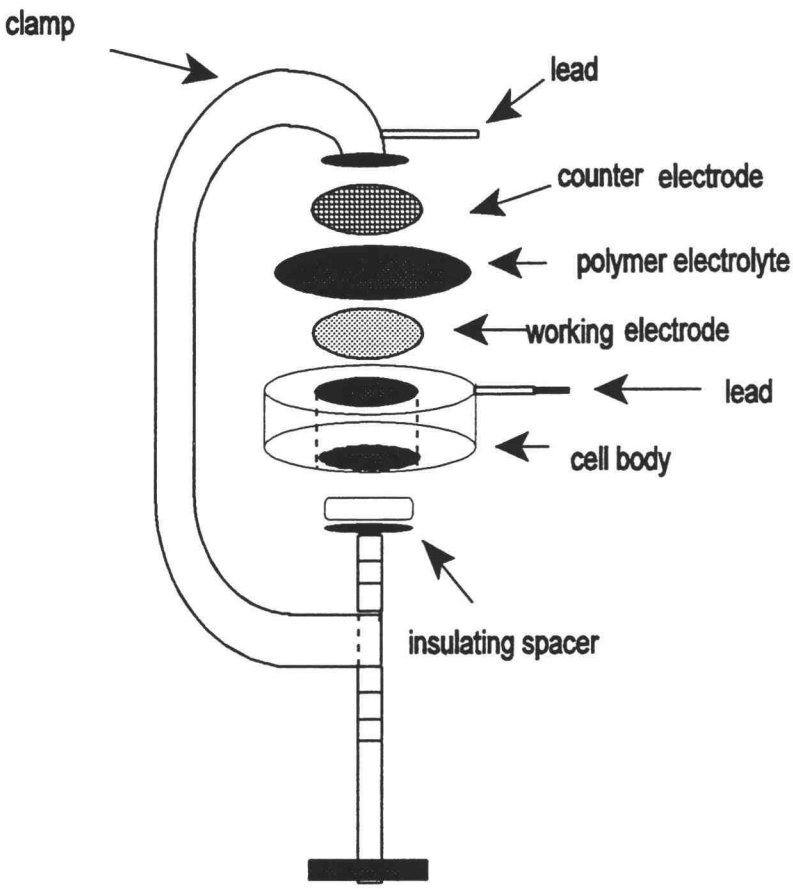

Figure 1.6 Apparatus and cell employed in electrochemical experiments involving polymer salt complexes and/or nanocomposites. The apparatus can be loaded in an air-tight container filled with a dry inert Ar atmosphere.

1.9 Tables

Table 1.I Alkali ion conducting electrolytes and typical conductivites.

Composition	Example	Conductivity Scm^{-1}	Temperature Range °C
A_2MO_4 (A = alkali metal; M = W, S, Mo)	Li_2WO_4	10^{-4} - 10^{1}	500 - 800
A_4MO_4 A_5MO_5 (A = alkali metal; M = Si, Ge, Al, Ga)	Li_4SiO_4 Li_5AlO_4	10^{-3} - 10^{3}	200 - 500
A_yAlX_z (A = alkali metal; X = Cl, F; y = 1-3; z = 4-6)	$LiAlCl_4$ K_2AlF_5 K_3AlF_6	10^{-6} - 10^{1}	200 - 1000
amorphous glasses	Li_2O-B_2O_3	10^{-6} - 10^{-3}	300 - 400

TABLE 1.II Thermal transitions and room temperature conductivities of several polymer electrolytes (20).

Polymer	Repeat Unit	Glass-Transition Temperature, T_g, °C	Melting Point, T_m, °C	Typical Polymer Electrolyte	Conductivity S/cm at 25°C
Poly(ethylene oxide)	$-CH_2CH_2O-$	-60	64	$(PEO)_8$-$LiClO_4$	$\sim 10^{-8}$
Poly(oxymethylene)	$-CH_2O-$	-82	181	-	-
Poly[(oxymethylene) oligo(oxyethylene)] (PEM)	$-(CH_2O)-(CH_2CH_2O)_n-$ n = 5 - 8	-66	13	$(PEM)_{25}$-$LiCF_3SO_3$	3×10^{-5}
Poly(propylene oxide) (PPO)	$-(CH_3)CHCH_2O-$	-60	amorphous	$(PPO)_8$-$LiClO_4$	$\sim 10^{-8}$
MEEP[a]	$OCH_2CH_2OCH_2CH_2OCH_3$ | $-P=N-$ | $OCH_2CH_2OCH_2CH_2OCH_3$	- 83	amorphous	$(MEEP)_4$-$LiBF_4$	2×10^{-5}
PEO poly(methyl-siloxane)	$-CH_3SiO$-PEO	-80	amorphous	PEO-polysiloxane-($LiClO_4$)	5×10^{-5}

[a] Poly[bis-(2-(2-methoxyethoxy)ethoxy)phosphazene].
- Not known.

Chapter 2
Effect of Salt Concentration on the Ionic Conductivity of Amorphous Poly(ethylene oxide)-Sodium Salt Complexes

John P. Lemmon and Michael M. Lerner*

Department of Chemistry and Center for Advanced Materials Research
Oregon State University
Corvallis, OR 97331

Macromolecules **1992**, *25*, 2907-2909

2.1 Abstract

Amorphous poly(ethylene oxide) (aPEO) is prepared by the oxy-methylene linkage of PEG400 and complexed with NaI and $NaClO_4$ with a range of stoichiometries, $aPEO_xNaAn$, x = 15-150. Transmission IR spectra and X-ray diffraction data indicate that the aPEO and all salt complexes prepared are amorphous at ambient temperature. The complexes are characterized by impedance and dc methods, with bulk conductivities determined from 263 to 343 K. A broad conductivity maximum is obtained at low salt concentrations for each series. Ionic conductivities on the order of 10^{-4}-10^{-5} S cm^{-1} are observed at ambient temperature. Arrhenius plots of the data indicate VTF behavior between T = 293 and 343 K.

2.2 Introduction

Poly(ethylene oxide) (PEO) forms salt complexes which exhibit high ionic conductivities above 333 K, but this conductivity rapidly decreases at lower temperatures due to the formation of a crystalline phase (1). The utility of the complexes as electrolytes in ambient temperature cells is therefore limited. Booth and co-workers (2,3) and others (2,4,5) have demonstrated that high molecular weight polymers, $[OCH_2(OCH_2CH_2)_m]_n$, can be produced by the oxy-methylene linkage of poly(ethylene glycol) to form amorphous salt complexes over a broad temperature range. Optimal properties for an amorphous-phase poly(ethylene oxide) (aPEO) are obtained from PEG400 ($m \approx 8$). Complexes of

aPEO with alkali-metal salts have been found to exhibit ionic conductivities on the order of 10^{-4}-10^{-5} S cm^{-1} at ambient temperature, which is 1-2 orders of magnitude greater than that in comparable PEO complexes. Research on sodium salt complexes of aPEO has indicated that ionic conductivities comparable to those observed in the Li complexes may be obtained (3-5), but a systematic study of the effect of concentration on conductivity has not yet been reported for the sodium complexes. This work describes the preparation and characterization of a range of stoichiometries for two sodium salt complexes, $aPEO_xNaClO_4$ and $aPEO_xNaI$ with x = 15-150.

2.3 Experimental Procedures

Amorphous PEO was prepared by a modification of the method published by Booth and co-workers (3). PEG400 (50 g; Aldrich) was added to a suspension of finely-ground KOH (Ashland Chemical; high-purity grade) in dry CH_2Cl_2 and mechanically stirred under N_2 for approximately 30 min until the solution became too viscous to stir. Another 50 mL of CH_2Cl_2 was then added, and the mixture was allowed to react overnight. Excess CH_2Cl_2 may be subsequently removed by evacuation. The crude product was dialyzed against distilled water (Spectrum cellulose tubing, MW cutoff = 3000) for 10 days to remove impurities of low molecular weight. Excess water was distilled away at reduced pressure and the product dried by heating under vacuum. A typical yield was 10 g of tacky, faintly yellow, polymer. ^{13}C and ^{1}H NMR spectra

obtained closely matched those reported previously for the high molecular weight polymer (1). All subsequent manipulations were performed in a drybox or under dry N_2 to exclude moisture.

Salt complexes were prepared by codissolving stoichiometric quantities of the polymer and salt in CH_3CN and then removing the solvent by evacuation. The complexes were further dried by evacuation at 70 °C for several hours. Cylindrical samples (diameter = 6 mm, thickness = 1.6 mm) for electrical measurements were formed in air-tight Kel-F cells and annealed at 70 °C prior to data collection. Some samples were cast into films (approximate diameter = 1.2 cm; thickness = 150 μm) from a CH_3CN solution, dried under vacuum, and pressed between disk electrodes in an air-tight cell. Stainless steel (irreversible) electrodes were generally employed, although some data were acquired with Na metal (reversible) electrodes.

Variable-temperature impedance spectra were collected using a computer-controlled Solartron 1260 impedance analyzer and Sun ECO1 environmental chamber. Impedance measurements were acquired in the frequency range 15 MHz to 1 Hz, applying a 1-V sine wave. A computer-controlled PAR362 potentiostat/galvanostat was used for dc measurements. Transmission IR spectra were acquired on a Nicolet 510P FTIR (64 scans averaged, resolution = 2 cm^{-1}). Samples for IR spectroscopy were cast onto polyethylene films and dried under vacuum. The FTIR sample chamber was purged continuously with dry air. X-ray diffraction data, collected on a D5000

Siemens powder diffractometer ($2° < 2\theta < 60°$, scan rate 2°/min), showed no evidence of a crystalline phase in aPEO or any of its complexes.

$NaClO_4$ (EM; reagent grade) and NaI (Mallinckrodt; analytical reagent, recrystallized from ethanol/water) were evacuated for several days at 70 °C and stored under N_2. CH_3CN (Mallinckrodt; HPLC grade) was distilled over P_2O_5 prior to use. PEO (Aldrich; MW = 100 000) was used as received for comparison studies.

2.4 Results and Discussion

Transmission IR data for aPEO, PEO, and salt complexes are presented in Figure 2.1. Previous studies (6) have ascribed the splitting of the peak near 1390 cm^{1-} to the presence of a symmetric and asymmetric —CH_2 wag and found that this peak is split only in a crystalline phase (7). The split peak is readily observed in the spectra of PEO and its complexes but is not split in ambient temperature spectra of aPEO and its complexes, indicating the amorphous nature of the latter. This result is confirmed by X-ray diffraction, which shows no diffraction peaks for aPEO or its complexes.

Representative impedance spectra obtained on pellets and thin films are shown in Figure 2.2a-c. The Cole-Cole plots obtained have a single arc for cells with irreversible electrodes. Measurements of samples with different geometries confirm that this arc corresponds to a bulk conduction process, and the bulk ionic conductivity was taken to be the touchdown of the high-frequency arc.

Conductivities for the salt complexes are on the order of 10^{-4}-10^{-5}S cm^{-1} at ambient temperature. Cole-Cole plots with two arcs are observed with reversible electrodes, with the high-frequency arc corresponding to bulk conduction and the low-frequency arc ascribed to an interfacial process. Although a previous report has indicated that the $aPEO_xLiAn$/Li interface is highly unstable (8), the measured $aPEO_xNaAn$ interfacial impedance remained relatively constant over a period of several hours at 323 K. The alkali-metal electrode interface is highly vulnerable to air and especially moisture, and the differences in the results obtained here and previously may represent the experimental difficulty of maintaining an inert environment within the cell. In agreement with the above model, the impedance measured at the low-frequency touchdown is similar to the total cell resistance obtained by cyclic voltammetry (Figure 2.3).

Arrhenius plots of the impedance data for the $aPEO_xNaClO_4$ and $aPEO_xNaI$ (Figure 2.4) are similar, and the curved lines are consistent with the VTF behavior observed in many polymer electrolytes. The VTF equation may be expressed as

$$\sigma T = A \exp(-B/(T-T_o)) \qquad [2.1]$$

and reasonable VTF parameters obtained from a fit of the data between 293 and 343 K are A = 0.47, B = 0.091 eV, and T_o = 165 K for $aPEO_{150}NaClO_4$ and A = 3.0, B = 0.096 eV, and T_o = 171 K for $aPEO_{15}NaClO_4$. The onset of a rapid decrease in conductivity is observed at 293 K, but the conductivities at ambient temperature are far greater than those of corresponding PEO complexes. The general slope of the curves becomes gradually steeper with increasing

concentration, indicating a small increase in the activation energy and/or glass transition temperature.

It is notable that the conductivity is not greatly affected by the salt concentration over the wide concentration range studied, although a broad maximum can be observed near x = 25-50 for the complexes at 333 K with a somewhat sharper maximum near x = 50 at 303 K (Figure 2.5). The conductivities obtained at low salt concentrations agree well with those found for $aPEO_xLiClO_4$ (4); these results differ markedly from the conductivity-concentration relation of crystalline PEO complexes (1), which exhibits a maximum near x = 8. This dissimilarity can be explained by the multiphase nature of the PEO complexes at these temperatures: the PEO complexes contain a crystalline phase, PEO_xNaAn (x = 3-6), of low conductivity along with an amorphous, conductive phase. The very shallow dependence of the conductivity of the salt concentration, resulting, for example, in a conductivity greater than 10^{-5} S cm^{-1} for at least a range of concentration for PEO_xNaClO_4, $150 < x < 25$, may prove useful in cell applications where nonequilibrium processes result in an ion concentration gradient.

Further characterization of the $aPEO_xNaAn$ complexes by NMR spectroscopy and differential scanning calorimetry is discussed in Chapter 3.

2.5 References

1. (a) Armand, M. B. In *Polymer Electrolyte Reviews - 1*; MacCallum, J. R., Vincent, C. A., Eds.; Elsevier: New York, 1987; and references therein. (b) Ratner, M.; Shriver, D. F. *Chem. Rev.* **1988**, *88*, 109.

2. Booth, C.; Nicholas, C. V.; Wilson, D. J. In *Polymer Electrolyte Reviews - 2;* MacCallum, J. R., Vincent, C. A., Eds.; Elsevier: New York, 1989; and references therein.

3. Nicholas, C. V.; Wilson, D. J.; Booth, C.; Giles, J. R. M. *Br. Polym. J.* **1988**, *20*, 289.

4. Gray, F. M. *Solid State Ionics* **1990**, *40/41*, 637.

5. Wintersgill, M. C.; Fontanella, J. J.; Pak, Y. S.; Greenbaum, S. G.; Al-Mudaris, A.; Chadwick, A. V. *Polymer* **1989**, *30*, 1123.

6. Nazri, G. A.; MacArthur, D. M.; O'Gara, Aroca, R. J. F. *Mater. Res. Soc. Symp. Proc.* **1991**, *210*, 163.

7. Matsuura, H.; Fukuhara, K. *J. Polym. Sci., Part B* **1986**, *24*, 1383.

8. Murugesamoorthi, K. A.; Owen, J. R. *Br. Polym. J.* **1988**, *20*, 227.

2.6 Figures

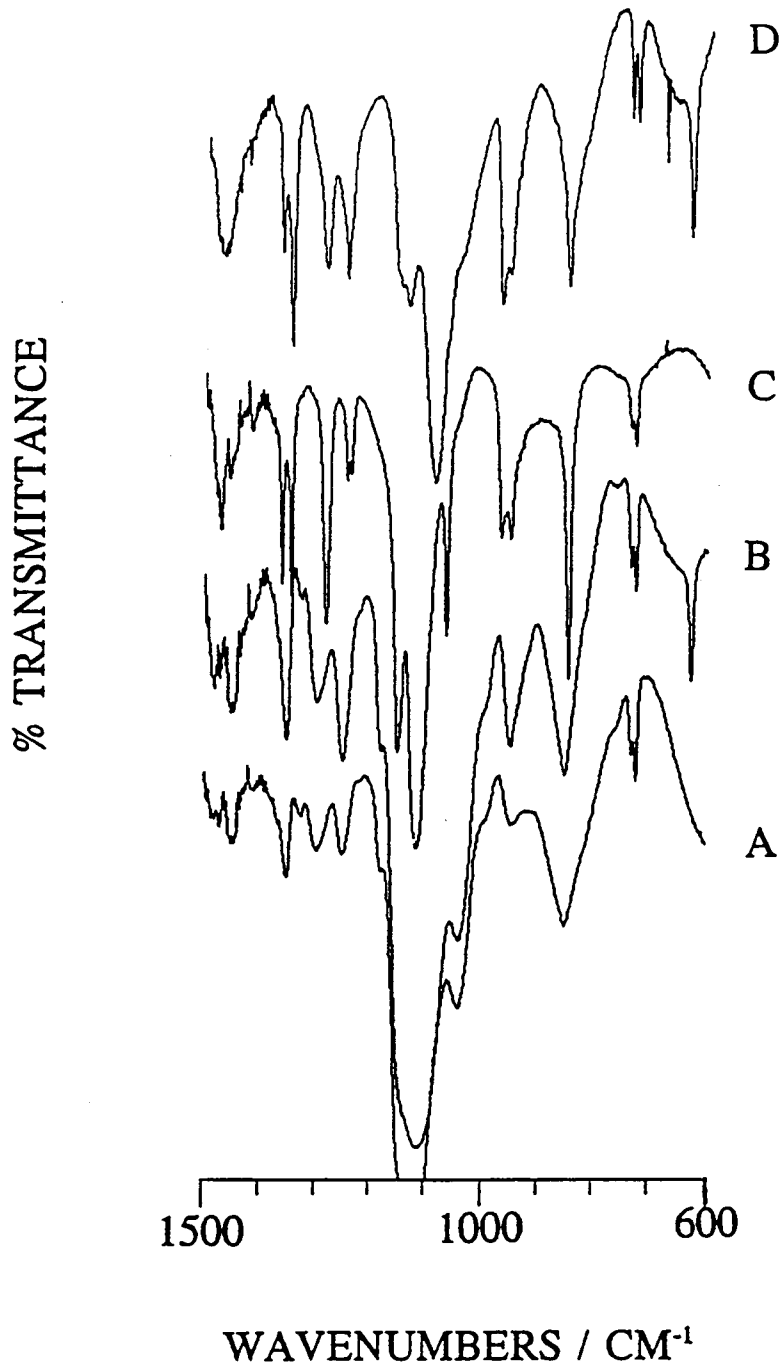

Figure 2.1 Transmission IR spectra of thin films of (A) aPEO, (B) $aPEO_{50}NaClO_4$, (C) PEO, and (D) $PEO_{50}NaClO_4$

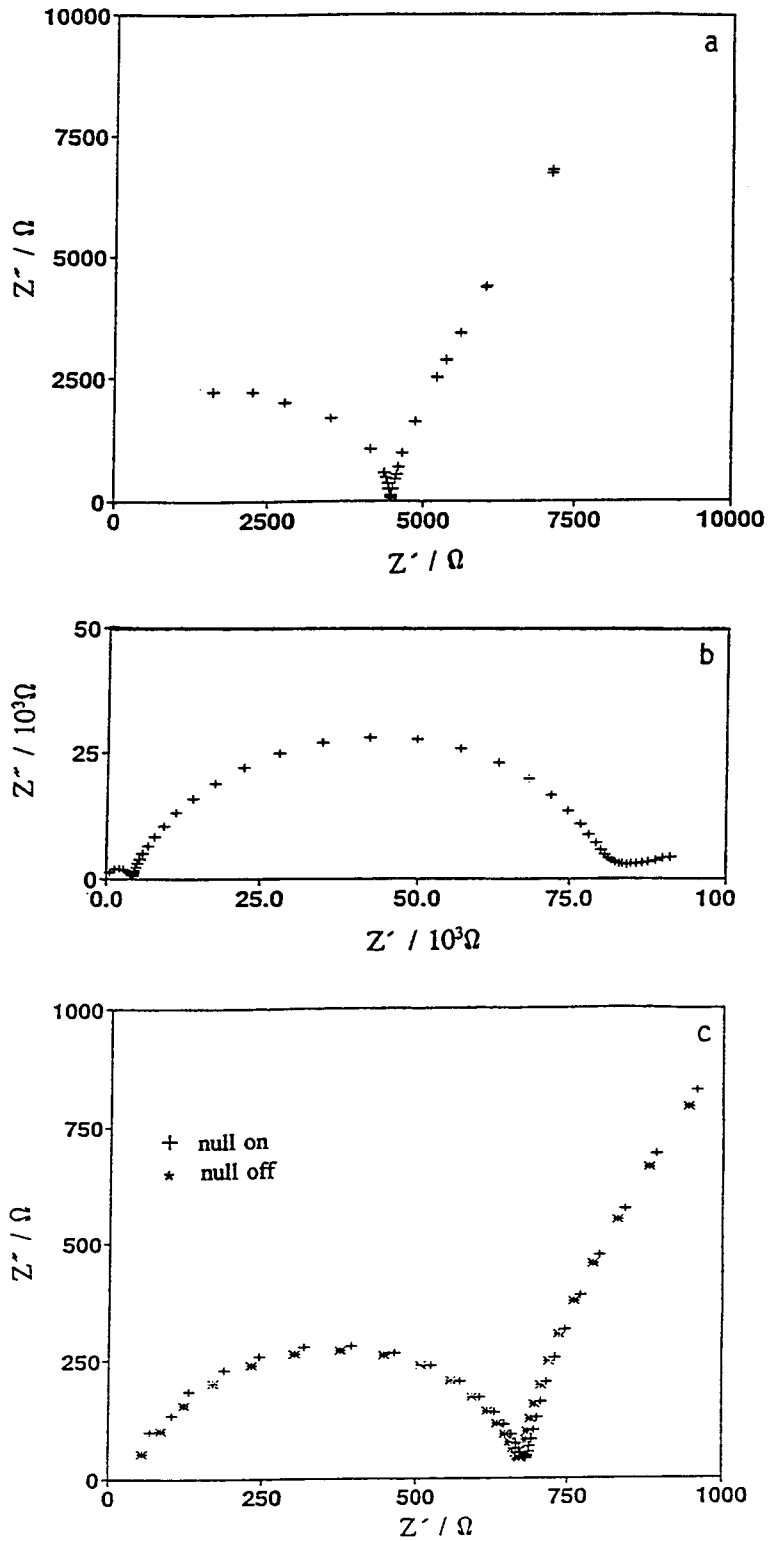

Figure 2.2 Cole-Cole plots of impedance data from $aPEO_{75}NaClO_4$; (a) pellet sample with steel electrodes at 323 K, (b) pellet sample with Na electrodes at 323 K, and (c) 150-μm film sample with steel electrodes at ambient temperature. In c, pluses indicate data corrected with a null circuit and asterisks indicate uncorrected data.

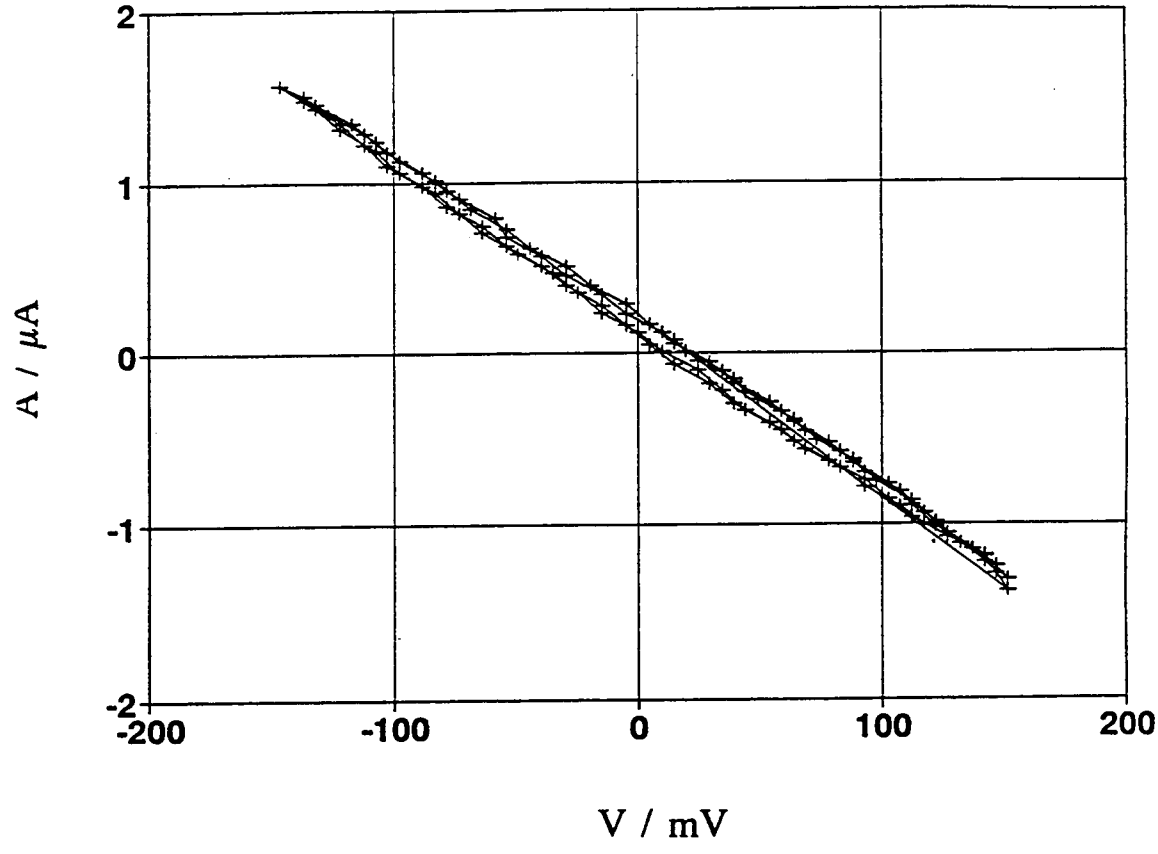

Figure 2.3 Cyclic voltammogram using two Na metal electrodes (scan rate = 20 mV/s, T = 323 K) and a thin film of $aPEO_{75}NaClO_4$ as electrolyte. The inverse slope = $R = \Delta V/\Delta I = 1.0 \times 10^5\ \Omega$.

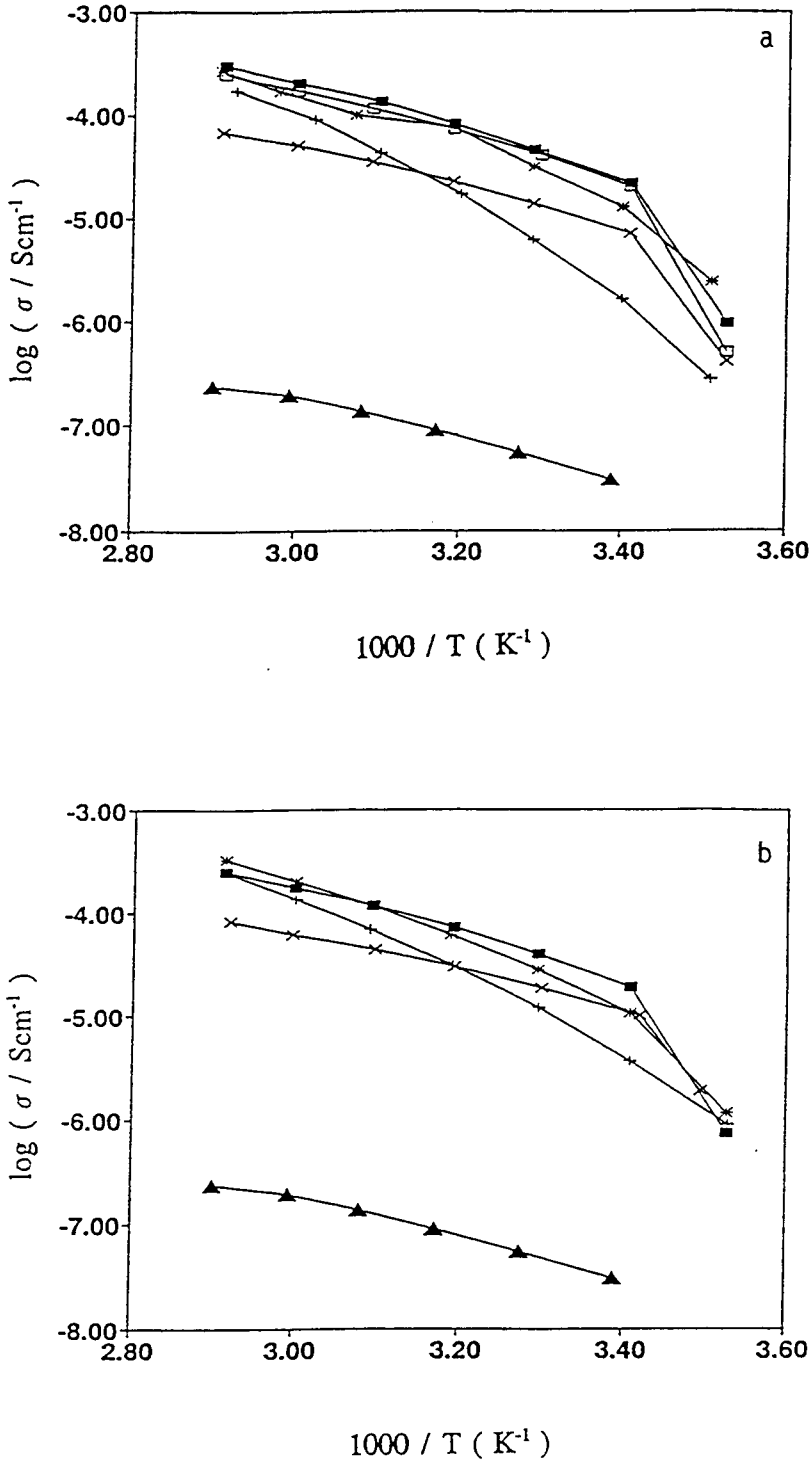

Figure 2.4 Arrhenius plots for (a) $aPEO_xNaClO_4$ and (b) $aPEO_xNaI$: (+) $x = 15$, (✱) $x = 25$, (■) $x = 50$, (□) $x = 75$, (X) $x = 150$, and (▲) uncomplexed aPEO.

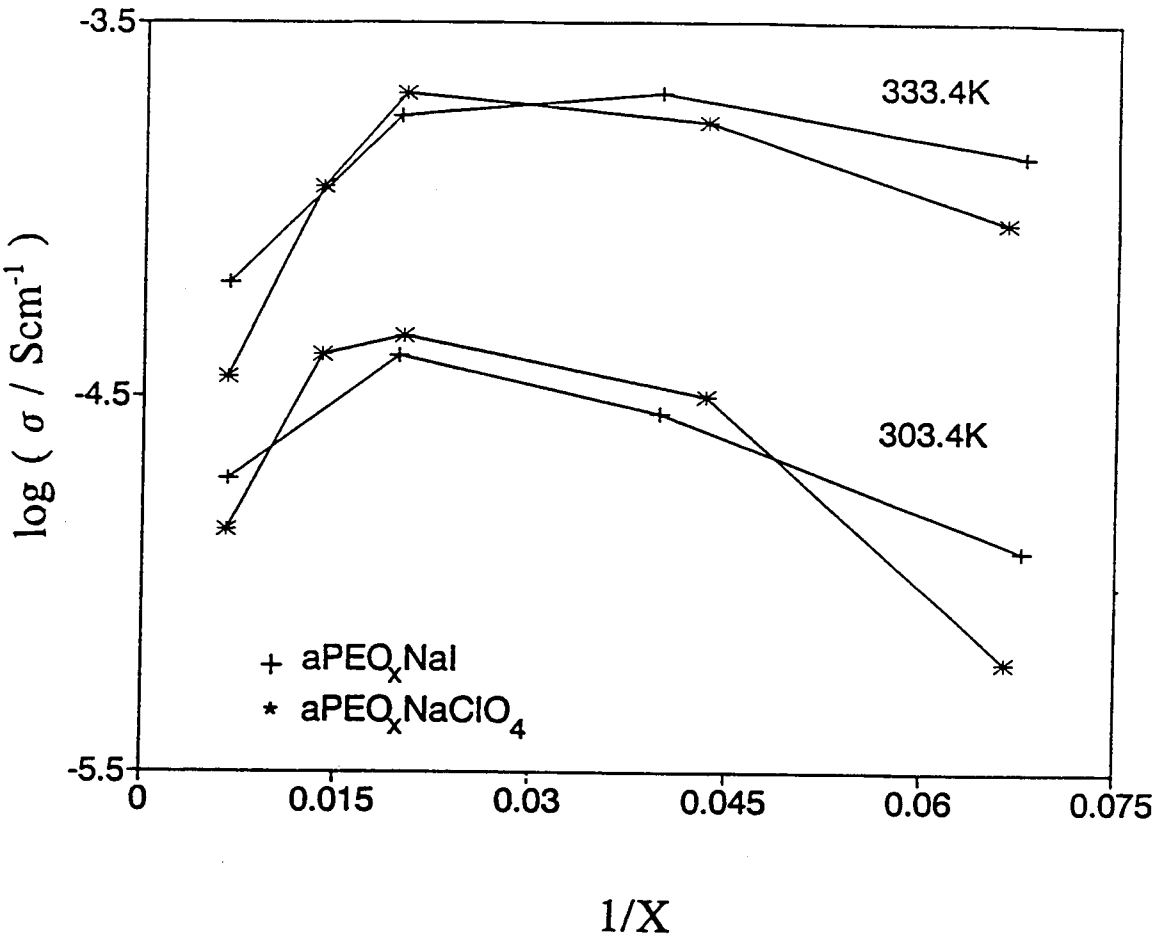

Figure 2.5 Conductivity vs composition at 303 and 333 K for aPEO$_x$NaClO$_4$ and aPEO$_x$NaI.

Chapter 3
Characterization of a Stoichiometric Range of Sodium Salt Complexes of Amorphous Poly[(oxymethylene)oligo(oxyethylene)] by Differential Scanning Calorimetry and ^{23}Na NMR

John P. Lemmon and Michael M. Lerner*

Department of Chemistry and Center for Advanced Materials Research
Oregon State University
Corvallis, OR 97331

Macromolecules **1993**, *26*, 2767-2770

3.1 Abstract

Sodium salt complexes of poly[(oxymethylene)oligo(oxyethylene)], $[OCH_2(OCH_2CH_2)_m]_n$ (m = 8-10), are characterized by (1) DSC between 190 and 295 K and (2) ^{23}Na NMR spectroscopy between 208 and 358 K using an inversion-recovery pulse sequence. The complexes studied (polymer$_x$NaAn, An = ClO_4 and I, x = 8-150) crystallize near 280 K only for $x > 25$; higher salt concentrations result in complexes which remain amorphous throughout the temperature range studied. Glass transition temperatures are determined for each complex, and the conductivity-temperature plots fit to the VTF equation using the relation $T_o = T_g - 27$ K. ^{23}Na NMR studies on complexes with x = 50, 25, and 8 show two components distinguished by relaxation rates. Mole fraction, molal concentration, and T_2^* are determined for each component over the temperature range studied, and observed trends are discussed in terms of mobile charge carriers and cross-link sites.

3.2 Introduction

Amorphous polyether-salt complexes can exhibit high ionic conductivities and are presently being considered for applications as electrolytes in energy storage devices (1). Poly(ethylene oxide) (PEO)-salt complexes have been demonstrated to perform adequately above the melting point of the complex (typically 60-100 °C) but are predominantly crystalline, and therefore far less conductive, at ambient temperature. Booth and co-workers (2-4) have described

a simple chemical route to high-molecular-weight poly[(oxymethylene)oligo(oxyethylene)] copolymers, $[OCH_2(OCH_2CH_2)_m]_n$, subsequently denoted as (poly(ME_m), which are amorphous at ambient temperature. As the synthesis involves the oxymethylene linkage of a distributed sample of poly(ethylene glycol), the average value for *m* is presented (m_{avg} = 8.7 when PEG 400 is utilized). Complexes of poly($ME_{8.7}$) with alkali-metal salts are also amorphous at ambient temperature and exhibit ionic conductivities on the order of 10^{-4}- 10^{-5} S cm^{-1} (2-6). We have previously described the characterization of a range of stoichiometries for two sodium salt complexes -- poly$(ME_{8.7})_xNaClO_4$ and poly$(ME_{8.7})_xNaI$, x = 15-150 -- by IR spectroscopy, X-ray diffraction, impedance, and dc measurements between 283 and 343 K (6). Broad maxima in the ionic conductivities were found at x = 25-50, and there was no significant difference in the results obtained on the two salt complexes studied. To further evaluate the relation between polymer dynamics and ionic conduction in amorphous polyether-salt complexes, we here describe results obtained on these complexes using differential scanning calorimetry and ^{23}Na NMR spectroscopy.

3.3 Experimental Section

Poly($ME_{8.7}$) was prepared by a modification of the method published by Booth and co-workers (3). The ^{13}C and ^{1}H NMR spectra obtained on the resulting polymers closely matched those reported previously for high-molecular-

weight polymers (2). All subsequent manipulations were performed in a drybox or under dry N_2 to exclude moisture.

$NaClO_4$ (EM, reagent grade) and NaI (Mallinckrodt, analytical reagent, recrystallized from ethanol/water) were evacuated for several days at 70 °C. CH_3CN (Mallinckrodt, HPLC grade) was distilled over P_2O_5 prior to use. Salt complexes were prepared by codissolving stoichiometric quantities of the polymer and salt in CH_3CN, removing the solvent by evacuation, and heating at 70 °C in vacuo for several hours to remove traces of solvent or volatile impurities.

DSC data were obtained between 190 and 295 K using a Netzsch, Inc., STA 419C scanning calorimeter with a low-temperature measuring head and liquid-nitrogen-cooled heating element. Samples (approximately 10 mg) were loaded into aluminum pans in a dry atmosphere and made airtight by wrapping with Teflon tape. The DSC sample chamber was evacuated prior to use and back-filled with dry He. Samples were stabilized by slow cooling to 190 K and subsequently heated at 10, 5, and 2 K/min. Reported transition temperatures are extrapolated to zero heating rate.

^{23}Na NMR data were obtained using a Bruker 400-MHz spectrometer with a 5-mm broad-band probe. Neat samples of polymer-salt complexes were loaded into the tubes under an inert atmosphere. An inversion-recovery (INVREC) pulse sequence at 105.8 MHz, with variable delays in the range of 10 μs to 1 s, was utilized to examine samples between 208 and 358 K at intervals of 15 K.

3.4 Results and Discussion

Arrhenius plots of the impedance data for the poly($ME_{8.7}$)$_x$$NaClO_4$ and poly($ME_{8.7}$)$_x$NaI were previously reported for x = 150-15 (6) and are presented (Figure 3.1) for poly($ME_{8.7}$)$_x$NaI to include recent results for the complex with x = 8. Data were also obtained for poly($ME_{8.7}$)$_x$$NaClO_4$ complexes and are essentially identical. The curved-line response observed in the temperature-conductivity plots is consistent with the VTF behavior common in polymer electrolytes. A rapid decrease in conductivity is observed below 293 K for lower salt concentrations. This effect, due to the formation of a crystalline complex, occurs well above ambient temperature for the corresponding PEO complexes (1). DSC data (Table 3.I, Figure 3.2) are presented for poly($ME_{8.7}$)$_x$NaI and poly($ME_{8.7}$)$_x$$NaClO_4$ complexes and agree with data obtained by other workers (7,8) on related materials. A melting transition is observed near 280 K at lower salt concentrations (x = 150, 50) only, indicating that poly($ME_{8.7}$)$_x$NaAn complexes with x < 50 do not crystallize in the temperature range studied. These results therefore follow the trends observed in the conductivity-temperature plots. The glass transition for the poly($ME_{8.7}$) complexes is markedly stronger at higher salt concentrations, which is reasonable as the entire sample is amorphous for these complexes and undergoes the glass transition. As with other polyether complexes, the glass transition temperature increases with salt concentration, reflecting a change in polymer dynamics due to polymer-salt interactions. The conductivity plots above T_m were fit to the VTF equation:

$$\sigma = (A/T) \exp(-B/(T-T_o)) \qquad [3.1]$$

and the calculated parameters A and B are presented in Table 3.I. The experimental T_g data were employed directly to determine T_o (T_o was taken to be T_g - 27 K to minimize undue correlation between the parameters employed in the fit).

A large exotherm near 230 K is reproducibly observed at x = 50 for both sodium salt complexes and is unaffected by thermal cycling of the samples. The origin of this transition is uncertain, but it is perhaps significant that the transition is observed only at a stoichiometry of x = 50, which is near the maximum salt concentration for the formation of a crystalline phase.

^{23}Na NMR spectroscopy has been employed to examine the chemical environment for Na^+ in amorphous polyether complexes. Two Na^+ species, distinguished on the basis of relaxation rates, have been detected by Greenbaum and co-workers (8-14) and other groups (15-17). These two components to the ^{23}Na NMR signal have been ascribed to mobile and bound sodium species, corresponding to the Na^+ species with short and long relaxation times, respectively.

The inversion-recovery method is employed to examine polymer-salt complexes with three different salt concentrations (x = 8, 25, and 50) in the temperature range of 208-358 K. Complexes with salt concentrations lower than x = 50 are difficult to study because of the low concentration of Na^+ in the sample, which is compounded in these complexes because, below T_m, much of the Na^+ is in a crystalline phase and cannot be detected. The results we

describe agree well with those of other workers and extend the NMR technique to the examination of a range of stoichiometries.

A typical series of NMR spectra obtained (Figure 3.3) displays the inversion of two overlapping peaks, one sharp and one broad, which are ascribed to Na^+ species Na_A^+ and Na_B^+, respectively. The typical separation of 2 orders of magnitude for the T_1 relaxation times of these signal components provides a unique solution for the relation

$$I(\tau) = M_A e^{-\tau/T1A} + M_B e^{-\tau/T1B} + C \qquad [3.2]$$

where I = total signal intensity, τ = pulse delay, M_A and M_B = magnetization coefficients for Na_A^+ and Na_B^+, T_{1A} and T_{1B} = spin-lattice relaxations for these two species, and C = a machine constant. Parameters derived by fitting the peak integrals in Figure 3.3 are displayed in Table 3.II, and a plot of these calculated and experimental values is displayed in Figure 3.4. The mole fractions of Na_A^+ and Na_B^+, are then determined from magnetization coefficients:

$$X_A = M_A/(M_A + M_B) \qquad [3.3a]$$

$$X_B = M_B/(M_A + M_B) \qquad [3.3b]$$

and molal concentrations (mol/kg polymer), c_A and c_B, for Na_A^+ and Na_B^+ can be derived using the mole fraction and the overall salt concentration.

In addition, line widths were measured at appropriate pulse delays, τ, to provide T_2^* for each of the Na^+ species. The parameters c_A, c_B, T_{2A}^*, and T_{2B}^* were evaluated for each complex at each of 11 temperatures.

The line width for Na_A^+ increases markedly near the glass transition temperature (Figure 3.5), demonstrating that the relaxation rate for Na_A^+ is

correlated to polymer dynamics. In contrast, the relaxation rate for species Na_B^+ is continuous through the glass transition temperature. These observations indicate that Na_A^+ is involved in charge transport and that a principal mode of relaxation involves ionic motion. The number of charge carriers should therefore be dependent on c_A, although the exact relation cannot be determined without the transport number of Na_A^+. The preexponential factors (A) derived from the VTF relation, which are directly related to the total number of charge carriers in the complexes, and the values obtained for c_A show similar trends for the complexes studied.

The results obtained strongly argue against the notion that Na_A^+ represents a single ion and Na_B^+ an ion aggregate since (1) the concentration ranges examined are all beyond the range where free ions predominate (4) and (2) χ_A increases, rather than decreases, with salt concentration. A more plausible explanation is that these two species are distinguished by their degree of interaction with the polymer (hence the previous notation mobile and bound). The VTF behavior of these complexes already suggests that the mobility of Na_A^+ is dependent on polymer dynamics; Na_B^+ must be still more strongly bound.

Previous studies have indicated that the relative abundance of Na_A^+ decreases for complexes with softer anions (8). One possibility is the assignment of Na_B^+ to cross-links of the type $R_2O\text{-}Na_B^+ - An^-\text{-}Na_B^+\text{-}OR_2$. There is some evidence for the action of Na_B^+ as a cross-linker: a plot of $1000/T_g$ vs c_B (Figure 3.8) shows the approximately linear relation expected if c_B is associated with the cross-link density for the complex. An unexpected result, however, is the strong

relation of c_B with temperature above T_g for poly($ME_{8.7}$)$_8$NaI, which indicates a more complicated relation between polymer dynamics and salt concentration than indicated by the VTF model alone.

3.5 References

1. (a) Armand, M. B. In *Polymer Electrolyte Reviews - 1*; MacCallum, J. R., Vincent, C. A., Eds.; Elsevier: New York, 1987, and references contained therein. (b) Ratner, M.; Shriver, D. F. *Chem. Rev.* **1988**, *88*, 109.

2. Booth, C.; Nicholas, C. V.; Wilson, D. J. In *Polymer Electrolyte Reviews - 2;* MacCallum, J. R., Vincent, C. A., Eds.; Elsevier: New York, 1989, and references contained therein.

3. Nicholas, C. V.; Wilson, D. J.; Booth, C.; Giles, J. R. M. *Br. Polym. J.* **1988**, *20*, 289.

4. Nekoomanesh, M.; Nagae, S.; Booth, C.; Owen, J. *J. Electrochem. Soc.* **1992**, *139*, 3046.

5. Gray, F. M. *Solid State Ionics* **1990**, *40/41*, 637.

6. Lemmon, J. P.; Lerner, M. M. *Macromolecules* **1992**, *25*, 2907.

7. Doan, K. E.; Heyen, B. J.; Ratner, M. A.; Shriver, D. F. *Chem. Mater.* **1990**, *2*, 539.

8. Wintersgill, M. C.; Fontanella, J. J.; Pak, Y. S.; Greenbaum, S. G.; Al-Mudaris, A.; Chadwick, A. V. *Polymer* **1989**, *30*, 1123.

9. Adamic, K.; Greenbaum, S.; Wintersgill, M.; Fontanella, J. *J. Appl. Phys.* **1986**, *60*, 1342.

10. Wintersgill, M.; Fontanella, J.; Smith, M.; Greenbaum, S.; Adamic, K.; Andeen, C. *Polymer* **1987**, *28*, 633.

11. Greenbaum, S.; Pak, Y.; Wintersgill, M.; Fontanella, J. *Solid State Ionics* **1988**, *31*, 241.

12. Greenbaum, S.; Pak, Y.; Wintersgill, M.; Fontanella, J.; Schultz J. *J. Electrochem. Soc.* **1988**, *135* (1), 235.

13. Greenbaum, S.; Pak, Y.; Adamic, K.; Wintersgill, M.; Fontanella, J. *Mater. Res. Symp. Proc.* **1991**, *210*, 237.

14. Panero, S.; Scrosati, B.; Greenbaum, S. *Electrochim. Acta* **1992**, *37* (9), 1535.

15. Gorecki, W.; Belorizky, E.; Berthier, C.; Donoso, P.; Armand, M. *Electrochim. Acta* **1992** , *37* (9), 1685.

16. Kim, D.; Ryoo, B.; Park, J.; Maeng, K.; Hwang, T. *Polym. J.* **1992**, *24*, 509.

17. Johansson, A.; Wendsjo, A.; Tegenfeldt, J. *Electrochim. Acta* **1992**, *37* (9), 1487.

3.6 Figures

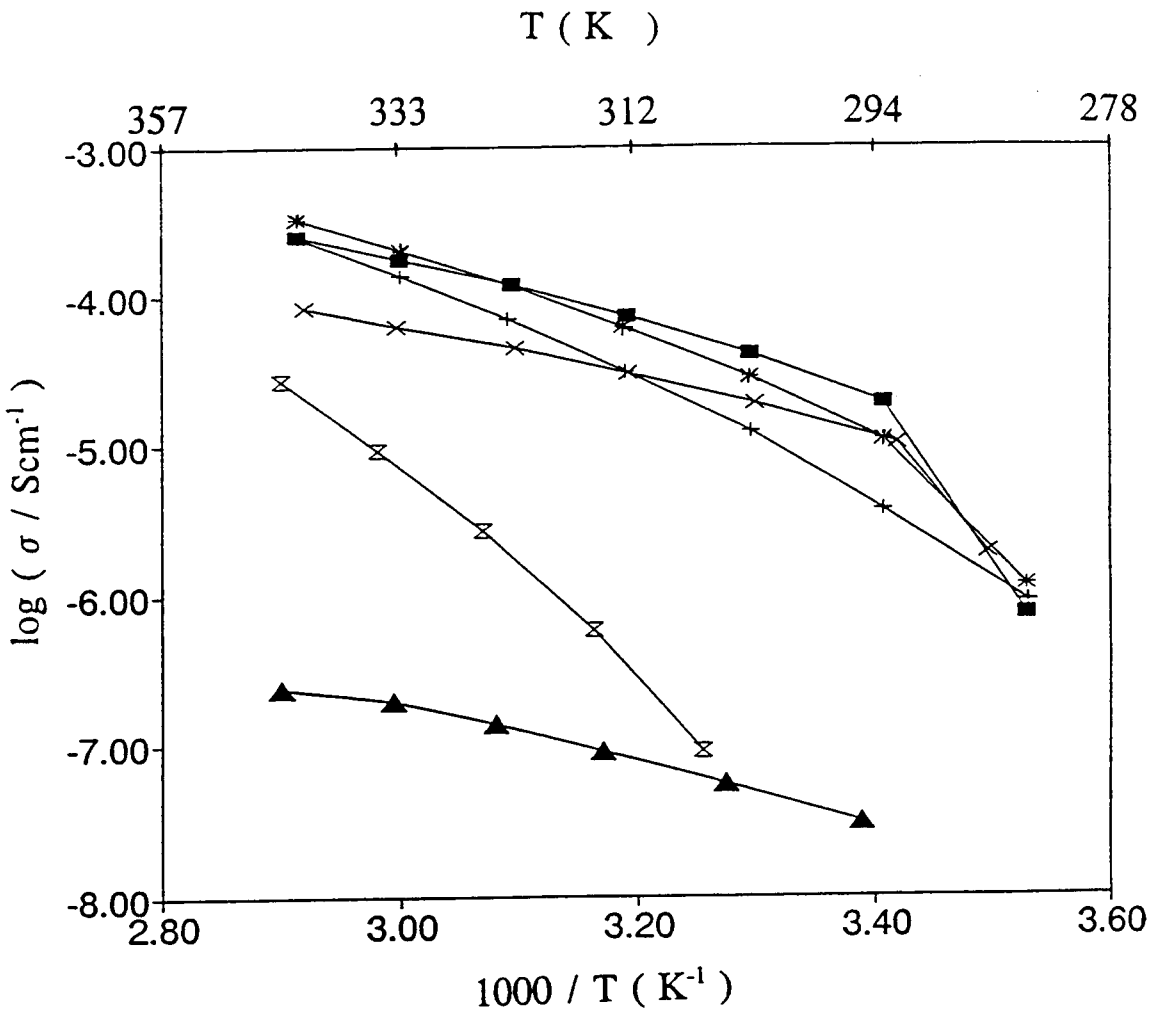

Figure 3.1 Arrhenius plots for poly($ME_{8.7}$)$_x$NaI; (⧖) x = 8; (+) x = 15; (*) x=25; (■) x = 50; (X) x =1 50; (▲) uncomplexed poly($ME_{8.7}$).

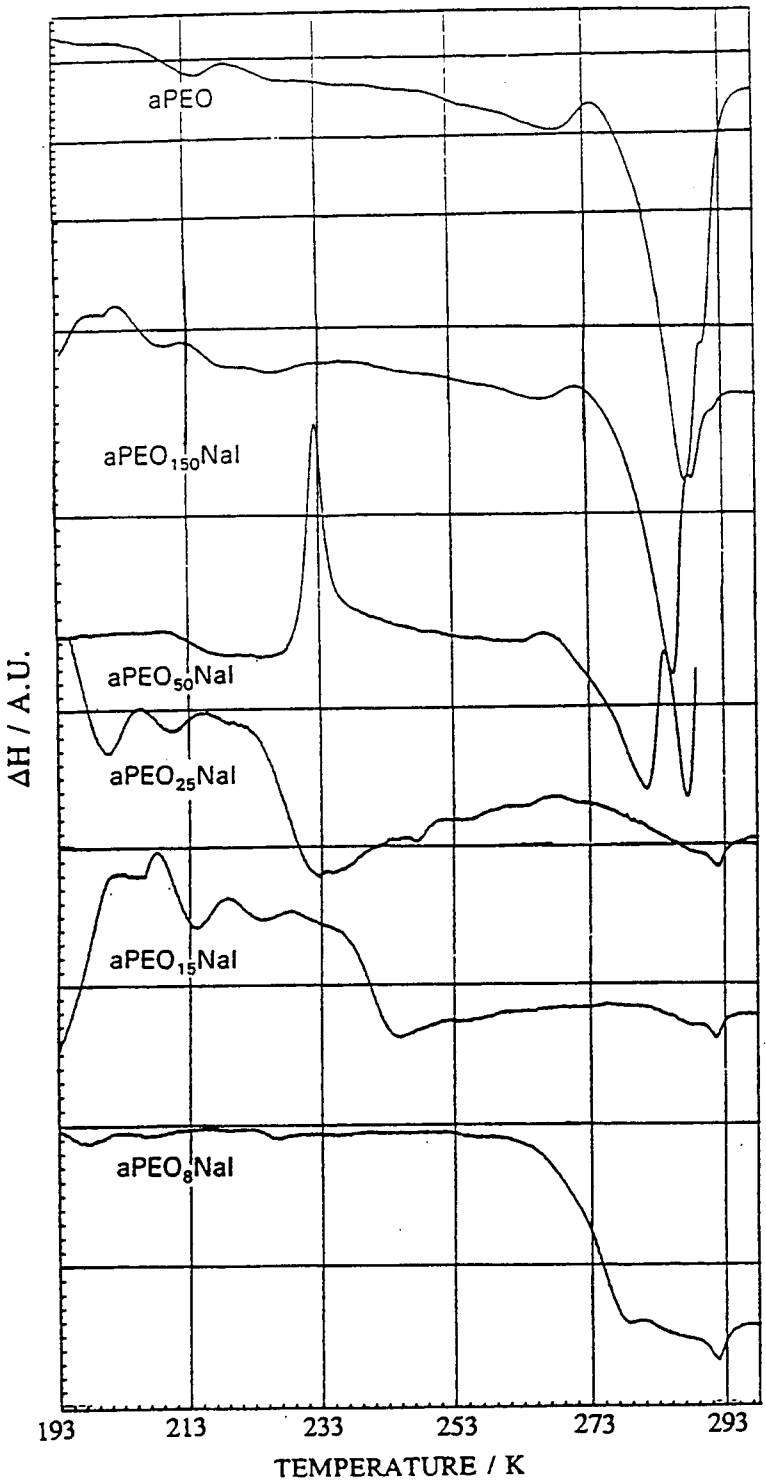

Figure 3.2 Differential scanning calorimetry data obtained on poly($ME_{8.7}$)$_x$NaI. Traces shown were collected at 5 K/min.

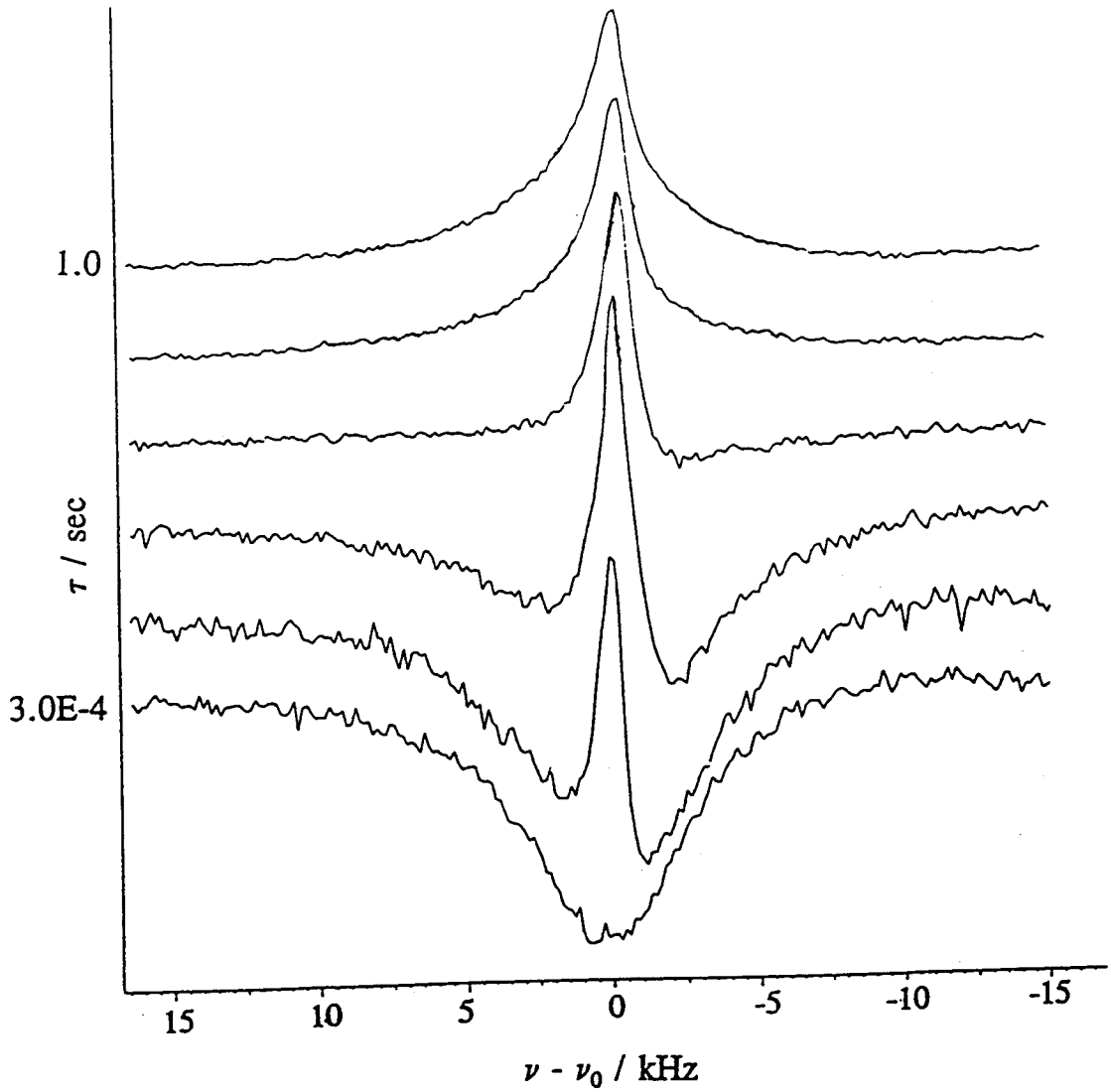

Figure 3.3 ^{23}Na NMR spectra obtained on poly($ME_{8.7}$)$_{25}$NaI at 343 K using an inversion-recovery pulse sequence with τ = 10 μs to 1 s.

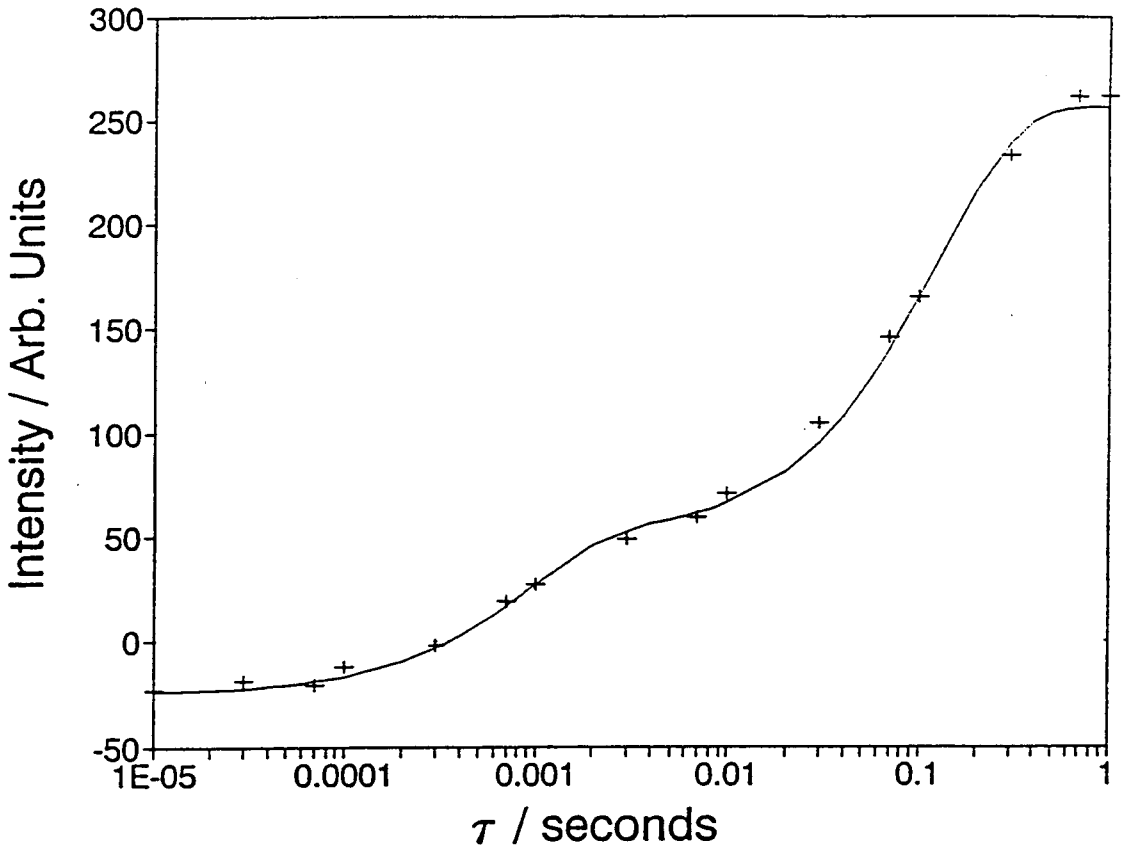

Figure 3.4 ^{23}Na signal peak intensity vs pulse delay, τ, in inversion-recovery experiments for poly($ME_{8.7}$)$_{25}$NaI at 343 K. The solid line corresponds to the best fit using calculated parameters.

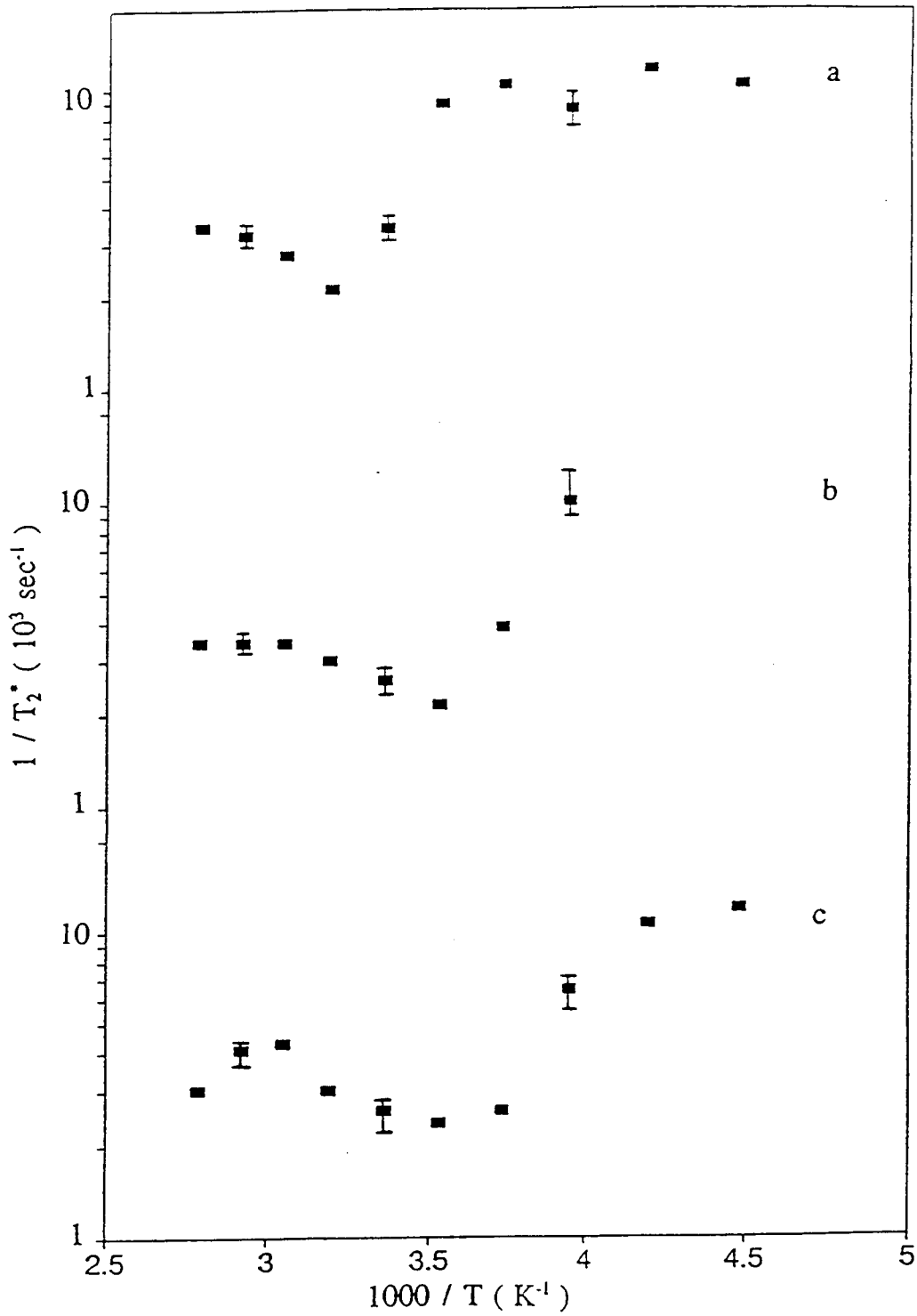

Figure 3.5 $1/T_2^*$ vs 1000/T for the mobile component (Na_A^+) in poly($ME_{8.7}$)$_x$NaI: (a) $x = 8$; (b) $x = 25$; (c) $x = 50$.

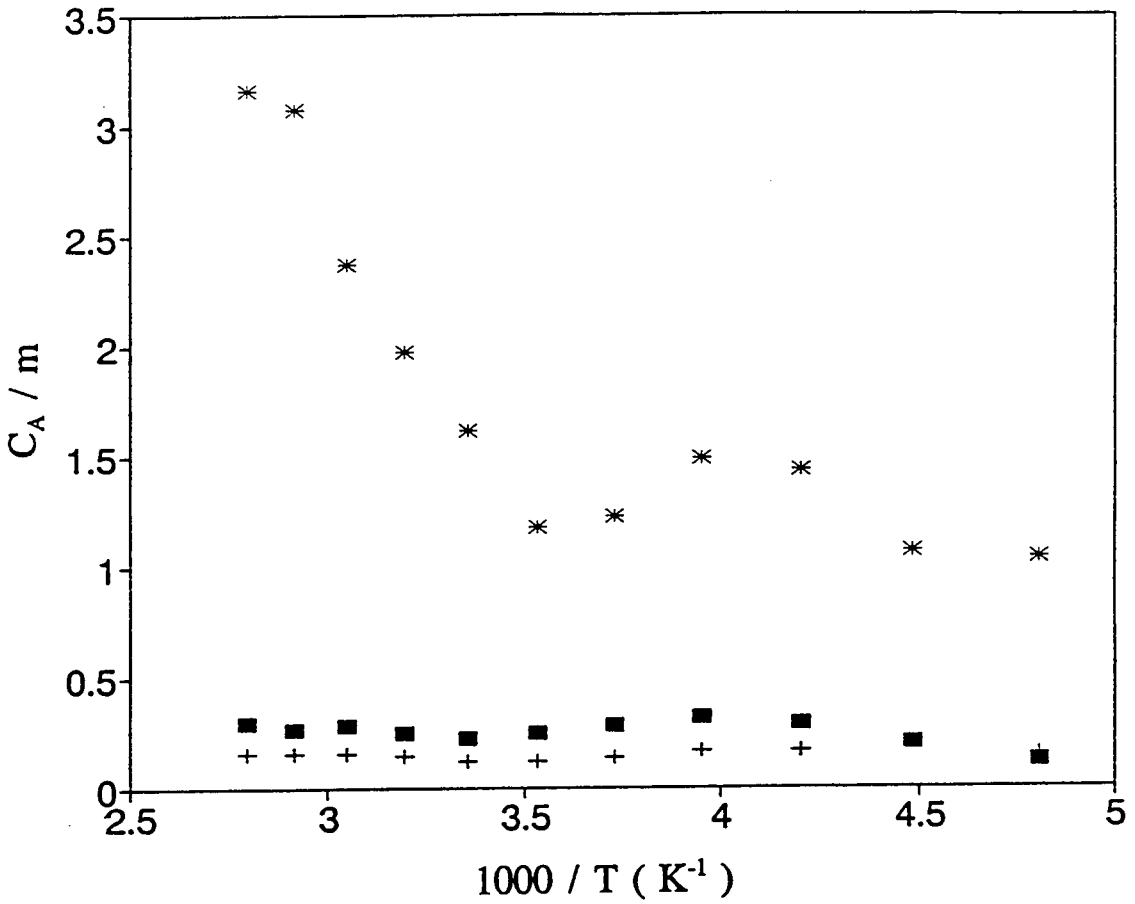

Figure 3.6 Concentration of Na_A^+ in poly($ME_{8.7}$)$_x$NaI vs 1/T: (+) $x = 50$; (■) $x = 25$; (*) $x = 8$.

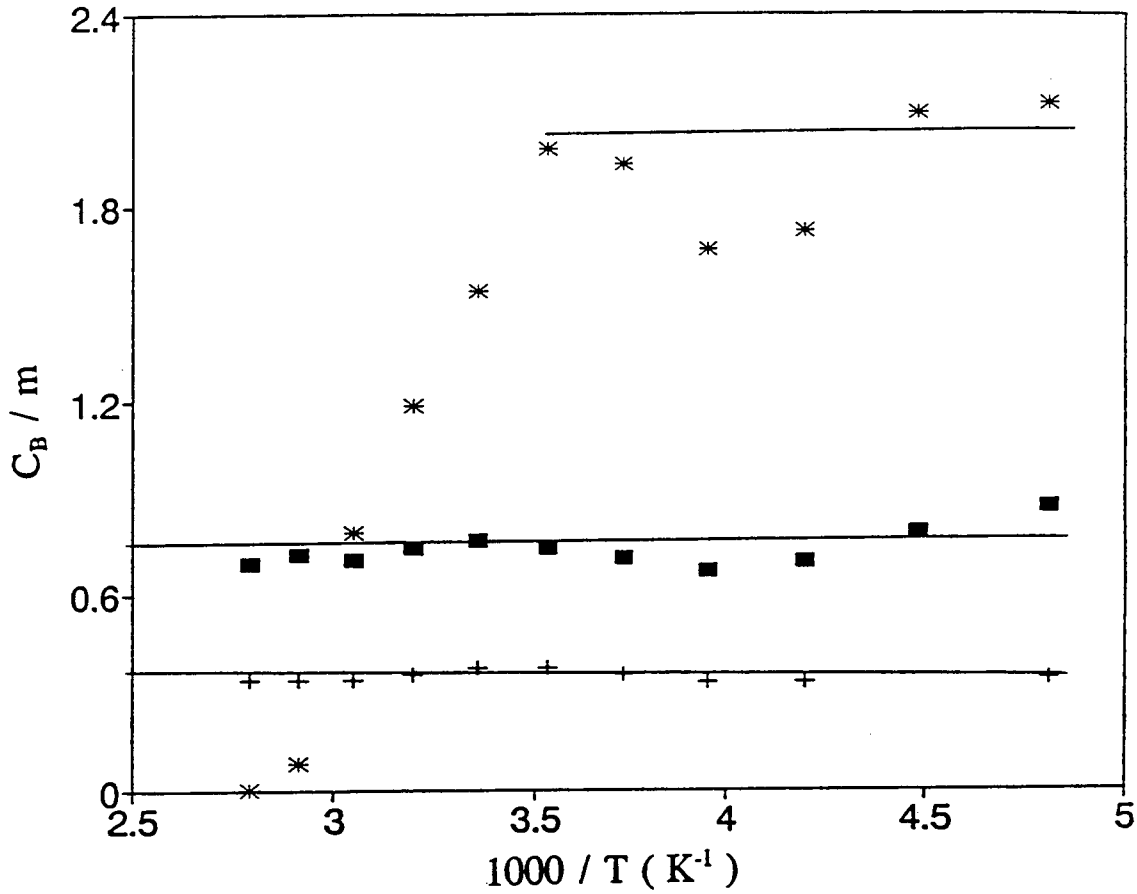

Figure 3.7 Concentration of Na_B^+ in poly($ME_{8.7}$)$_x$NaI vs 1/T: (+) $x = 50$; (■) $x = 25$; (*) $x = 8$. The line drawn through each set indicates the value for c_B in Figure 3.8.

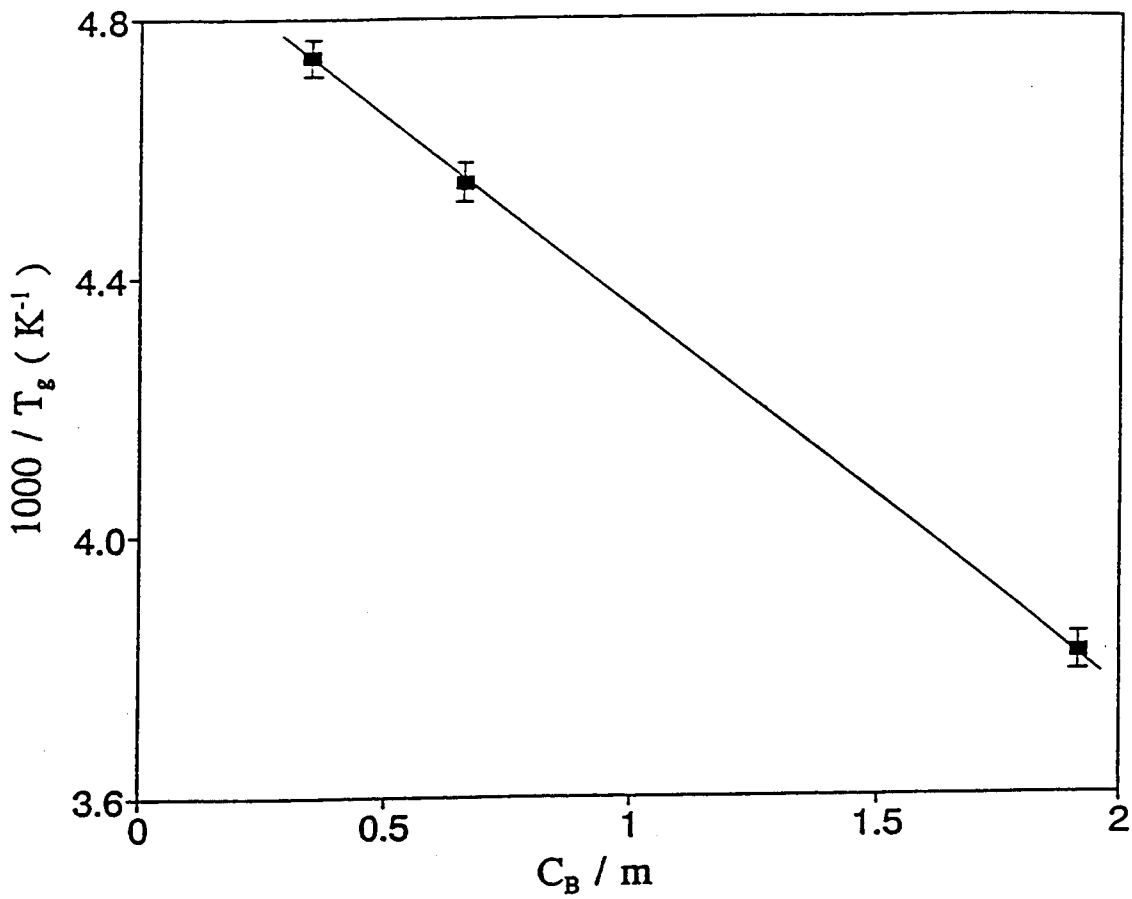

Figure 3.8 1000/T_g vs c_B for poly($ME_{8.7}$)$_x$NaI complexes with x = 50, 25, and 8.

3.7 Tables

Table 3.I DSC Results obtained on poly($ME_{8.7}$)$_x$NaI complexes and calculated VTF parameters using $T_0 = T_g - 27$ K.

Poly($ME_{8.7}$)$_x$NaI

x	T_g(±3K)	T_m(±3K)	B (eV)	A (S $K^{1/2}$ cm^{-1})
aPEO	205	281	---	---
150	212	278	0.063	0.15
50	211	272	0.080	1.6
25	220	---	0.090	6.0
15	234	---	0.090	9.7
8	262	---	0.103	28.0

Poly($ME_{8.7}$)$_x$$NaClO_4$

x	T_g(±3K)	T_m(±3K)
aPEO	205	281
150	208	278
75	214	274
50	211	280
25	220	---
15	228	---
8	258	---

Table 3.II Parameters derived for poly($ME_{8.7}$)$_{25}$NaI by fitting equation 3.2 to the integrated peak intensities from the INVER experiment.

Temp (K)	T_{1A} (s)	T_{1B} (s)	M_a	M_b	C	X_A	X_B
358	0.0012	0.12	31	73	115	0.30	0.70
343	0.00090	0.12	38	103	116	0.27	0.73
328	0.0008	0.14	52	130	108	0.29	0.71
313	0.0010	0.16	52	157	87	0.25	0.75
298	0.0014	0.19	38	131	79	0.22	0.78
283	0.0024	0.19	53	159	62	0.25	0.75
268	0.004	0.21	73	185	51	0.28	0.72
253	0.008	0.24	87	184	54	0.32	0.68
238	0.0098	0.14	74	179	15	0.29	0.71
223	0.010	0.11	52	206	-3	0.20	0.80
208	0.014	0.11	33	237	-5	0.12	0.88

Chapter 4
Synthesis of Planar-sheet Graphite Fluorides Using Fluorometallate Salts of Transition Metals in Anhydrous Hydrogen Fluoride

John P. Lemmon and Michael M. Lerner*

Department of Chemistry and Center for Advanced Materials Research
Oregon State University
Corvallis, OR 97331

Carbon, Vol 31, No. 3, pp. 437-443, 1993

4.1 Abstract

Planar-sheet graphite fluorides, C_xF, are prepared at ambient temperature by the reaction of graphite with the transition fluorometallates K_2MnF_6 and K_2NiF_6 in anhydrous hydrogen fluoride (AHF). In the case of K_2MnF_6, this represents the first chemical route to graphite fluorides without use of elemental fluorine. For each reagent, the net reactions are identified by stoichiometry and X-ray diffraction of the solid products. The graphite fluorides generated at the oxidation limit have stoichiometries close to C_6F and C_2F for the Mn^{4+} and Ni^{4+} fluorometallates, respectively. Na_3FeF_6 will also oxidize graphite to C_xF in AHF, although homogenous products were not obtained due to rapid solvolysis of the fluorometallate. CoF_3 and KF react in AHF to release F_2. C_xF is produced when graphite is reacted with this oxidizing combination. The reactions and oxidation limits are discussed in terms of a thermodynamic model for graphite intercalation. A synthetic strategy for the preparation of planar-sheet graphite fluorides in organic solvents is proposed.

4.2 Introduction

Two classes of graphite fluorides are known, polycarbon fluorides, $(C_xF)_n$ ($1 \leq x \leq 2$), and planar-sheet graphite fluorides, C_xF ($x \geq 1.3$). Both compounds are prepared by the fluorination of graphite and retain the hexagonal carbon sheets of the graphite structure. Polycarbon fluorides are gray or white insulators where covalent C-F bonds (similar to those in PTFE) are formed, carbon is

sp^3-hybridized, and the hexagonal carbon sheets are therefore puckered. Polycarbon fluorides are prepared by the high temperature oxidation of graphite with elemental fluorine (1-3). Planar-sheet graphite fluorides are typically black semiconductors which have a semi-ionic interaction between carbon and fluorine, and the carbon sheets remain planar as in graphite (3-5). Syntheses for the planar-sheet graphite fluorides are described below. The polycarbon fluorides are currently employed as positive electrodes in lithium cells and as industrial lubricants, and similar uses have been explored for the planar-sheet graphite fluorides (3,6-8).

All the chemical preparations for the planar-sheet graphite fluorides to date have employed elemental fluorine as an oxidant. The chemical reactions are generally carried out at ambient temperature and utilize a carrier to introduce fluoroanions into the carbon galleries. Upon exposure to excess fluorine, the graphite fluoroanion salts are further oxidized and converted to planar-sheet graphite fluorides. The details of the intercalation reaction and products, utilizing HF as a carrier (and HF_2^- as the corresponding fluoroanion), have been described by Mallouk and Bartlett (4). In these reactions, graphite bifluoride salts are formed initially:

$$C_y + \tfrac{1}{2}F_2 \xrightarrow[298\ K]{AHF} C_y\ HF_2 \cdot nHF \qquad [4.1a]$$

(AHF = anhydrous hydrogen fluoride)

and the first-stage bifluoride salt ($C_y HF_2 \cdot n$HF, $y \approx 12$) is oxidized to planar-sheet graphite fluorides of composition, $C_x F \cdot m$HF ($2 < x < 6$), when further reacted with fluorine:

$$C_y\ HF_2 \cdot nHF \xrightarrow[298\ K]{F_2,\ HF} y/xC_xF \cdot mHF \qquad [4.1b]$$

Electrochemical methods can also be employed to oxidize graphite in anhydrous HF/KF and generate planar-sheet graphite fluorides; electrochemical studies confirm the mechanism described in reaction [4.1a] and [4.1b] (9). The oxidation of graphite fluorometallate salts such as $C_y AsF_6$ with fluorine in anhydrous HF (AHF) results in even more highly oxidized products (C_xF, $x \geq 1.3$) (10). Other groups have also reported on similar methods to generate the graphite fluorides using a bifluoride or fluoroanion carrier (11-13).

Previous examinations of the interaction of transition fluorometallate anions with graphite have yielded conflicting results. Nikolaev and co-workers (14) reported that K_2NiF_6 in AHF reacts with graphite to produce a graphite fluoronickellate product of approximate composition $C_{19}NiF_3 \cdot 5HF$. A more recent study (15) concluded that neither K_2MnF_6 nor K_2NiF_6 in AHF reacts with graphite. A preliminary study by one of the authors (16,17) found that graphite does undergo a redox reaction with K_2MnF_6 to generate graphite fluorides and MnF_3.

A simple thermodynamic model for graphite intercalation, detailed in the Discussion section, suggests that MnF_6^{2-}, in the presence of bifluoride, might provide sufficient oxidizing power to generate graphite bifluoride salts and, upon further reaction, graphite fluorides. The NiF_6^{2-} anion, which is a more powerful oxidant, is even more likely to react. If this synthetic route is feasible, at least two major advantages can be envisioned: (1) the direct use of F_2 is avoided; and (2) the degree of graphite oxidation may be stoichiometrically controlled. The

aim of this project was to clearly identify the products and net reaction, if any, of graphite with these oxidizing fluorometallates complexes.

4.3 Experimental

Graphite (Union Carbide, SP1 grade, avg. part. dia. = 100 μm) was dried by evacuation at 400°C. Anhydrous HF (AHF) (Matheson) was dried in a Kel-F trap over SbF_5, subjected to two freeze/pump/thaw cycles to remove H_2, and then removed at 0°C. K_2MnF_6 was synthesized from $KMnO_4$ (Mallinckrodt, reagent) in 49% hydrofluoric acid (Fischer Scientific) by literature methods (18). KF (Aldrich, 99%) was dried by heating under a dynamic vacuum. K_2NiF_6, Na_3FeF_6, and CoF_3 (Ozark Mahoning) were used as purchased. All solids were handled in the dry argon atmosphere of a glovebox.

A typical experiment consisted of loading approximately 100 mg of graphite and the desired mass of fluorometallate salt into individual 3/8" FEP Teflon tubes which had each been heat-sealed at one end. These were connected via 316 stainless-steel Swagelok fittings to a 1KS4 Whitey valve (see Fig. 4.1). A coarse PTFE membrane was placed within the union tee connection to allow filtration of the products. The assembled reactor was connected to a metal vacuum line and the fluorometallate salt dissolved by condensing AHF into the reactor tube. The desired quantity of fluorometallate solution was then poured onto the graphite in ≈0.25-mL aliquots. The reaction limit was readily observed when the added solution no longer reacted with the graphite and

retained the color of the fluorometallate salt for several hours. The amount of fluorometallate salt utilized could then be estimated to within 10%. In reactions where a predetermined stoichiometry was employed, the graphite and fluorometallate were initially loaded into the same tube.

The product was filtered through the PTFE membrane by carefully pouring the solution through the filter and then condensing AHF back into the original tube. This procedure was repeated a minimum of five times to separate any soluble bifluoride salts or unreacted fluorometallates from insoluble graphite compounds and metal fluorides. The reactor was finally evacuated for several hours and the products loaded into 0.5-mm quartz capillaries (Charles Supper Co.). The capillaries were plugged with halocarbon grease and sealed with a microtorch. Powder X-ray diffraction data were collected using CuK_{α} radiation and the Debye-Scherrer geometry or with $CuK_{\alpha 1}$ radiation and an Enraf-Nonius Guinier camera, with SP1 graphite employed as an external standard. A Siemens D5000 powder diffractometer was used to evaluate some air-stable products.

Atomic absorption analyses were collected on a Buck Scientific 200 analyzer. Samples were dissolved in 0.1 M HCl and compared with a calibrated standard over the range of 2.5 to 10 mg Fe/L. Densities were determined by flotation in an acetone/$CHBr_3$ solution for some samples.

4.4 Results

Experimental results and diffraction data are summarized in Table 4.I. A discussion specific to each reagent or set of reagents is given below.

4.4.1 Graphite + K_2MnF_6

K_2MnF_6 forms a stable, yellow-orange solution in AHF. When poured onto graphite so that the ratio C/Mn = 28, the solution becomes colorless within a few minutes and a purple solid, very sparingly soluble in AHF, appears. In experiment 1, the principal products observed by diffraction are a second-stage graphite bifluoride salt, MnF_3, and KHF_2. No X-ray diffraction lines from unreacted graphite are observed, a very weak pattern for K_2MnF_6 is present. As described above, the graphite bifluoride salts are also intermediates in the preparation of graphite fluorides with HF/F_2 or by electrochemical methods, and earlier studies have established that a vacuum stable, second-stage graphite bifluoride is consistent with $C_xHF_2 \cdot n$HF, $18 < x < 36$. The reaction observed is therefore formulated as the reduction of Mn^{4+} to Mn^{3+} and the corresponding one-electron oxidation of graphite:

$$28/x C_x + K_2MnF_6\ (sol) \xrightarrow[298\ K]{AHF} C_{28}HF_2 \cdot nHF + MnF_3\ (ppt) + 2KHF_2\ (sol) \qquad [4.2]$$

As more K_2MnF_6 is added, and C/Mn approaches 5 to 6, the yellow color due to MnF_6^{2-} disappears more slowly. When the mole ratio C/Mn < 5 to 6 (see experiments 2 and 3), the added solution retains its yellow color overnight and

the soluble products observed by diffraction include unreacted K_2MnF_6. The insoluble product now contains MnF_3 along with a three-line pattern of reflections, corresponding to (*001*), (*100*), and (*110*), characteristic of a planar-sheet graphite fluoride (first stage, $c \approx 6.0$ Å) (4). The net reaction at the oxidation limit is therefore formulated as:

$$6/x C_x + K_2MnF_6\ (sol) \xrightarrow[298\ K]{AHF} C_6F \cdot mHF + MnF_3\ (ppt) + 2\ KHF_2\ (sol) \qquad [4.3]$$

It should be noted, however, that a small amount of unreacted K_2MnF_6 remains at the observed endpoint, so that the true stoichiometry of the graphite product, C_xF, has x somewhat greater than 6. As the graphite fluoride is not readily isolated from the MnF_3 byproduct by washing in AHF, the stability of the graphitic products obtained was examined in 49% aqueous HF (which could effectively remove MnF_3). The $C_{28}\ HF_2 \cdot n$HF graphite bifluoride salt is unstable in aqueous HF, reverting rapidly to graphite. The product at the oxidation limit, $C_6F \cdot m$HF proved somewhat more stable, but partial decomposition is observed following filtration in aqueous HF. These results are consistent with the known chemistry of graphite fluorides and bifluorides (3).

The reaction of graphite with K_2MnF_6 was also attempted in aqueous HF. K_2MnF_6 forms a stable, bright yellow solution in aqueous HF, which rapidly turns colorless when graphite is added. As described above, however, graphite bifluoride is unstable in the solution and rapidly decomposes to graphite, presumably by water oxidation. Graphite may therefore be seen to have a catalytic role in the hydrolytic decomposition of MnF_6^{2-} (Figure 4.2). This activity

does not appear to be limited to the graphite surface. Diffraction profiles of the graphitic product obtained reveal a highly disordered stacking of carbon sheets, indicative of a bulk intercalation/deintercalation process (Fig 4.3).

4.4.2 Graphite + K_2NiF_6

The deep red/violet solution of K_2NiF_6 in AHF is relatively stable at ambient temperature in the reactors employed. A slow decomposition of NiF_6^{2-} to NiF_2 (approx. 100 mg/week), presumably arising from the diffusion of moisture through the Teflon tubing, is observed. This side reaction does not pose a significant obstacle in evaluating the graphite reactions of interest, which occur far more rapidly.

When the deep red/violet fluoronickellate solution is poured onto graphite with a C/Ni ratio of 56 (experiment 4), the solution loses its color within minutes. The diffraction pattern obtained from the insoluble products includes diffraction lines due to unreacted graphite, a planar-sheet graphite fluoride (c = 5.7 Å), and a broad-line pattern corresponding to disordered NiF_2. Diffraction of the soluble products show KHF_2 only, and no unreacted K_2NiF_6 is present. Therefore, the oxidation of graphite by K_2NiF_6 does occur, but a homogenous product is not obtained under these conditions. No diffraction lines corresponding to the graphite fluoronickellate product described by Nikolaev and co-workers (14) are observed. The possible role of this salt as an intermediate in the formation of the graphite fluoride cannot be ruled out, although the graphite bifluoride salt

intermediates described previously are more consistent with previous observations (see Section 4.4.1). Simple methods of obtaining a more homogenous product, such as using a smaller particle graphite or a more dilute solution of NiF_6^{2-}, are likely to succeed but were not attempted in this study.

The oxidation limit is observed at approximately C/Ni = 4 (experiment 5), where the insoluble product shows the characteristic three-line diffraction pattern of a planar-sheet graphite fluoride (c = 5.9 Å), and also contains lines corresponding to NiF_2. The soluble product from this experiment contains only KHF_2. The addition of a greater stoichiometry of NiF_6^{2-} (experiment 6) for approx. 48 h results in a similar graphite fluoride product, and the slow decomposition of unreacted K_2NiF_6 is parallel to the control reaction without graphite. The graphite oxidation is therefore compensated by the two-electron reduction of Ni^{4+}:

$$4/xC_x + K_2NiF_6\ (sol) \xrightarrow[298\ K]{AHF} 2C_2F \cdot mHF + NiF_2\ (ppt) + 2KHF_2\ (sol) \qquad [4.4]$$

As in the fluoromanganate reactions, the byproduct generated, NiF_2, is insoluble in AHF, and therefore difficult to separate from the graphite fluoride. The graphite fluorides produced at the oxidation limit (experiments 5 and 6), show little or no signs of decomposition after washing in aqueous HF and are subsequently stable in air. This agrees with the general observation that the water and air stability of the planar-sheet graphite fluorides increases as x approaches 2. The density of the graphite fluoride following treatment with aqueous HF was determined to be 2.20 g/cm^3 (C_2F, c = 6.0 Å: ρ_{calc} = 2.27).

4.4.3 Graphite + Fe^{3+}

When AHF is condensed onto the white, solid Na_3FeF_6, without graphite being present, a colorless and highly viscous solution is immediately produced, and a fluffy white precipitate then appears over the course of one to several minutes. The diffraction data show only $NaHF_2$ in the soluble products, and several unindexable lines in the insoluble fraction. The reaction may be formulated as the solvolysis of FeF_6^{3-} in HF:

$$FeF_6^{3-} + (3 - \delta)HF \rightarrow FeF_{3+\delta}^{\delta-} (ppt) + (3 - \delta)HF_2^- \qquad [4.5]$$

The generation of an oligomeric anion is consistent with the notable increase in viscosity of the solvent. The value of δ is uncertain but is supposed to be close to 3. Similar results have been observed with FeF_6^{3-} salts of XeF^+ as well as other trivalent hexafluoroanions (19), and it is reasonable that these highly charged hexafluorometallates will show diminished fluoracidity. In the present case, solvolysis occurs by reaction with the stronger fluoracid HF. Atomic absorption analyses of the soluble and insoluble products of reaction [4.5] indicate that 99.5 to 99.9 mol% of the Fe remains in insoluble form.

The solvolysis of FeF_6^{3-} in AHF limits the effectiveness of this reagent in graphite oxidation. Reproducible products are difficult to obtain for these reactions, which proceed only during the initial period when the viscous, Fe^{3+}-containing solution is present. The graphite reactions were therefore performed in a single Teflon tube, using a predetermined ratio of C/Fe. All products contain unreacted graphite, but experiments with initial Fe^{3+}-rich conditions (experiments

8 and 9) may also exhibit the characteristic (*001*) line, near d = 5.6 Å, of a graphite fluoride product. A number of unindexed lines, presumably due to the oligomeric fluoroferric salts, $Na_5FeF_{3+\delta}$, and perhaps mixed Fe^{3+}/Fe^{2+} complexes, are also observed.

The inhomogeneity of these reactions appears to result from the short period of solvation of Fe^{3+}. A method of generating more homogenous products in AHF and, therefore, of establishing the thermodynamic oxidation limit, is not obvious. These desired results might, however, be obtained in a less acidic solvent (see Discussion section).

4.4.4 Graphite + Co^{3+}

Literature methods have been described for the synthesis of K_3CoF_6, for example, by the action of F_2 on $K_3Co(CN)_6$ (20). However, the solvolysis of CoF_6^{3-} by HF has previously been noted (21), so the direct use of CoF_3 is explored in these studies. CoF_3 is stable in AHF, but its solubility is not appreciable. No direct reaction of graphite with CoF_3 in AHF is observed (experiment 10). This may be a consequence of the limiting solubility of CoF_3; an alternate explanation is the lack of a suitable fluoroanion carrier such as HF_2^-. To overcome the latter problem, the addition of KF along with CoF_3 was examined.

As a control, the interaction of CoF_3 with KF/AHF was first examined without graphite. When HF is condensed onto a mixture of CoF_3 and KF, a colorless gas is evolved and diffraction of the products shows $KCoF_3$ along with

other unindexable phases. The evolved gas rapidly tarnishes a clean Hg surface, which suggests the reduction of CoF_3 according to:

$$CoF_3 + KHF_2(sol) \xrightarrow{AHF} KCoF_3 + HF + \tfrac{1}{2}F_2(g) \qquad [4.6]$$

This decomposition is also consistent with earlier observations on the solvolysis of Co^{3+} by HF (21). In repeating these experiments, it appears that the nature and extent of this reaction is dependent on the mass of solid reactants (KF and CoF_3) employed. This might arise from a temperature effect due to the heat of solvation for KF; additionally, the basicity of the solution may be important.

When AHF is condensed onto a mixture of graphite, CoF_3, and KF, the products obtained included $KCoF_3$ and other unindexable phases. No graphite or graphite compounds are observed directly by diffraction of the insoluble products. After washing away the cobalt fluorides in aqueous HF; however, a planar-sheet graphite fluoride (c = 6.0 Å, ρ_{exp} = 2.18 g/cm^3) is observed. The stoichiometric endpoint of the reaction with Co^{3+} cannot be determined by the above method, and the indirect production of graphite fluorides by reaction with F_2 is a possibility in this case.

4.5 Discussion

Bartlett and McQuillan (22) have previously described a simple thermodynamic model for graphite intercalation which relates the degree of intercalation to four enthalpic terms: the energy required to overcome van der Waals' interactions between graphite sheets, the work function or ionization energy of

graphite (which is a function of the partial charge per carbon atom), the electron affinity of the reagents employed (i.e., the oxidizing power of the reagent or reagent combination), and the lattice enthalpy of the intercalation compound (Fig. 4.4).

As the first two terms are properties of graphite alone, the relative degree of intercalation observed for different reagents with graphite should be determined by only two energy terms: the oxidizing power of the reagent(s) and the lattice enthalpy of the intercalation compound. This model can be refined to include other energy terms such as entropic contributions and solvation effects, yet it has been demonstrated that even this simple model can successfully explain a large number of observations on reactivities and products. An important advantage of a simple thermodynamic model is that it allows the consideration of reasonable new routes to intercalation compounds. As an example, the preparation of main-group graphite fluorometallates via the oxidizing combination of Cl_2 with metal fluorides has recently been described (23) and was originally derived from these simple thermodynamic considerations.

The thermodynamic threshold for the preparation of the graphite hexa- and tetrafluorometallates has been well established. Intercalation products are only obtained when the electron affinity of the reagents exceeds 105 kcal/mol, and a vacuum-stable first-stage compound arises for systems with EA > 125 kcal/mol. Planar-sheet graphite fluorides and graphite bifluorides salts have smaller gallery heights than graphite fluorometallates (≈6 Å as compared with ≈8 Å) and, therefore, have greater lattice energies. Whether the solids are consid-

ered ionic or covalently bound is of lesser consequence; the cohesive energy, which may be modeled by ionic or covalent forces, will be more favorable when the salts contain smaller anions. Thus, the oxidative half-reaction for the production of graphite bifluorides and, ultimately, planar-sheet graphite fluorides in the graphite/F_2/HF reaction:

$$e^- + HF + \tfrac{1}{2}F_2 \rightarrow HF_2^- \qquad [4.7]$$

with H≈90 kcal/mol falling well below the thermodynamic limit for intercalation of larger fluorometallates, yet providing a route to first-stage compounds due to the greater lattice energy contribution.

The tabulated thermodynamic data are presently insufficient to estimate with confidence the ethalpy for the reduction half-reactions which were identified in each reagent system examined. For instance, in the fluoromanganate system, $\Delta H_{rxn,298}$ (e^- + 2HF + MnF_6^{2-}(sol) → MnF_3(ppt) + 2HF_2^-(sol) + F^-), is required, but cannot be estimated with any reasonable degree of certainty. However, the oxidizing power for the fluorometallates in AHF may be ranked as NiF_6^{2-} > MnF_6^{2-} > FeF_6^{3-} based on (1) the known chemistry of these species, e.g., NiF_6^{2-} in AHF will oxidize Xe to XeF_2, FeF_6^{3-} will not (24); and (2) a comparison of the tabulated reduction potentials of the related oxometallates in aqueous acid (Table 4.II).

The experimental data obtained show that the oxidation limit for the NiF_6^{2-} reagent is approximately C_2F, while that of MnF_6^{2-} is only C_6F, which therefore agrees with the above model. The oxidation limit for FeF_6^{3-} could not be established, although planar-sheet graphite fluorides were obtained. As $FeCl_3$ is known to react with graphite to form a chloroferrate salt (21), which is certainly a

less stable lattice than for the graphite fluorides ($c \approx 9$ Å for $C_xFeCl_4 \cdot nFeCl_3$), the observation of a graphite fluoride product for the Fe^{3+} reagent system studied is reasonable. It is to be expected, however, that the oxidation limit for this reagent should be $x > 6$. Finally, if a suitable solvent can be found, the Co^{3+} fluoroanion should be a powerful oxidant and may result in an even more fluorine-rich material than those obtained.

The results described in the experimental section (see Figure 4.2) indicate that the preparation of planar-sheet graphite fluorides is unlikely in aqueous HF, due to the rapid decomposition of both the graphite bifluoride intermediate and C_xF for $x \gg 2$. The potential of utilizing transition fluorometallates with bifluoride to form graphite fluorides is presently being explored in more suitable solvents, such as the oxidatively robust organics nitromethane and acetonitrile. Synthesis in organic solvents are experimentally less demanding than those in AHF, and could thus provide an even more accessible route to the graphite fluorides. An added advantage in using organic solvents may be in avoiding the problems of solvolysis described above.

The principal difficulty in using the organic solvents lies in the limited solubility of ionic salts in even polar organic media. The fluorometallate anions themselves may be paired with large cations to produce reasonably soluble salts. Suitable large cations are already known: for example, tetramethylammonium salts of strong oxidizers such as ClF_4^- and BrF_4^- have been shown to be stable and soluble in dry CH_3CN (26). It has been seen, however, that the formation of planar-sheet graphite fluorides requires a carrier such as bifluoride

to introduce fluoride into the galleries. We are presently examining whether sufficiently soluble forms of HF_2^- can be found for these oxidizing conditions. Alternatively, larger anions might also be examined as carriers in these systems.

4.6 References

1. Kita, Y.; Kadono, K.; Fujii, Y.; Watanabe, N. *Z. Anorg. Allg. Chem.* **1987**, *544*, 7 and references contained therein.

2. Kita, Y.; Watanabe, N.; Fujii, Y. *J. Am. Chem. Soc.* **1979**, *101*, 3832.

3. Watanabe, N.; Touhara, H.; Nakajima T.; Bartlett, N.; Mallouk, T.; Selig, H In *Inorganic Solid Fluorides*, Hagenmuller, P. Ed.; Academic Press: New York, 1985, (pp 331-369) and references contained therein.

4. Mallouk, T.; Bartlett, N.; *J. Chem. Soc., Chem. Comm.* **1983**, *103.*

5. Mallouk, T.; Hawkins, B.; Conrad, M.; Zilm, K.; Maciel, G.; Bartlett, N. *Phil. Trans. R. Soc. Lond.* **1985**, *A314*, 179.

6. Hagiwara, R.; Lerner, M.; Barteltt, N. *J. Electrochem. Soc.* **1988**, *35*, 2393.

7. Yazami, R.; Hamwi, A. *Solid State Ionics* **1990**, *40/41*, 982.

8. Hamwi, A.; Daoud, M.; Cousseins, J. *Synth. Met.* **1989**, *30*, 23.

9. Takenaka, H.; Kawaguchi, M.; Lerner, M.; Bartlett, N. *J. Chem. Soc., Chem. Comm.* **1987**, 1431.

10. Hagiwara, R.; Lerner, M.; Bartlett, N. *J. Chem. Soc., Chem. Comm.* **1989**, 573.

11. Nakajima, T.; Ino, T.; Watanabe, N.; Takenaka, H. *Carbon* **1988**, *26*, 397.

12. Nakajima, T.; Molinier, M.; Motoyama, M. *Carbon*, **1991**, *29*, 429.

13. Hamwi, A.; Daoud, M.; Cousseins, J. *Synth. Met.* **1988**, *28/30*, 1756.

14. Nikolaev, A.; Nazarov, A.; Yudanov, N.; Ikorsky, V. *Izv. Sib. Otd. Akad. Nauk SSSR* **1972**, *7*, 1366.

15. Flandrois, S.; Hun, B.; Grannec, J.; Tressaud, A.; Hauw, C. *Synth. Met.* **1988**, *23*, 435.

16. Lerner, M. Ph.D. Thesis, University of California at Berkeley **1988**.

17. Lemmon, J.; Lerner, M. *Proc. Oregon Acad. Sci.* **1991**, Salem, OR.

18. Bode, H.; Jenssen, H.; Bandte, F. *Angew. Chem.* **1953**, *65*, 304.

19. Zemva, B. private communication, University of California at Berkeley **1992**.

20. Hoppe, R. *Rec. Trav. Chim.* **1956**, *75*, 569.

21. Court, T.; Dove, M. *J. Chem. Soc., Chem. Comm.* **1971**, 726.

22. Bartlett, N.; McQuillan, B. In *Intercalation Chemistry*, Whittingham, S., Jacobsen, A. Eds.; Academic Press: New York, 1982, (pp 19-53) and references contained therein.

23. Lerner, M.; Hagiwara, R.; Bartlett, N. *J. Fluor. Chem.* (in press).

24. Bartlett, N. private communication, University of California at Berkeley **1992**.

25. *Standard Potentials in Aqueous Solution*, Bard, A., Parsons, R., Jordan, J. Eds.; Marcel Dekker: New York, **1985**.

26. Wilson, W.; Christe, K. *Inorg. Chem.* **1989**, *28*, 4172.

4.7 Figures

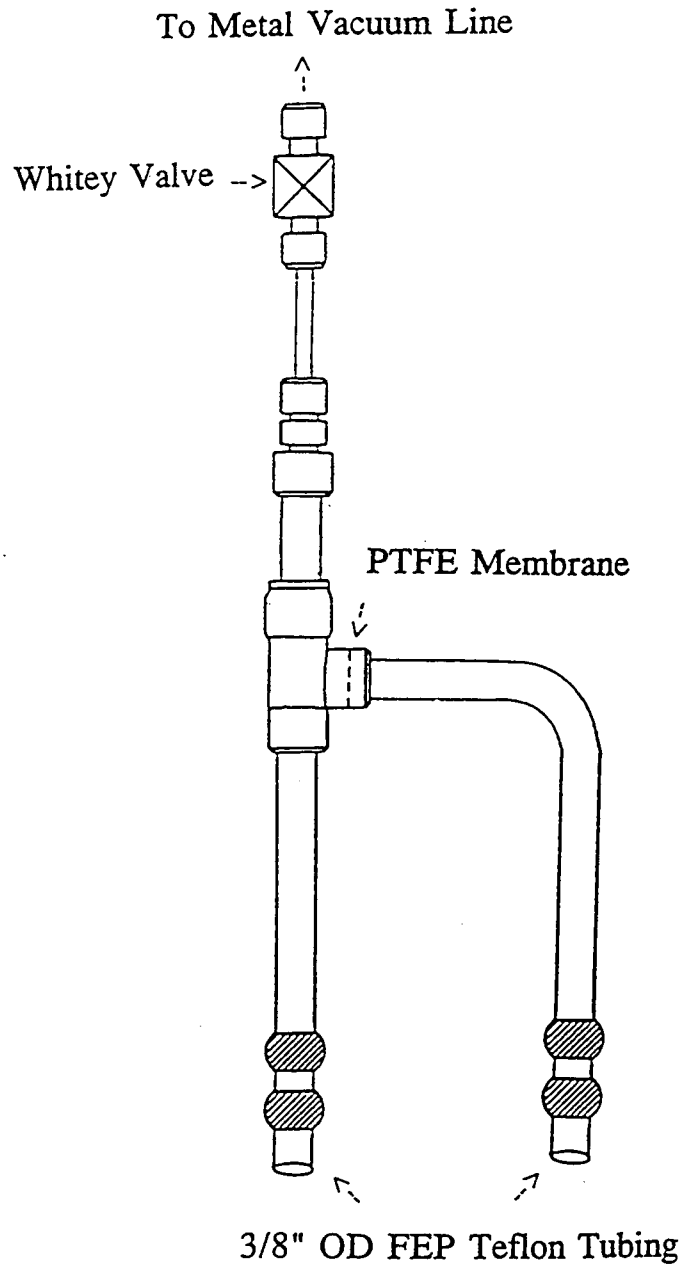

Figure 4.1 General design for reactors employed.

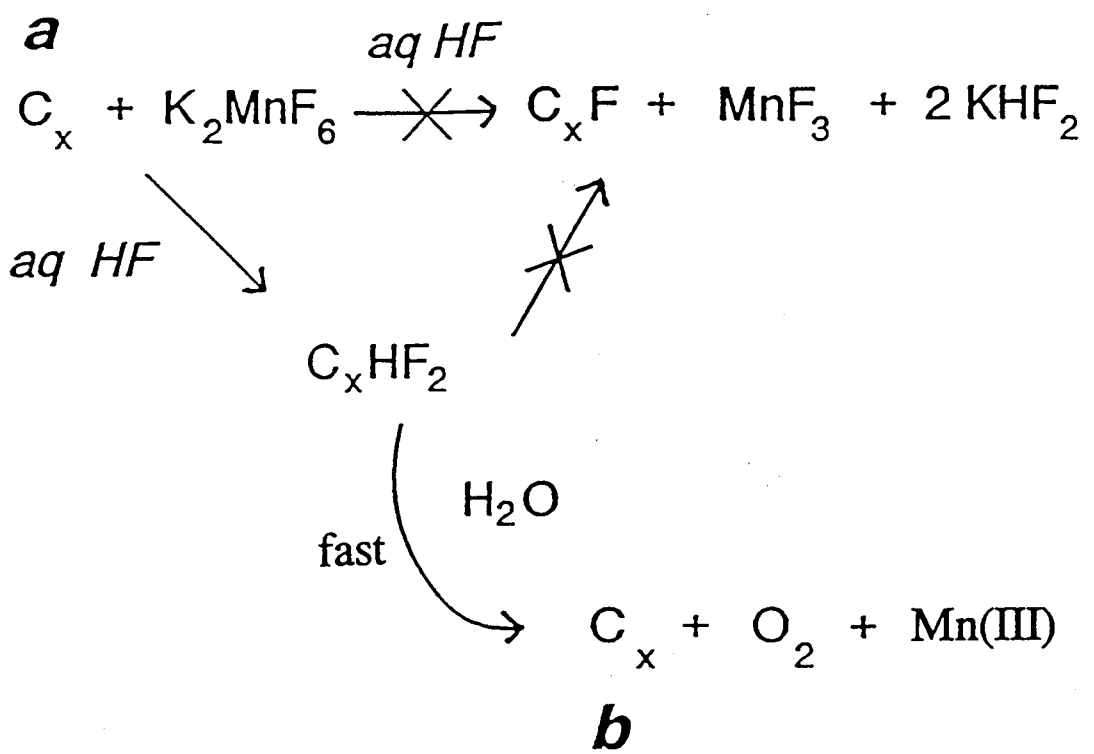

Figure 4.2 Reaction scheme for catalytic decomposition of MnF_6^{2-}.

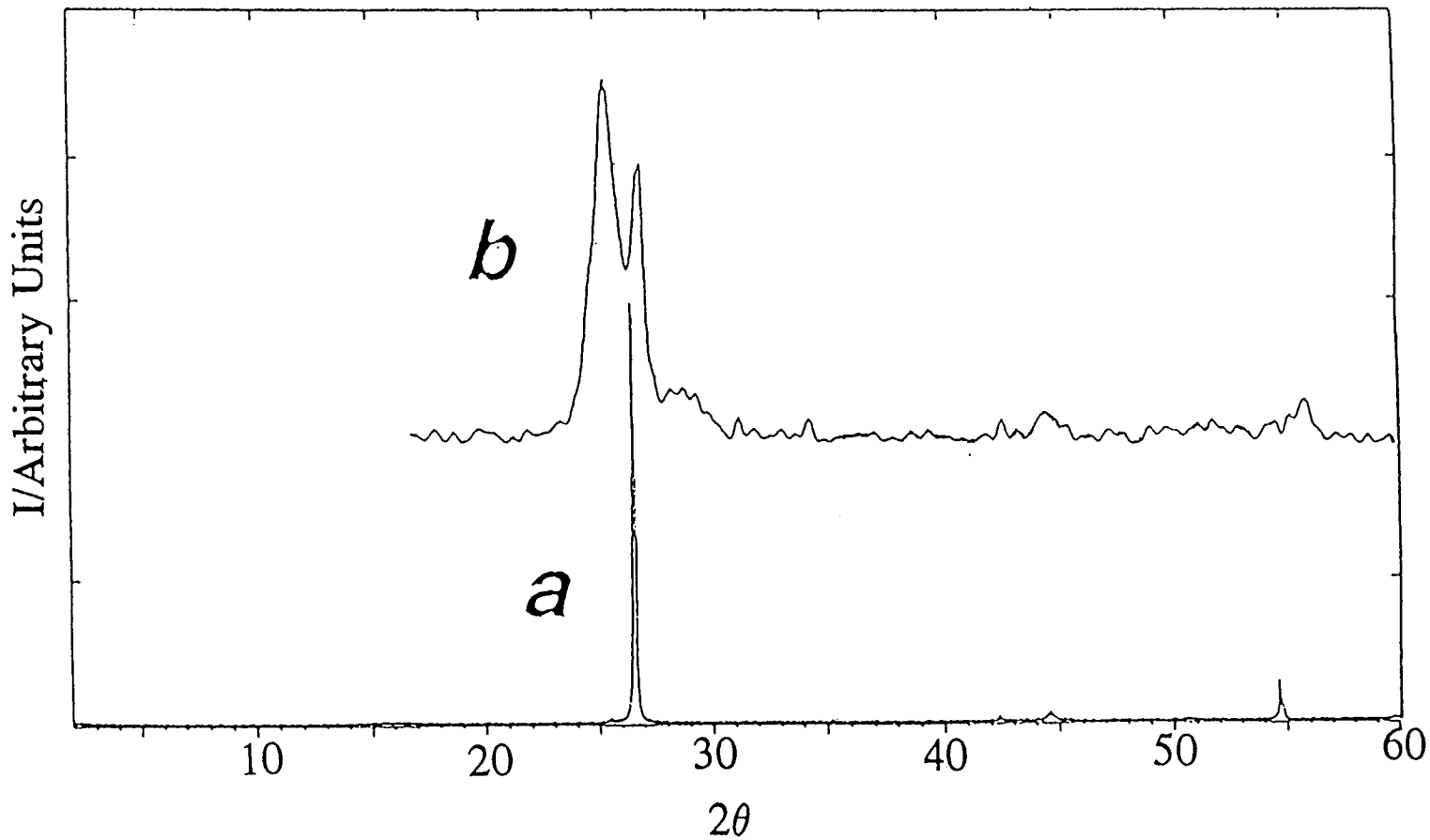

Figure 4.3 X-ray diffraction profiles for (a) unreacted graphitre, and (b) graphite reacted with a solution of K_2MnF_6 in 49% aqueous HF at ambient temperature (See Figure 4.2). Scan rate = 5° (2θ)/minute; 2° < 2θ < 60 °.

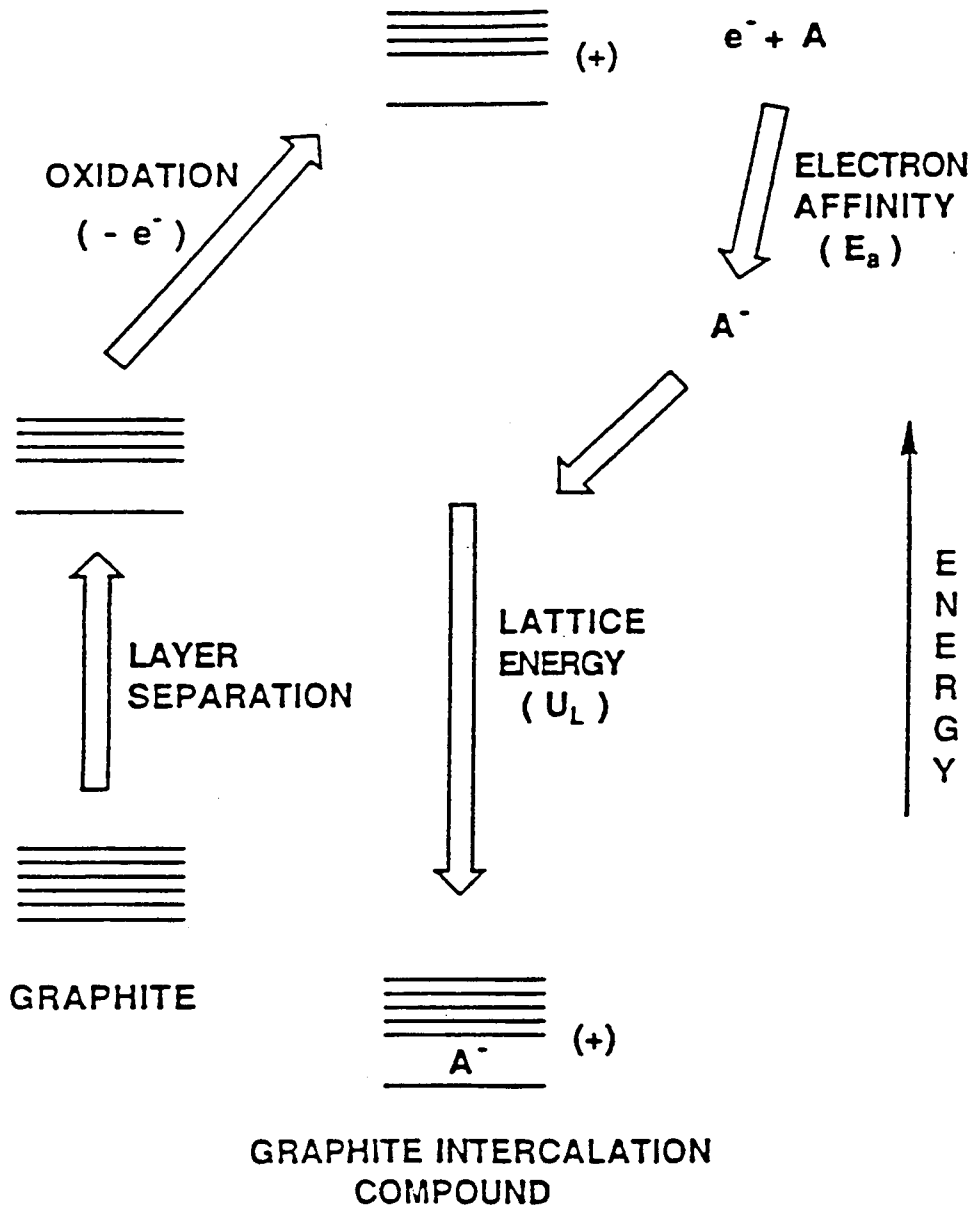

Figure 4.4 Principal energy terms associated with graphite intercalation.

4.8 Tables

Table 4.I Reactivity and X-ray diffraction data for reactions of graphite with K_2MnF_6, K_2NiF_6, Na_3FeF_6 and CoF_3 in anhydrous HF at ambient temperature.

Exp#	Reagent	C:M ratio	Insoluble product	Soluble product
1	K_2MnF_6	28	$C_{28}HF$ (2nd stage, c = 9.35 Å) MnF_3	KHF_2 K_2MnF_6 (v. weak)
2	K_2MnF_6	5-6	C_xF (1st stage, c = 5.9 Å) MnF_3	K_2MnF_6
3	K_2MnF_6	4	C_xF (1st stage, c = 6.0 Å) MnF_3	KHF_2 K_2MnF_6
4	K_2NiF_6	56	graphite C_xF (1st stage, c = 5.7 Å) NiF_2 (broad)	KHF_2
5	K_2NiF_6	4	C_xF (1st stage, c = 5.9 Å) NiF_2	KHF_2
6	K_2NiF_6	2	C_xF (1st stage, c = 5.9 Å) NiF_2	KHF_2
7	Na_3FeF_6	28	graphite unindexed lines	$NaHF_2$
8	Na_3FeF_6	20	graphite C_xF (1st stage, c = 5.6 Å)	$NaHF_2$ unindexed lines
9	Na_3FeF_6	4	graphite C_xF (1st stage, c = 5.6 Å) unindexed lines	$NaHF_2$ unindexed lines
10	CoF_3	4	graphite CoF_3	none

Table 4.II Standard reduction potentials in aqueous acid.

Half-reaction	E_o/V (25)
$e^- + Fe^{3+} \rightarrow Fe^{2+}$	0.8
$e^- + Mn^{4+} \rightarrow Mn^{3+}$	1.0
$e^- + Ni^{4+} \rightarrow Ni^{2+}$	1.6
$e^- + Co^{3+} \rightarrow Co^{2+}$	1.9

Chapter 5
Preparation and Characterization of Nanocomposites of Polyethers and Molybdenum Disulfide

John P. Lemmon and Michael M. Lerner*

Department of Chemistry and Center for Advanced Materials Research
Oregon State University
Corvallis, OR 97331

Chem. Mater., **1994**, *6*, 207-210

5.1 Abstract

Nanocomposites of poly(ethylene oxide) and molybdenum disulfide are prepared by the hydrolysis of lithiated molybdenum disulfide in an aqueous solution of PEO (mw 100 000) or poly[oxymethylene-oligo(oxyethylene)] (PEM, mw ≈ 70 000). X-ray diffraction indicates an expansion of 8.3 Å in the interlayer spacing (c ≈ 14.5 Å), consistent with the incorporation of a polymer double layer within the disulfide galleries. Reaction stoichiometries and elemental analyses indicate a composition of $Li_{0.12}(PEO)_yMoS_2$ (y = 1.0-1.3) for the single-phase product. Analyses of extracted polymer demonstrate that high-molecular-weight polymer is present within the disulfide galleries. Scanning calorimetry of the nanocomposites indicates exothermic peaks at approximately 200 and 310 °C, which are demonstrated to be associated with an order/disorder phase transition and polymer decomposition, respectively. A fully amorphous, unstacked phase is irreversibly generated by heating the nanocomposites at 200 °C for several hours.

5.2 Introduction

The intercalation of organic compounds into layered transition metal dichalcogenides has been widely studied since the 1970s (1-8). Recent interest in the incorporation of polymers within inorganic hosts stems from the potential mechanical, structural, and electrical properties of organic/inorganic nanocomposites (9-12).

In general, layered ternary chalcogenides of the transition metals, A_xMCh_2 (A = alkali metal; M = Ti, Nb, Ta; Ch = S, Se, Te) spontaneously incorporate water or polar organic molecules to form stable compounds with solvated cations:

$$A_xMCh_2 + nL \rightarrow A_xL_nCh_2 \qquad [5.1]$$

Exchange reactions can also be utilized to expand the chemistry of these materials. An example is the incorporation of the oligoether poly(ethylene glycol) by exchange of water in the hydrated lithium salt (5):

$$A_x(H_2O)_yMS_2 + PEG \rightarrow A_x(PEG)MS_2 + yH_2O \qquad [5.2]$$

A topotactic mechanism for the above reactions, in which the intersheet galleries expand or contract but the solid retains its two-dimensional character will be ineffective for the introduction of high-molecular-weight polymers due to the slow diffusion of macromolecules into the galleries.

One alternate route to polymer-containing nanocomposites involves the *in situ* polymerization of monomeric intercalants, and the preparation of materials such as poly(styrene)/MoS_2 (13), polyaniline/V_2O_5 (14) and polyaniline/MoO_3 (15) have been reported by this method.

Murphy and co-workers (4) and Schöllhorn and co-workers (5) first observed that, under appropriate conditions, single-sheet colloids can be obtained by chemical oxidation of the lithiated metal disulfides. Morrison and co-workers (13,16-18) and other groups (19) have demonstrated that a colloidal suspension of single-sheet MoS_2 can incorporate molecular organics, organometallic complexes, or other complex cations when the single sheets are restacked.

More recently, the incorporation of polyaniline into MoS_2 has been reported by this method (20).

We have previously reported the formation of nanocomposites of poly(ethylene oxide) and poly[oxymethylene-oligo(oxyethylene)] with MoS_2 (21) and here describe the preparation of single-phase materials and their characterization by X-ray powder diffraction, differential scanning calorimetry, thermogravimetric and elemental analyses, and electrical measurements.

5.3 Experimental Section

Li_xMoS_2 was prepared by the reaction of MoS_2 (Aldrich, 99% purity) with butyllithium (Aldrich, 1.6 M in hexane) using a literature method (22). Lithium analysis of the product by atomic absorption spectroscopy gives a stoichiometry of $Li_{1.15}MoS_2$. Poly(ethylene oxide) (PEO, Aldrich, mw = 100 000 Da) was used as received. Poly[oxymethylene-oligo(oxyethylene)] (PEM) was prepared as described previously (23). The preparation of nanocomposites proceeds by exfoliation of the layered disulfide to form a stable colloid [5.3a], adsorption of polymer to these separated lamella [5.3b], and then restacking to form a layered nanocomposite [5.3c]. Exfoliation of MoS_2 into single-sheet lamella was achieved

$$Li_xMoS_2 + xH_2O \rightarrow MoS_2(coll) + (x/2)H_2 + xLiOH(aq) \qquad [5.3a]$$

$$Poly(aq) + MoS_2(coll) \rightarrow Poly/MoS_2(coll) \qquad [5.3b]$$

$$Poly/MoS_2(coll) \rightarrow Poly/MoS_2(ppt) \qquad [5.3c]$$

via the rapid hydrolysis and sonication of Li_xMoS_2. Polymer/MoS_2 nanocomposites (Figure 5.1) were synthesized by the exfoliation of MoS_2 in deionized, deaerated (DI/DA) water containing a stoichiometric amount of polyether. Typical reactions involved 10-100 mg of PEO, 200 mg of Li_xMoS_2, and a total water volume of 20 mL. The reaction stoichiometries were varied from 0.05-0.45 g of polymer/g of MoS_2. The solutions were then neutralized with dilute acid; the solid product was separated by centrifugation at 13 000 rpm and washed several times with small amounts of DI/DA to ensure removal of LiOH and other soluble products. The nanocomposites were dried *in vacuo* at 70 °C for several hours, and subsequent manipulations were performed in a drybox or under dry nitrogen to exclude moisture and oxygen.

X-ray powder diffraction data were collected at ambient temperature on a Siemens D5000 powder diffractometer ($2° < 2\theta < 30°$, scan rate 0.002°). Pressed pellets of the reaction products were loaded into a holder modified to contain an inert atmosphere.

Simultaneous DTA/TGA data were obtained using a Netzsch, Inc. STA 419C thermal analyzer. Samples (20-25 mg) were loaded into aluminum pans, the sample chamber was evacuated and back-filled with He. Thermal scans from 50 to 400 °C were performed at 5 °C/min.

Lithium analysis utilized a Varian Techtron AA6 atomic absorption spectrophotometer at 670.8 nm with a sensitivity of 0.017 μg/mL. Polymer/MoS_2 composites were analyzed following dissolution in hot, concentrated HNO_3.

Carbon and hydrogen analyses were performed by Desert Analytical (Tucson, AZ).

Gel permeation chromatography was performed on a Hewlett-Packard 1050 HPLC system using an ultrahydrogel linear column (Waters Chromatography) and Waters 410 RI detector. Samples were eluted at 0.85 mL/min in deionized water containing 0.05% NaN_3.

Electrical conductivites between 77 and 274 K were determined using a four-probe method on pressed pellets maintained under a blanket of dry N_2.

5.4 Results and Discussion

The powder diffraction data (Figure 5.2) for products of reactions *a-d* exhibit peaks near 6, 12, and 18°, corresponding to $d \approx 14.5$, 7.3, and 4.8 Å, which are indexed as the (001), (002), and (003) reflections for a nanocomposite phase. Preferred orientation in these pressed pellets reduces the intensity of all but (00*l*) reflections. The c-repeat distances obtained increase slightly with higher polymer content (in *a*, 14.56(8) Å; *b*, 14.34(6); *c*, 14.21(12)), and the change in relative peak intensities is reproducible. The intensity changes are probably associated with different packing densities of the polymer layers in the nanocomposites (*vide infra*). Peak widths are similar for reaction products *a-c* and indicate stacking coherence lengths in the range of approximately 200-400 Å (20-25 repeat units). Reaction products *d* and *e*, prepared at lower polymer

stoichiometries, show a broad peak associated with restacked MoS_2. Similar diffraction data are obtained using PEM.

The distances between Mo planes observed in products *a-c* is 8.0-8.3 Å greater than in $LiMoS_2$. This expansion is similar to that obtained by insertion of poly(ethylene glycol) into MS_2(5) oligo- or polyethers into montmorillonite (24), and PEG or PEO into MPS_3(25) and suggests that a polymer bilayer is incorporated into the intersheet region. A schematic structure of this arrangement is displayed in Figure 5.3. A greater expansion, indicating a phase containing more than a double layer of polymer, is not observed in these reactions or other experiments utilizing a large excess of PEO. When the polymer stoichiometry is limiting, an ordered monolayer phase (with 4.0-Å expansion) can be obtained for the polyethers/montmorillonite nanocomposites (24); however, an ordered product with this smaller expansion is not evident in these data. The weak, broad peak obtained at 0.10g/g (Figure 5.2*e*) corresponding to a *c*-repeat distance of approximately 9.5 Å, might be ascribed to a poorly ordered monolayer phase. The broad peak near 14° at lower starting polymer stoichiometries (*d-f*) corresponds to the intersheet distance of restacked MoS_2.

The polymer conformation within the galleries cannot be determined directly from these diffraction studies, and a helical polymer conformation, as in crystalline PEO, cannot be excluded by steric arguments. Since the energy of polymer adsorption will decrease dramatically once monolayer coverage of the sheet surfaces is complete, a bilayer within the galleries (resulting from monolayer coverage of each sheet face) is a reasonable expectation from this

exfoliation-adsorption method. In addition, indirect evidence strongly support the bilayer structure. This evidence includes the similar 8-Å expansion observed in a variety of small-molecule ethers in layered structures, the similar expansion observed for PEM (which is amorphous at ambient temperature), and the existence of an ordered 4-Å expanded phase in PEO/Na montmorillonite. The latter structure contains galleries that are too small to contain helical polymer chains, is prepared under similar conditions, and is related stoichiometrically to the bilayer phase (24).

Elemental analyses for C, H, and Li for reactions *a-c* are indicated in Table 5.I. The polymer/MoS_2 ratio found in the product depends on the mixing stoichiometries utilized in the nanocomposite syntheses. The large difference between initial and final stoichiometry in *a* indicates a threshold for polymer content (residual polymer is removed when the product is washed with water). The final polymer/MoS_2 ratios in *b* and *c* are slightly greater than the mixing stoichiometry; these results can be explained by the loss of a small amount of MoS_2 when the product is washed. The change in polymer content found for these products indicates a higher packing density of polymer within the disulfide galleries. This explanation is consistent with the reproducible change in relative peak intensities and slight increase in *c*-repeat distance with polymer content.

The Li content in the composites was analyzed, and the overall stoichiometry was determined to be close to $Li_{0.12}(PEO)_xMoS_2$ for all three samples. The lithium content most likely reflects a negative charge on MoS_2 sheets similar to that present in the hydrated lithium salts. Indeed, the lithium stoichiometry

($x \approx 0.1$) is consistently similar to that obtained for hydrates prepared under similar conditions. Electrical measurements (Figure 5.6) indicate a semimetallic conductivity and thermal response, which are again consistent with negatively charged MoS_2 layers (26). Although Morrison *et al.* have suggested (18) the presence of hydroxide in restacked MoS_2 to account for the negative charge associated with the MoS_2 layers, this explanation is inconsistent with our observations that similar colloids and restacked solids can be generated in polar organic solvents such as DMSO and DMF. The significant presence of LiOH is unlikely because our products have been washed with water, are not deliquescent, and display no unexplained diffraction peaks. Electrochemical studies to directly determine the charge state of the MoS_2 sheets within these nanocomposites are currently in progress.

A simultaneous DTA/TGA scan of the product from reaction *a* is presented in Figure 5.4. The absence of a melting endotherm at 60 °C indicates that no crystalline PEO phase occurs in the nanocomposite and illustrates again that the polymer conformation within these galleries is different than that of the bulk polymer. The exotherm near 310 °C arises from degradation of the polymer and the associated weight loss of 27 wt %, due to volatilization of the decomposition products, corresponds to the entire polymer content within the nanocomposite. X-ray diffraction of the nanocomposite after heating to 450 °C shows only a restacked MoS_2 phase. For comparison, the decomposition of pure PEO is observed at 360 °C in an inert atmosphere.

An additional exotherm between 125 and 255 °C is not associated with any significant sample weight loss. PEM/MoS_2 nanocomposites were also scanned and showed similar behavior. To further examine this transition, ambient-temperature X-ray diffraction pattern of a single pellet of the nanocomposite following heating at 200 °C in an Ar atmosphere for 3-6 h (Figure 5.5) were obtained and indicate an irreversible loss of sample order. After 6 h, the material appears entirely disordered. Subsequent heating of the pellet above 400 °C under inert conditions to remove the polymer component for several hours generates crystalline MoS_2. We conclude, therefore, that the disordered phase must contain MoS_2 sheets without a coherent stacking arrangement (28). The generation of the disordered state requires a large rearrangement in the structure. The driving energy for this process may be provided by the thermally activated rearrangement of adsorbed polymer. The potentially high electroactive area for the disordered phase makes it an attractive candidate for electrochemical applications. Experiments on the charge-discharge performance of these materials are currently underway.

GPC data on polymer extracted from the nanocomposites indicates that the polymeric component of these materials is not degraded into low-molecular-weight fragments, although the results of crosslinking and scission are evident. Figure 5.7 shows that the extracted polymer from $Li_{0.12}PEO_{1.34}MoS_2$ contains significant molecular weight components centered at 450 000 and 20 000 Da. After heat treatment to form the unstacked nanocomposite, the extracted polymer has a single peak centered at 45 000 Da. In these samples, only 10-

50% of the total polymer component can be extracted into an organic solution for analysis. Low-molecular-weight and other highly soluble products should be more readily desorbed from the disulfide surfaces, so the data obtained may not be representative of the entire polymer component. As no low-molecular-weight fragments are observed, however, the gross degradation of PEO dos not occur. The details of polymer interaction with the disulfide lamella, and the mechanism of cross-link formation and bond cleavage, are of considerable interest and will be further explored by ^{13}C NMR studies on these solids.

5.5 References

1. Gamble, F. R.; DiSalvo, F. J.; Klemn, R. A.; Geballe, T. H. *Science* **1970**, *168*, 568.

2. Gamble, F. R.; Osiecki, J. H.; DiSalvo, F. J. *J. Chem. Phys.* **1971**, *55*, 3525.

3. Whittingham, M. S. *Mater. Res. Bull.* **1974**, *9*, 1681.

4. Murphy, D. W.; Hull, G. W. *J. Chem. Phys.* **1975**, *62*, 973.

5. Lerf, A.; Schöllhorn, R. *Inorg. Chem.* **1977**, *11*, 2950.

6. Subba Rao, G. V.; Shafer, M. W. *Intercalated Layered Materials*; Levy, F., Ed.; D. Reidel: Holland, 1979; Vol. 6.

7. *Intercalated Layered Materials*; Levy, F., Ed.; D. Reidel: Boston, 1979.

8. Schöllhorn, R. *Angew. Chem., Int. Engl. Ed.* **1980**, *19*, 983.

9. Stucky, G. D. *Prog. Inorg. Chem.* **1992**, *40*, 99-177.

10. Ozin, G. A. *Adv. Mater.* **1992** *4*, 613.

11. Stein, A.; Keller, S. W.; Mallouk, T. E. *Science* **1993**, *259*, 1558.

12. Behrens, P. *Adv. Mater.* **1993**, *5*, 127.

13. Divigalpitiya, W. M. R.; Frindt, R. F.; Morrison, S. R. *J. Mater. Res.* **1991**, *6*, 1103.

14. Liu, Y. J.; DeGroot, D. C.; Schindler, J. L.; Kannewurf, C. R.; Kanatzidis, M. G. *J. Chem. Soc., Chem. Commun.* **1993**, 593.

15. Bissessur. R.; DeGroot, D.; Schindler, J.; Kannewurf, C.; Kanatzidis, M. *J. Chem. Soc., Chem. Commun.* **1993**, 687.

16. Divigalpitiya, W. M. R.; Frindt, R. F.; Morrison, S. R. *Science* **1989**, *246*, 369.

17. Gee, M. A.; Frindt, R. F.; Joensen, P.; Morrison, S. R. *Mater. Res. Bull.* **1986**, *21*, 543.

18. Miremadi, B. K.; Cowan, T.; Morrison, S. R. *J. Appl. Phys.* **1991**, *69*, 6373.

19. Tagaya, H.; Hashimoto, T.; Karasu, M.; Izumi, T.; Chiba, K. *Chem. Soc. Jpn., Chem. Lett.* **1991**, 2113.

20. Kanatzidis, M. G.; Bissessur, R.; DeGroot, D. C.; Schindler, J. L.; Kannewurf, C. R. *Chem. Mater.* **1993**, *5*, 595.

21. Lemmon, J. P.; Sloop, S. E.; Lerner. M. M. *Proc. Am. Chem. Soc., Inorg. Chem. Soc., Inorg. Chem.* **1993**, Abstract No. 355.

22. Murphy, D. W.; DiSalvo, F. J.; Hull, G. W.; Waszczak, J. V. *Inorg. Chem.* **1976**, *15*, 17.

23. Lemmon, J. P.; Lerner, M. M. *Macromolecules* **1992**, *25*, 2907.

24. Wu, J.; Lerner, M. M. *Chem. Mater.* **1993**, *5*, 835.

25. Lagadic, I.; Léaustic, A.; Clément, R. *J. Chem. Soc., Chem. Commun.* **1992**, 1396.

26. Reports (27) have indicated the metallic nature of 1T-MoS_2, which can be prepared from single-sheet MoS_2. The uncharged sheets, however, are prepared only when an oxidant such as $K_2Cr_2O_7$ or I_2 was added to the suspension.

27. Wypych. F.; Schöllhorn, R. *J. Chem. Soc., Chem. Commun.* **1992**, 1386.

28. A structure consisting of a stacked arrangement of MoS_2 sheets of highly irregular intersheet spacing has also been suggested to the authors.

5.6 Figures

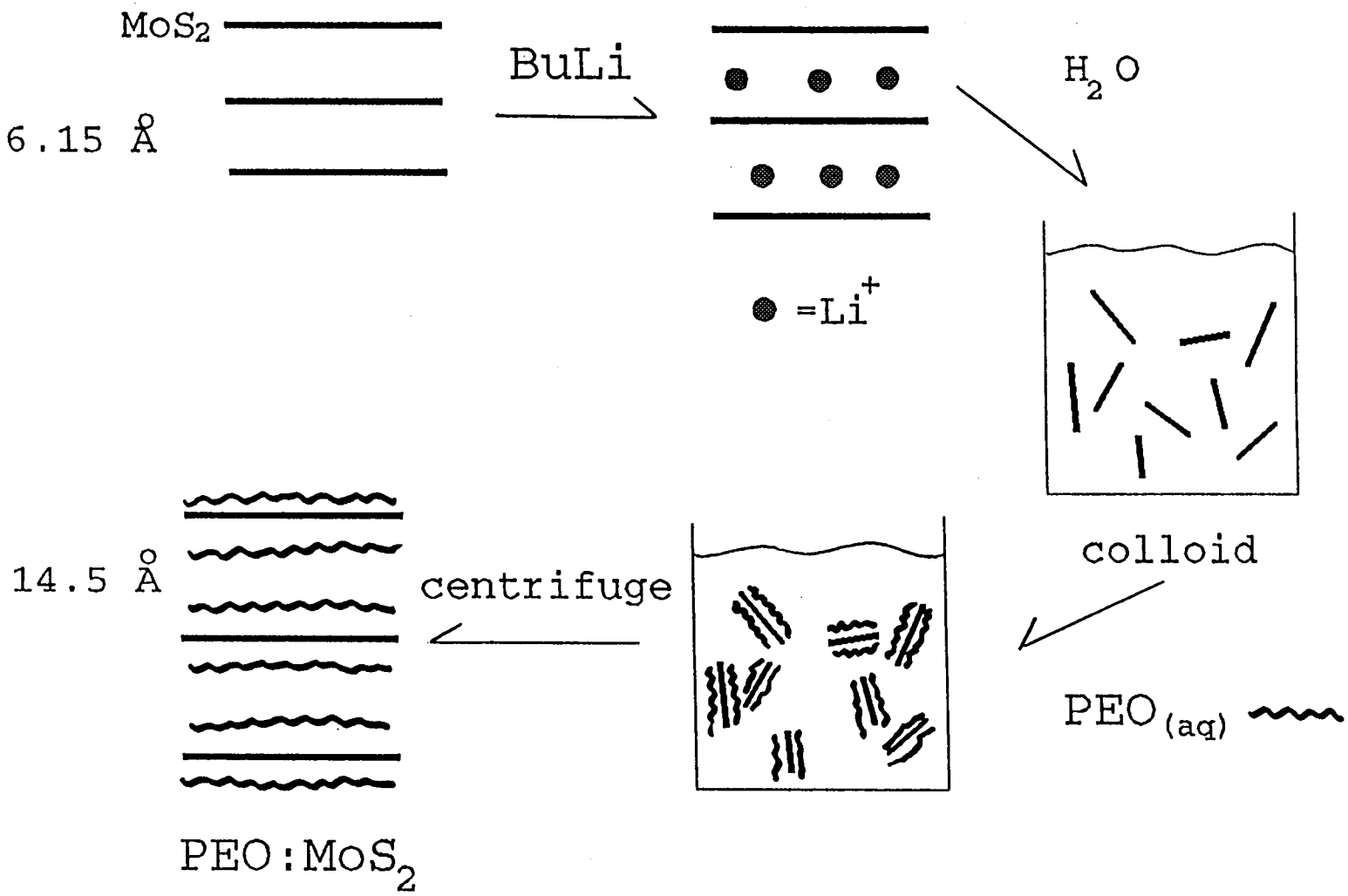

Figure 5.1 Preparative Route to PEO/MoS_2 Nanocomposites

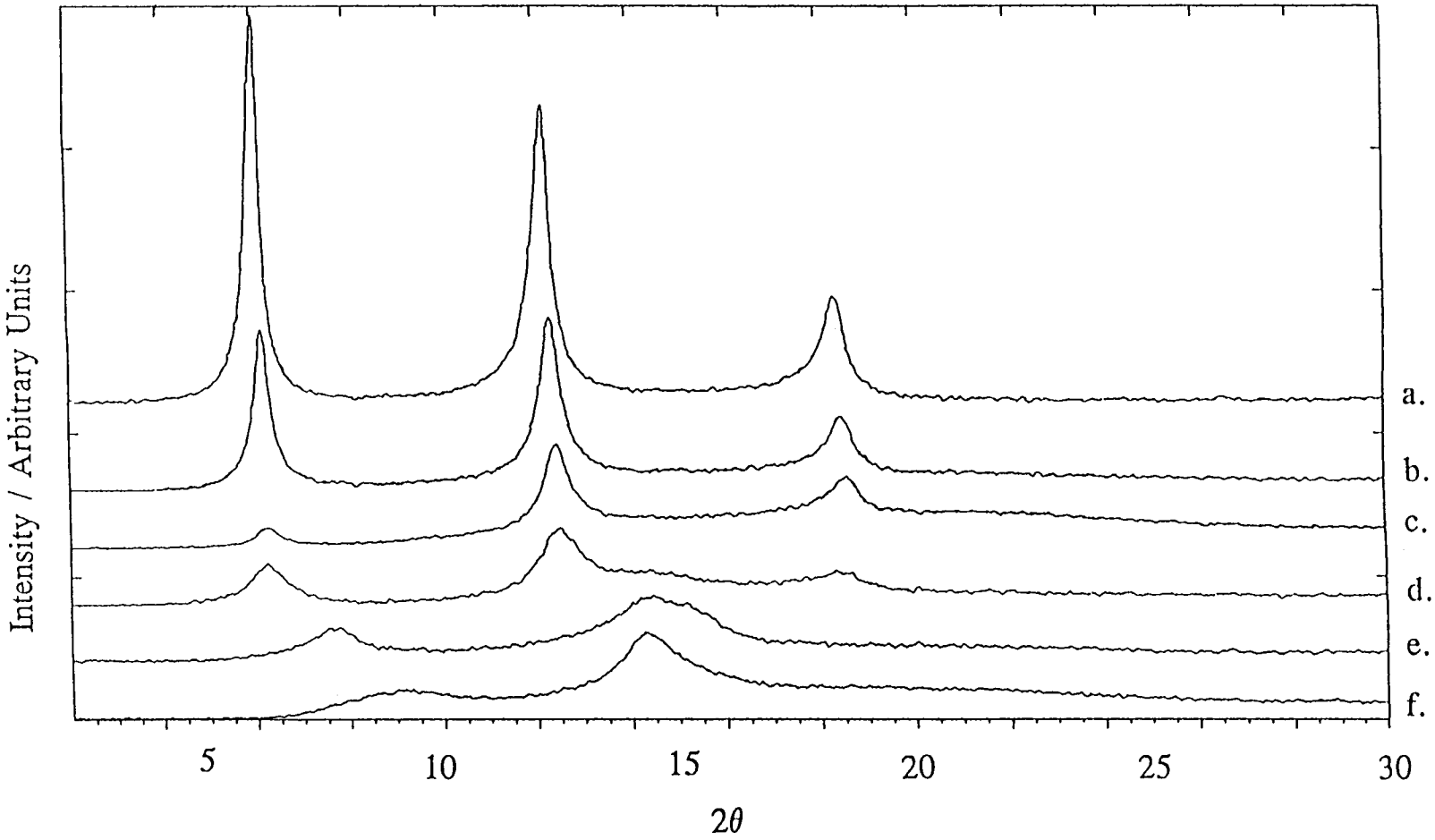

Figure 5.2 X-ray powder diffraction pattern of $Li_{0.12}PEO_xMoS_2$ prepared with reaction stoichiometries: (a) 0.45 g of polymer/g of MoS_2, (b) 0.30 g/g, (c) 0.25, (d) 0.20, (e) 0.10, (f) 0.05.

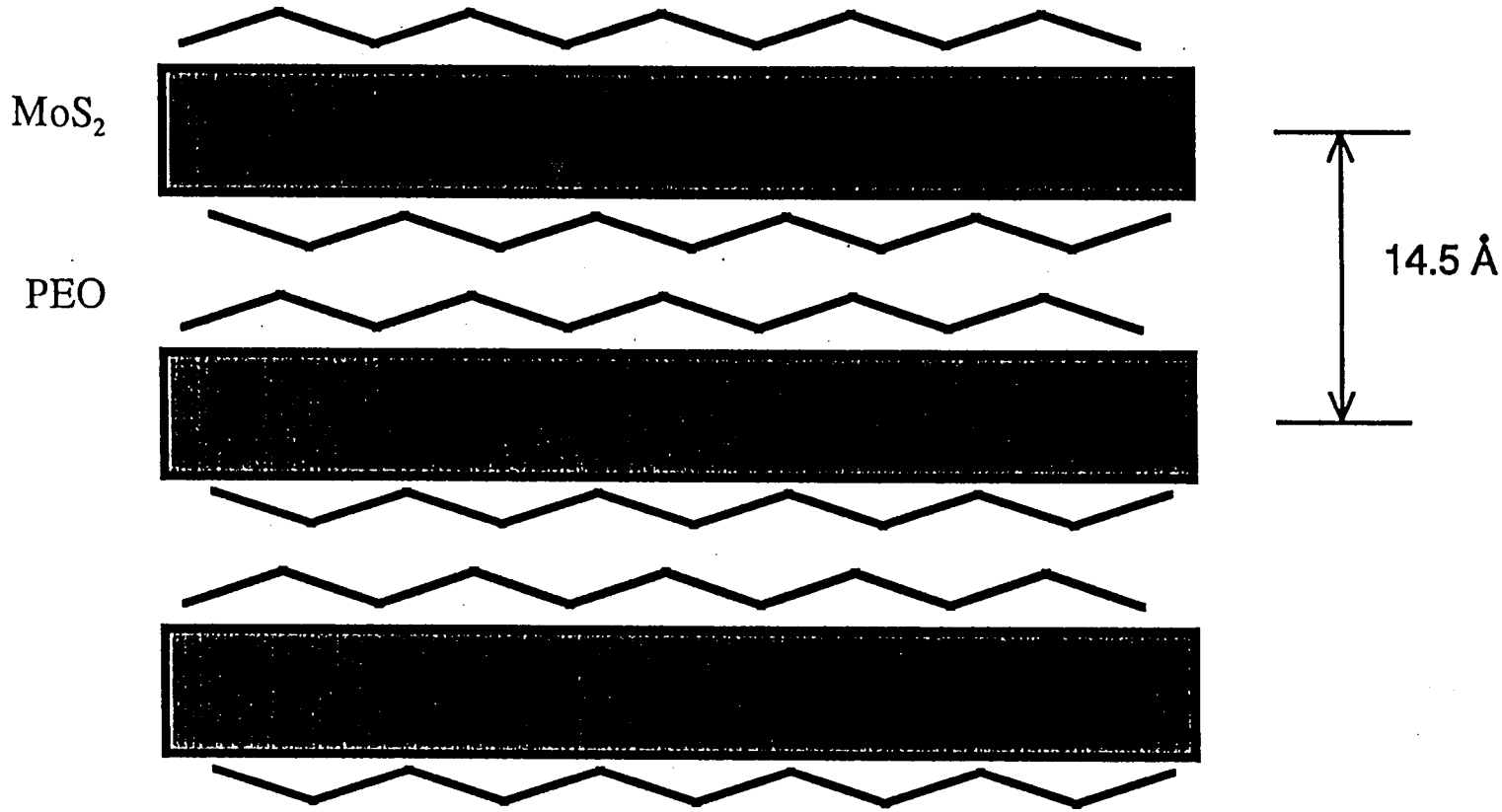

Figure 5.3 Arrangement of the double-layer nanocoposite structure.

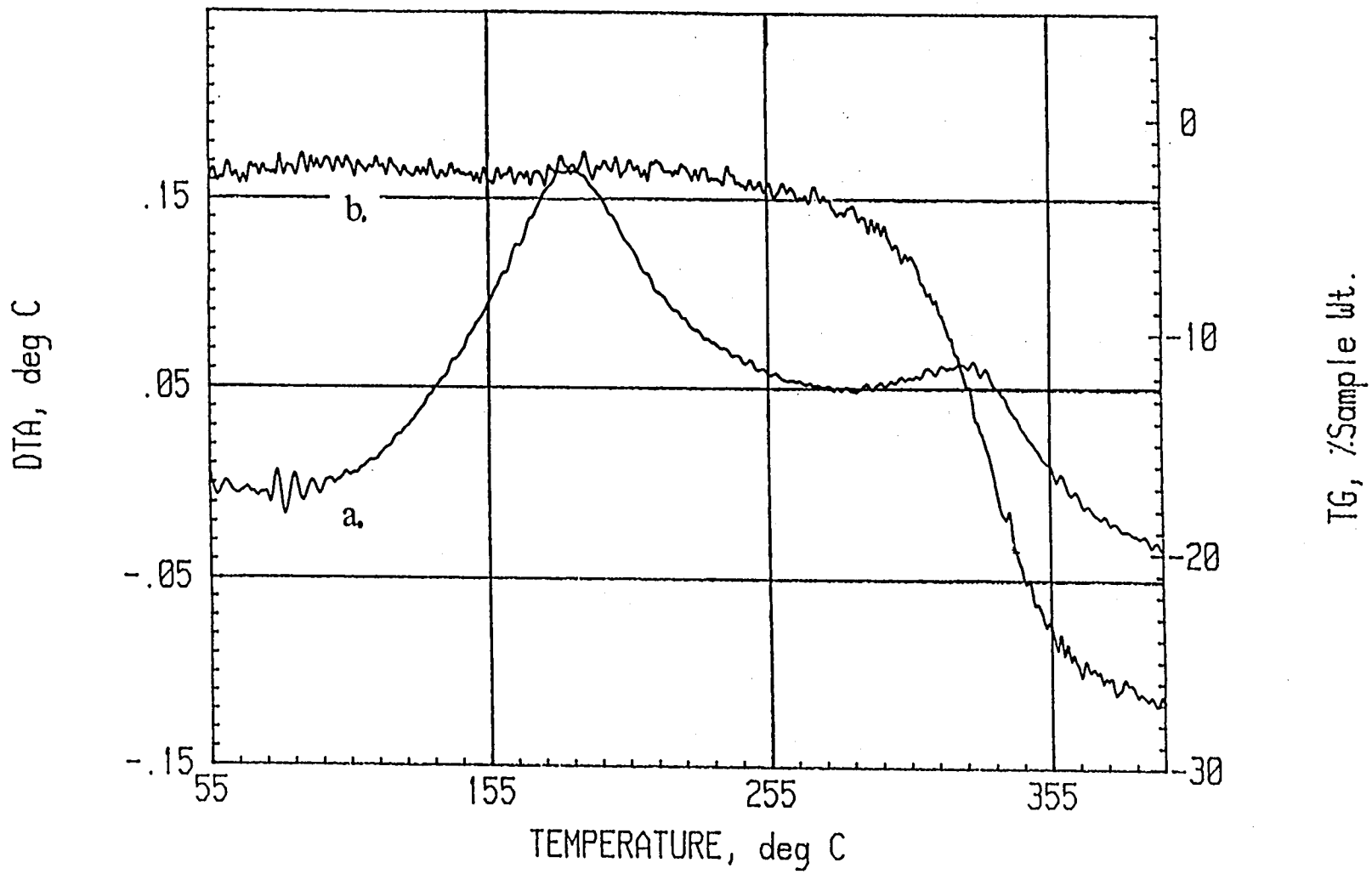

Figure 5.4 Simultaneous DTA/TGA scan obtained for $Li_{0.12}PEO_{1.34}MoS_2$: (a) DTA, (b) TGA.

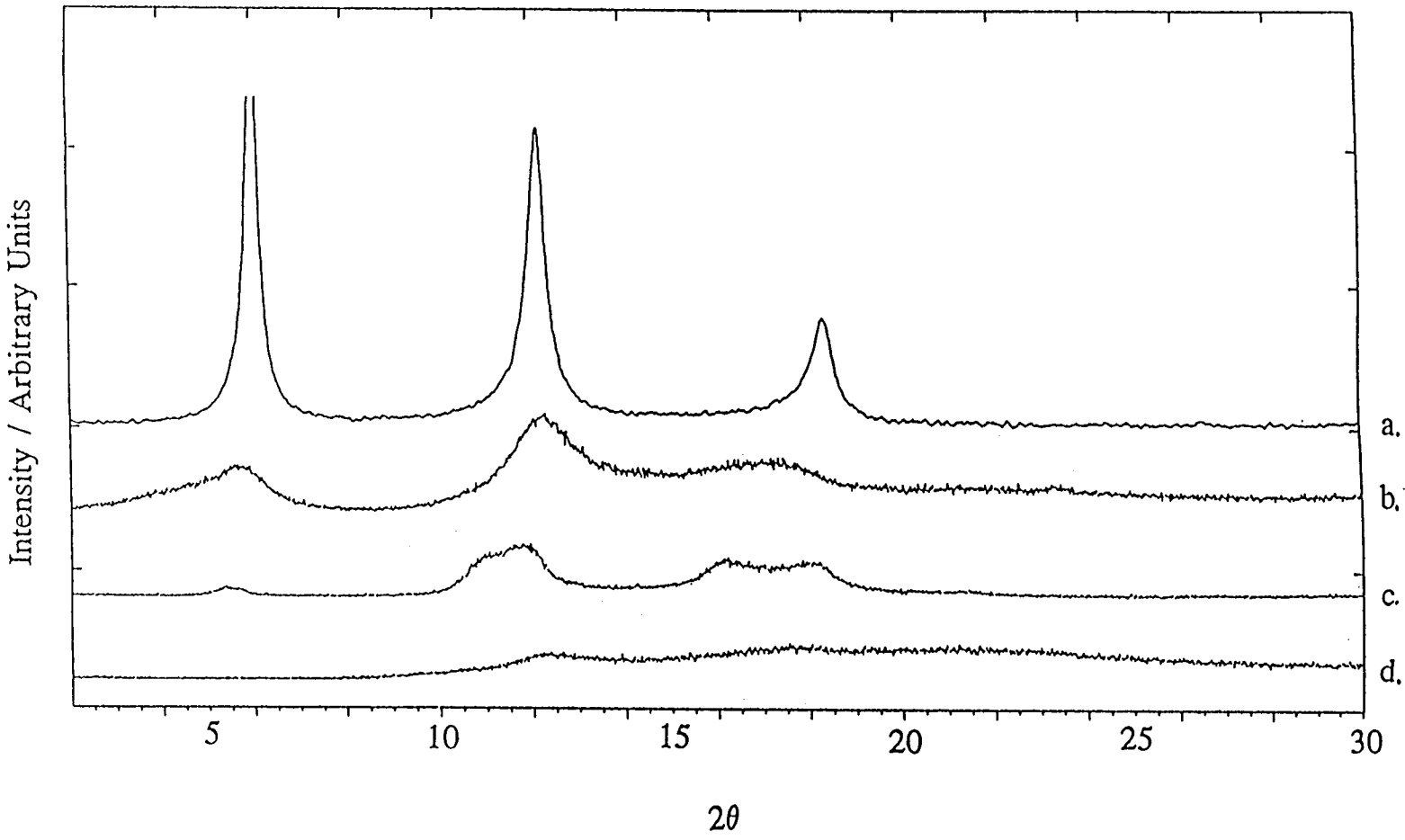

Figure 5.5 X-ray powder diffraction pattern for $Li_{0.12}PEO_{1.34}MoS_2$ heated to 200 °C: (a) 0 h; (b) 3 h; (c) 4.5 h; (d) 6 h.

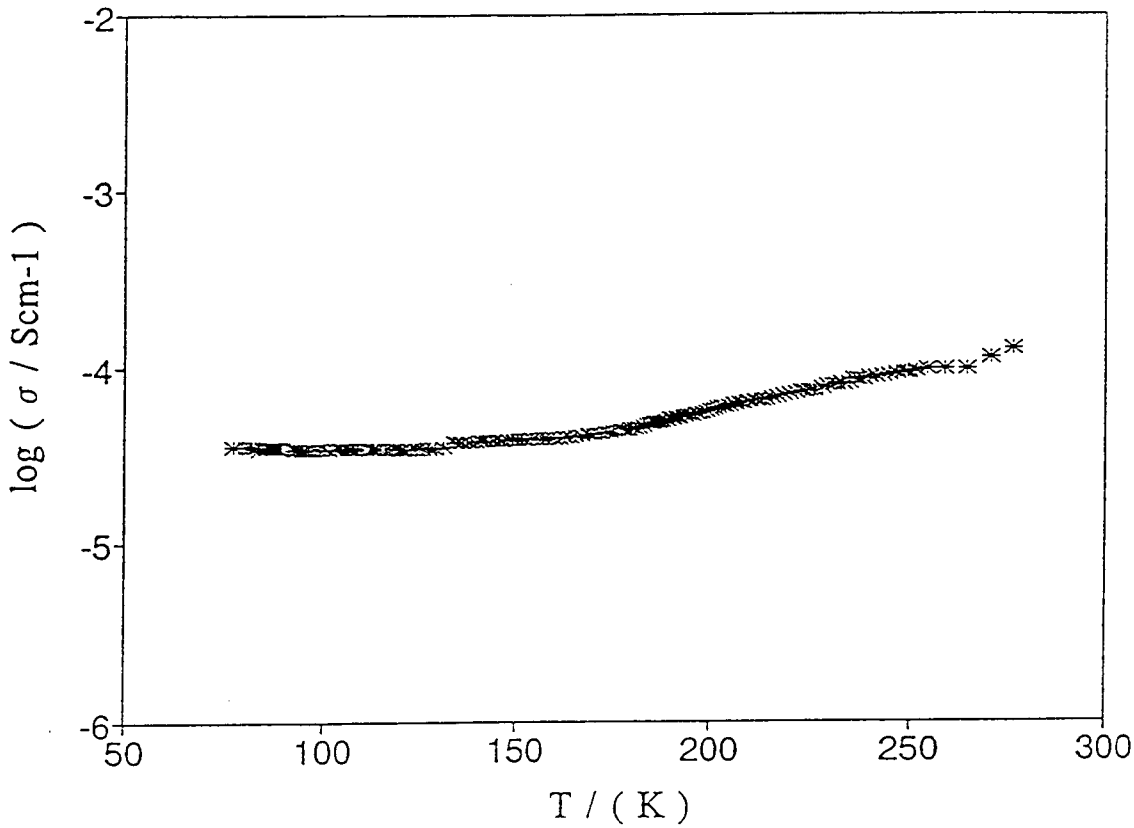

Figure 5.6 Electrical conductivity of $Li_{0.12}(PEO)_{1.34}MoS_2$ nanocomposite.

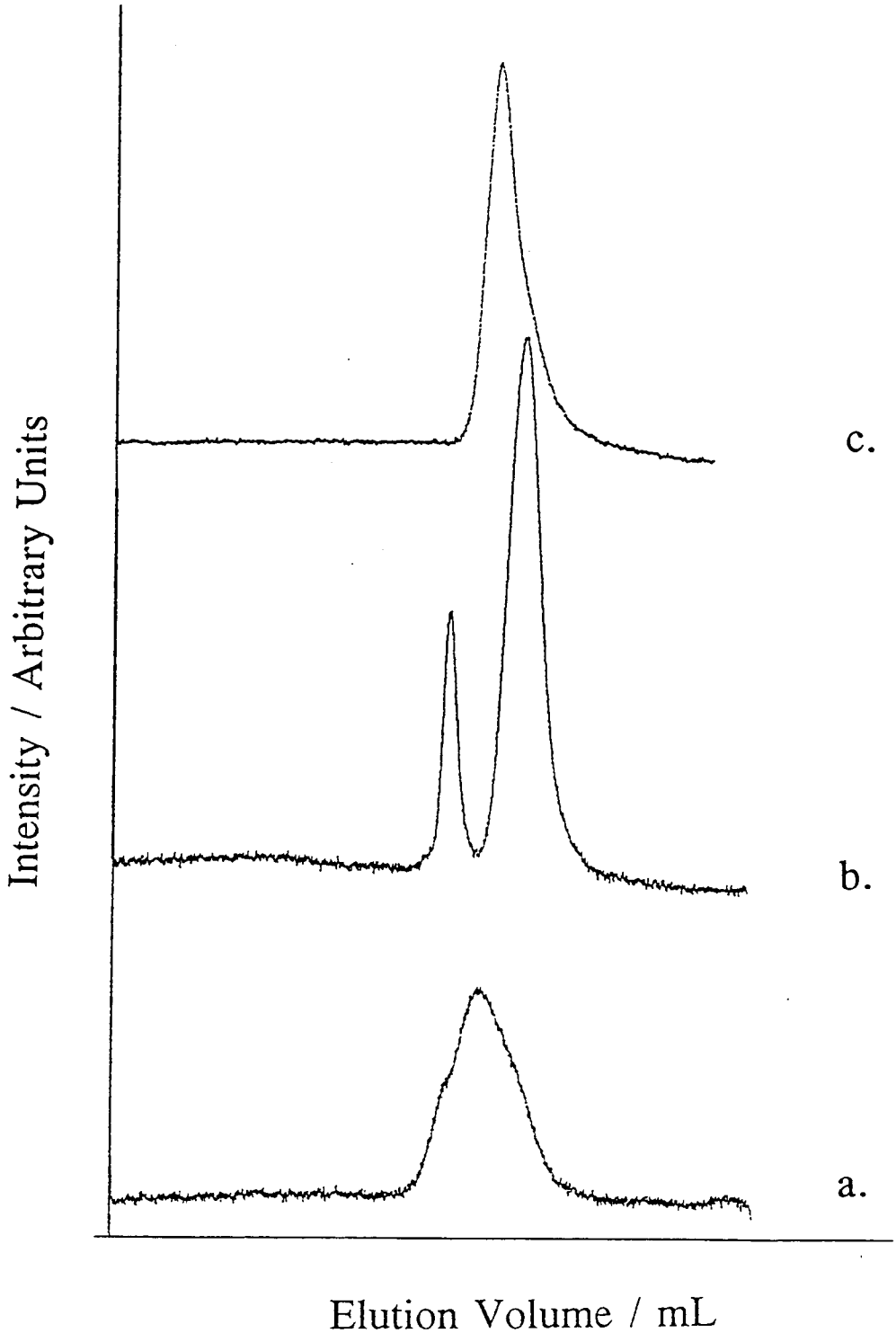

Figure 5.7 Gel permeation chromatography traces for (a) PEO starting reagent ($M_W \approx 100\,000$), (b) polymer extracted from $Li_{0.12}(PEO)_{1.34}MoS_2$, and (c) polymer extracted from $Li_{0.12}(PEO)_{1.34}MoS_2$ after heating at 200 °C. The calibration determined with PEO standards is log M_W = (-0.968 x elution volume) + 11.974.

5.7 Tables

Table 5.I Elemental analyses for C, H, and Li in PEO/MoS_2 nanocomposites[a]

expt	PEO/MoS_2 (g/g)	Li wt %	C wt %	H wt %	H/C	composition
a	0.45	0.39	14.75	2.42	1.97	$Li_{0.12}(PEO)_{1.34}MoS_2$
b	0.30	0.42	13.42	2.13	1.91	$Li_{0.13}(PEO)_{1.18}MoS_2$
c	0.26	0.75	12.25	2.01	1.97	$Li_{0.12}(PEO)_{1.05}MoS_2$

[a] The representation $(PEO)_n$ refers to *n* moles of the repeat unit (CH_2CH_2O).

Chapter 6
Preparation and Characterization of Nanocomposites of Poly(ethylene oxide) with Titanium Disulfide and Molybdenum Trioxide

John P. Lemmon and Michael M. Lerner*

Department of Chemistry and Center for Advanced Materials Research
Oregon State University
Corvallis, OR 97331

6.1 Abstract

Single-phase nanocomposites containing TiS_2 and poly(ethylene oxide) are prepared by the interaction of colloidal TiS_2 with a solution of PEO in N-methyl formamide (NMF). X-ray diffraction indicates a layered product (c = 14.2 Å), consistent with the incorporation of an 8 Å double layer of poly(ethylene oxide) between the disulfide sheets. A single-phase product is of approximate composition $Li_{0.02}Na_{0.25}(C_2H_4O)_{0.8}TiS_2 \cdot 0.1NMF$. Electronic measurements between 77 and 274 K indicate a conductivity between 10^{-2} and 10^{-3} Scm^{-1}, with little temperature dependence. PEO/MoO_3 nanocomposites are obtained following exfoliation of Li_xMoO_3 in a water/acetonitrile solution. Stacking repeats of 12.6 Å and 15.9 - 16.5 Å indicate expansions of approximately 4 Å or 8 Å relative to Li_xMoO_3. A stoichiometry of $Li_{0.2\text{-}0.3}(C_2H_4O)_{0.9}MoO_3 \cdot 0.1H_2O$ is obtained for the single-phase product with stacking repeat = 16.5 Å.

6.2 Introduction

Nanocomposites containing structural elements of inorganic solids and organic polymers are of both fundamental and practical interest. Potential applications for these materials include charge-storage, optics, and catalysis (1-6). The topotactic intercalation of polymers into layered hosts is kinetically limited by the slow diffusion of large molecules into the galleries; however, an exfoliation/adsorption process has proved successful for the preparation of nanocomposites containing a number of layered solids with soluble polymers. In

these syntheses, the layered host structure is exfoliated and forms a colloidal suspension; the soluble polymer is subsequently adsorbed onto the colloidal particles and the product obtained by flocculation of these nanoparticles.

One reason for interest in the inclusion of oligo- and polyethers within host structures is the rapid transport of ions through the related bulk polymers. It remains to be seen whether nanocomposites containing these polymers will exhibit electrical properties that combine the behavior of the assembled components. The conformation of the polymer within the host galleries is very different from that of the native polymer, and transport properties may also be effected. A potential for the systematic design of new mixed conductors, however, is apparent in the study of these nanocomposites. The preparation of nanocomposites of high-molecular-weight poly(ethylene oxide) with clays (7,8), MPS_3 (9), and MoS_2 (10,11), and V_2O_5 (12), using an exfoliation/adsorption process, has been described. The technique can likely be extended to other layered disulfides (TaS_2, WS_2, and NbS_2) or dichalcogenides that exfoliate following lithiation and hydrolysis.

Layered MoO_3 is readily exfoliated into aqueous solution. Poly(aniline) and poly(*p*-phenylenevinylene) have been incorporated into MoO_3 to form nanocomposites, the former by *in situ* polymerization of aniline (13), and the latter by adsorption of a soluble precursor onto colloidal MoO_3 and subsequent thermal conversion (14). We report below the formation and characterization of a PEO/MoO_3 nanocomposite.

Some layered hosts are not amenable to processing in aqueous solution or at elevated temperatures. A notable example is TiS_2, which is susceptible to hydrolysis under acidic conditions, and forms an unusually stable hydrate in aqueous base. The charge-storage properties of Li/TiS_2 cells using a polymer electrolyte have been widely studied (15) and naturally lead to interest in the study of PEO/TiS_2 nanocomposites. The preparation of this material, using a water/CH_3CN solvent, has recently been noted by Ruiz-Hitsky and coworkers (16). We here note that single-phase products are difficult to obtain in this manner, and describe a route using anhydrous conditions. In addition to the details of appropriate synthetic conditions, the products are characterized with X-ray powder diffraction, differential scanning calorimetry, thermogravimetric and elemental analysis, and electrical measurement.

6.3 Experimental

Li_xTiS_2 ($x \approx 1$) and Li_xMoO_3 were prepared by the reaction of TiS_2 (Johnson Matthey, 99.8 %) or MoO_3 (Aldrich, 99.5 %) with n-butyllithium (Aldrich, 1.6 M in hexane) using a literature method (14). Several days were allowed for the reaction with MoO_3. The product obtained after filtration, Li_xMoO_3 ($x < 0.5$) appears to contain a homogeneous distribution of lithium within the galleries (as evidenced by relatively sharp set of (00*l*) reflections). PEO (Aldrich, mw = 100,000 Da) was used as received. N-methyl formamide (NMF) (Aldrich, 99 %)

was distilled under vacuum prior to use and stored under dry conditions. All other solvents employed were reagent grade and used as received.

PEO/TiS_2 nanocomposites were synthesized by the sonication of Li_xTiS_2 ($x \approx 1$) in an NMF solution containing excess PEO. A typical experiment to produce a single-phase product involved the addition of $LiTiS_2$ (150 mg) to a solution of PEO (150 mg) in NMF (100 mL) and sonication for several hours under dry N_2. The colloid was stirred for several days. A small amount of dilute NaOH must then be added to complete the exfoliation of TiS_2. Although Li is far more abundant in the solution, Na was selectively incorporated into the nanocomposite. The pH of the solution was controlled as described in the discussion section. The product was flocculated from the solution by the addition of acetone (which serves to lower the solvent polarity), and the floc filtered and washed several times with acetone. The resulting solid was dried *in vacuo* at 70 °C for several hours, and subsequently handled in a dry box or under dry nitrogen. In control reactions, Li_xTiS_2 was exfoliated and precipitated without PEO, and similar experiments were performed in aqueous or a mixed aqueous/organic solvent.

A colloidal suspension of Li_xMoO_3 was obtained by sonicating the solid (1.5 g) in a 2:1 (*v/v*) solution of water and CH_3CN for 15 minutes. The nanocomposites were prepared by adding excess PEO to the colloid, stirring for 24 hours, and isolating a solid via centrifugation. The solid product was washed with CH_3CN to remove excess PEO, and dried *in vacuo* at 80 °C for 48 hours.

X-ray powder diffraction data were collected at ambient temperature on a Siemens D5000 powder diffractometer ($2° < 2\theta < 60°$). Pressed pellets were loaded into a sample holder modified to maintain an inert atmosphere.

Simultaneous DSC/TGA data were obtained using a Netzsch STA-419-C thermal analyzer. Samples (30 - 40 mg) were loaded into aluminum pans and the sample chamber maintained under an inert atmosphere. The temperature was increased from ambient at 5 or 10 °C / min.

Lithium and sodium analyses utilized a Buck Scientific 200 atomic absorption spectrophotometer reading at 670.8 and 590 nm, respectively; standard solutions were prepared from Li_2CO_3 (Aldrich, 99.997 %) and NaCl (Mallinckrodt, Analytical reagent). The PEO/TiS_2 nanocomposites were analyzed following dissolution into hot, concentrated HNO_3. PEO/MoO_3 nanocomposites were dissolved by (1) addition of hot, concentrated acid to decompose PEO, (2) neutralization, and (3) addition of KOH to dissolve MoO_3. Carbon and hydrogen analyses were performed by Desert Analytical (Tucson, AZ).

Electrical conductivities between 77 and 274 K were obtained by the four-probe method on pressed pellets maintained under a blanket of dry N_2.

6.4 Results and Discussion

Previous studies of the preparation of PEO/MoS_2 nanocomposites in our laboratory and by others have employed an aqueous solvent for exfoliation of

the lithiated host structure. Recent work by Ruiz-Hitsky and coworkers indicates that similar results can be obtained with TiS_2 (16). The synthetic method described involves the addition of a CH_3CN solution containing PEO and $NaClO_4$ to an aqueous suspension of TiS_2. We also observe that a PEO/TiS_2 nanocomposite results using this method: the nanocomposite is evident as a new phase with a stacking repeat of approximately 14.5 Å. The solid obtained, however, contains other phases, generally as major components of the overall product. Figure 6.1a indicates the presence of both the PEO/TiS_2 nanocomposite (peaks at 6, 12, and 18° 2θ) and a monolayer hydrate of $LiTiS_2$ (peak at 10° 2θ). Under acidic conditions (pH ≈ 4), the solid product contains a bilayer hydrate $M_x(H_2O)_yTiS_2$ ($x \approx 0.3$, c-repeat ≈ 11.5 Å) (two sharp peaks in Figure 6.1b) and a monolayer hydrate (peak at 10° 2θ). Aqueous solutions with pH < 4 are hydrolytically unstable and promote the decomposition of TiS_2 to titanates and TiO_2.

The stability of the hydrates, $M_x(H_2O)_yTiS_2$, which prevents the preparation of a single-phase nanocomposite product from aqueous solution, may be related to the extent of negative charge retained by the disulfide lamella. The disulfide is partially reoxidized by reaction with water, and the negative charge retained is determined by the associated redox couples. The charge retained determines the cation concentration within the galleries, the latter can be measured experimentally. The cation concentration within the galleries will in turn affect the relative solvation energies of water and polymer; for example, the polymer may be sterically restricted from effective solvation at high cation

concentrations. Alternatively, the extent of charge retained may change the polymer adsorption energy at the disulfide surface. The TiS_2^{x-} lamella in aqueous solution retain a charge of $x \approx 0.3$. For comparison, PEO/MoS_2 nanocomposites, which are readily formed from aqueous solution without contamination by a hydrate phase, are comprised of less highly charged lamella (MoS_2^{x-}, $x \approx 0.1$). It will be noted below that polymer content in the TiS_2 nanocomposites is somewhat less than in those with MoS_2.

The exfoliation of TiS_2 (and other disulfides) in NMF has been known for some time (17-19), and avoids the experimental difficulties described above. Two products can be identified following the interaction of $MTiS_2$ with NMF alone (not including PEO); $M_x(NMF)_yTiS_2$ (M = Li, Na), with c-repeat ≈ 13.7 Å, and $(RNH_2)_x(NMF)_yTiS_2$, containing $CH_3NH_2CHO^+(RNH_2^+)$ cations, with c ≈ 19.5 Å. The relative abundance of these phases is pH dependent, with the latter predominating when the reaction is carried out under acidic conditions (below the pK_a for NMF). The insertion of NMF has also been reported for other lithium or sodium transition metal disulfides (1).

The product obtained when PEO is added to the reaction also depends on the solvent pH. Under acidic conditions (final pH = 5.5 - 6.5) the product contains (Figure 6.2a) $(RNH_2)_x(NMF)_yTiS_2$, (peak at 4.5°), $M_x(NMF)_yTiS_2$ (peaks at 13.5, and 18.5°), and the PEO-containing nanocomposite (peaks at 6.5, 13, and 19°). Basic NMF yields a solid product (Figure 6.2b) that exhibits reflections of the nanocomposite alone. This route has subsequently been used to prepare single-phase products.

The products obtained in this manner do not contain a large component of the molecular solvent within the galleries. Elemental analysis for C, H, and N allows for a maximum ratio of NMF to monomer repeat near 0.1 mol/mol. Unlike the NMF-intercalated products, these nanocomposites show only a small (2%) loss in weight through 220 °C (Figure 6.3). The boiling point of NMF is 185 °C, and $M_x(NMF)_yTiS_2$ shows a significant loss beginning at 190 °C.

The powder diffraction data (Figure 6.2b) for the single-phase products obtained exhibit peaks at d = 14.2, 7.1, 4.7 Å and 3.6 Å, indexed as (001), (002), (003), and (004) reflections for a PEO/TiS_2 nanocomposite. Preferred orientation in the pressed pellets reduces the intensity of all but (00*l*) reflections; therefore, little useful information on the in-plane structure can be deduced from these data. Peak widths for the (00*l*) set indicate a stacking coherence length of 300 Å (approximately 20 repeat units). The absence of a peak at d = 5.7 Å shows that the product is devoid of unreacted TiS_2, and the absence of a melting endotherm at 60 °C in the DSC data (Figure 6.3) shows that crystalline PEO is not present in the product.

Thermal analysis of the nanocomposite (Figure 6.3) reveals a broad, weak endotherm between 90 and 140 °C. This endotherm is also observed with unreacted TiS_2. A sharper endotherm at 180 °C could be related to an order/disorder phase transition reported previously for PEO/MoS_2 (10), or may be associated with the residual NMF component in the product. Both TiS_2 and the nanocomposite are unstable to loss of sulfur above 220 °C.

The distance between the Ti planes in the nanocomposite is 8.0 - 8.2 Å greater than in $LiTiS_2$. This expansion is similar to that obtained by insertion of poly(ethylene glycol) into TiS_2 (18), oligo- or polyethers into montmorillonite (7,8), PEO into MoS_2 (10,11), and PEO or PEG in MPS_3 (9), and suggests that a polymer bilayer has been incorporated into the intersheet region. Indirect evidence strongly supports the bilayer structure rather than a helical polymer structure for these materials: for example, ordered phases with 4 Å expansion have been obtained in PEO/montmorillonite (7) and PEO/MoO_3 (see below). An expansion greater than 8 Å, indicating a phase containing more than a double layer of polymer, does not arise in these reactions, even though the reaction conditions employed an excess of polymer. To our knowledge, an expanded structure of this type has not yet been observed in any layered nanocomposite containing polyethers.

Elemental analyses indicate a product stoichiometry near $Li_{0.02}Na_{0.25}(PEO)_{0.8}TiS_2 \cdot 0.1NMF$. The notation $(PEO)_n$ refers to n moles of the monomer repeat unit CH_2CH_2O. The stoichiometry is obtained using analyses for C, H, N, Li, Na, the known weight uptake during the reaction, and setting Ti:S::1:2. The overall cation content is consistent with other compounds which retain the composition $A_x(solv)_yTiS_2$ ($x \approx 0.3$) (1,20) and reflects the partial re-oxidation of the TiS_2^{1-} sheets through interaction with solvents. The polymer content (and therefore polymer packing density) is less than in $Li_{0.12}(PEO)_yMoS_2$ (y = 1.0 - 1.3) (10).

Electrical measurements (Figure 6.4) on pellets pressed from powders indicate semimetallic conduction; the conductivity of the nanocomposite is lower than that of pure TiS_2. The conductivity for the partially reduced sheets, $TiS_2^{0.3-}$, is expected to be enhanced relative to TiS_2 (21); however, the 4-probe experiment records a bulk response rather than the conductivity of individual lamella. Several factors should decrease the observed bulk response in the nanocomposites relative to TiS_2, including the reduced crystalline order in the nanocomposite, and the dilution of conducting sheets with an electronically-insulating polymer.

The extraction of the polymeric component of the nanocomposites, and subsequent analysis by gel permeation chromatography and other methods has previously been reported with PEO/MoS_2 (10). In the case of the PEO/TiS_2 nanocomposite, extraction (via long-term stirring in water, alcohols, acetonitrile, or toluene), produces only a very small fraction of soluble polymer. The degradation of the layered host by addition of concentrated base also produces little soluble polymer. These results indicate that (1) PEO is more strongly bound to the TiS_2 lamella than MoS_2, and (2) the colloidal titanates generated by destruction of the TiS_2 structure also strongly adsorb PEO. The PEO/MoO_3 nanocomposite (described below) is also not amenable to polymer extraction. With these products, the nanocomposite becomes colloidal in water, and organic solvents do not extract a significant fraction of the polymer from MoO_3.

Li_xMoO_3 rapidly exfoliates during sonication in aqueous solution, and the nanocomposite with PEO is readily obtained. The extent of lithiation of the

Li_xMoO_3 employed (i.e. *x* in Li_xMoO_3) was not evaluated quantitatively, although other studies indicate that the maximum value for *x* by these methods may be less than 0.5 (22,23). Complete exfoliation is observed only for the highly-lithiated salts, as judged by the basal-plane expansion for the anhydrous lithiated compounds. The nanocomposites prepared by the exfoliation/adsorption method show an expansion of approximately 8 Å when excess PEO is employed: the stacking repeat of 8.2 Å in Li_xMoO_3 is increased to 15.9 - 16.5 Å (Figure 6.5). A 4.4 Å expansion to a stacking repeat of 12.6 Å is observed when the PEO content is limited to 0.1 g/g Li_xMoO_3 (Figure 6.5). As there are no obscuring peaks in the region of 10° 2θ, it can be seen that this sample does not contain Li_xMoO_3, it is inferred that this is also true with the sample expanded by 8.2 Å. These results are consistent with adsorbed bilayers (8 Å expansion) or monolayers (4 Å expansion) of PEO between MoO_3 sheets. The results obtained can be compared with the 5 - 6 Å expansion observed with inclusion of PPV or PAN, where aromatic rings are thought to be oriented perpendicular to the MoO_3 sheets (24,25).

Elemental analysis of the products provides Li:Mo::0.25:1, indicating that MoO_3 lamella retain a negative charge in aqueous solution. The nanocomposite rapidly reforms a colloid when placed in aqueous solution, and the products therefore cannot be washed to remove excess polymer. Some products therefore contain excess PEO; scanning calorimetry of these materials indicates a sharp endotherm near 60 °C, corresponding to a bulk PEO melting transition (Figure 6.7). Single-phase products are obtained by careful control of the

PEO:MoO_3 and solvent ratios. Elemental analysis for Li, C, and H, combined with thermal gravimetric data on the single-phase products, provide an approximate stoichiometry of $Li_{0.25}(C_2H_4O)_{0.9}MoO_3 \cdot 0.1H_2O$. Thermal analyses of the products (Figure 6.7) show an irreversible exotherm, associated with polymer decomposition, at 320 °C.

6.5 References

1. Schöllhorn,R. *Angew. Chem. Int. Engl. Ed.* **1980**, *19*, 983.
2. Stucky, G. D. In *Progress in Inorganic Chemistry Vol, 40*, Lippert, S. J., Ed,; Wiley & Sons Inc., **1992**.
3. Ozin, G. A. *Adv. Mater.* **1992**, *4*, 613.
4. Komarneni, S. *J. Mater. Chem.* **1992**, *2*, 1219.
5. Stein, A.; Keller, S. W.; Mallouk, T. E. *Science* **1993**,*259*, 1558.
6. Behrens, P. *Adv. Mater.* **1993,** *5,* 127.
7. Wu, J.; Lerner, M. M. *Chem.Mater* **1993**, *5*, 835
8. Aranda, P.; Riuz-Hitsky, E. *Chem. Mater.* **1992**,*4*, 1395.
9. Lagadic, I.; Léaustic, A.; Clément R. *J. Chem. Soc., Chem. Commun.* **1992**, 1396.
10. Lemmon, J. P.; Lerner, M. M. *Chem. Mater.* **1994**, *6*, 207.
11. Bissessur, R.; Kanatzidis, M. G.; Schindler, J. L.; Kannewurf, C. R. *J. Chem. Soc., Chem. Commun.* **1993**, 1582.
12. Liu, Y.; DeGroot, D.; Schindler, J.; Kannewurf, C.; Kanatzidis, M. *Chem. Mater.* **1991**, *3*, 992.
13. Bissessur, R.; DeGroot, D.; Schindler, J.; Kannewurf, C.; Kanatzidis, M. *J. Chem. Soc., Chem. Commun.* **1993**, 687.

14. Nazar, L.; Zhang, Z.; Zinkweg, D. *J. Am. Chem. Soc.* **1992**, *114*, 6239.

15. Hooper, A.; Gauthier, M.; Belanger, A. In *Electrochemical Science and Technology of Polymers Vol. 2*, Linford, R. G. Ed.; Elsevier, **1990**.

16. Ruiz-Hitzky, E.; Jimenez, R.; Casal, B.; Manriquez, V.; Santa Ana, A.; Gonzalez, G. *Adv. Mater.* **1993**, *5*, 738.

17. Murphy, D. W.; DiSalvo, F. J.; Hull, G. W.; Waszczak, J. V. *Inorg. Chem.* **1976**, *15*, 17.

18. Lerf, A.; Schollhorn, R. *Inorg. Chem.* **1977**, *16*, 2950.

19. Nazar, L. F.; Jacobson, A. J. *J. Chem. Soc., Chem. Commun.* **1986**, 570.

20. *Intercalated Layered Materials*, Levy, F. Ed. D. Reidel: Boston, 1979.

21. Uchida, T.; Kohiro, K.; Hinode, H.; Wakihara, M.; Taniguchi, M. *Mat. Res. Bull.* **1987**, *22*, 935.

22. Kuhlmann, R.; Schöllhorn, R. *Mat. Res. Bull.* **1976**, *11*, 83.

23. Thomas, D.; McCarron, E. *Mat. Res. Bull.* **1986**, *21*, 945.

24. Nazar, L. F.; Liblong, S. W.; Yin, X. T. *J. Am. Chem. Soc.* **1991**, *113*, 5889.

25. Bissessur, R.; DeGroot, D. C.; Schindler. J. L.; Kannewurf, C. R.; Kanatzidis, M. G. *J. Chem. Soc., Chem. Commun.* **1988**, 223.

6.6 Figures

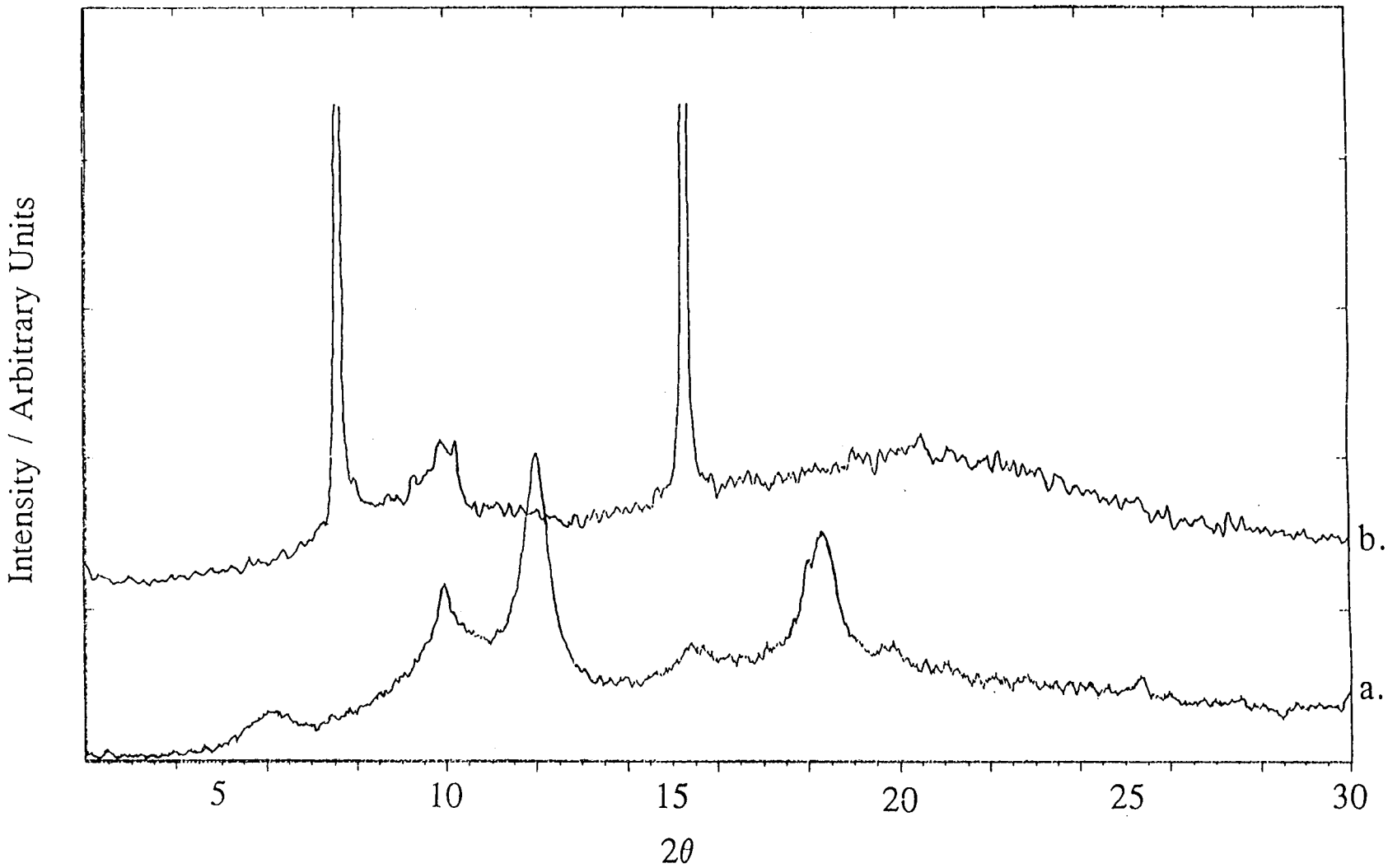

Figure 6.1 Diffraction patterns of products obtained with TiS_2 and PEO using an aqueous solution, (a) solid precipitated under basic conditions upon addition of $NaClO_4/CH_3CN$, (b) solid precipitated from an acidic aqueous solution.

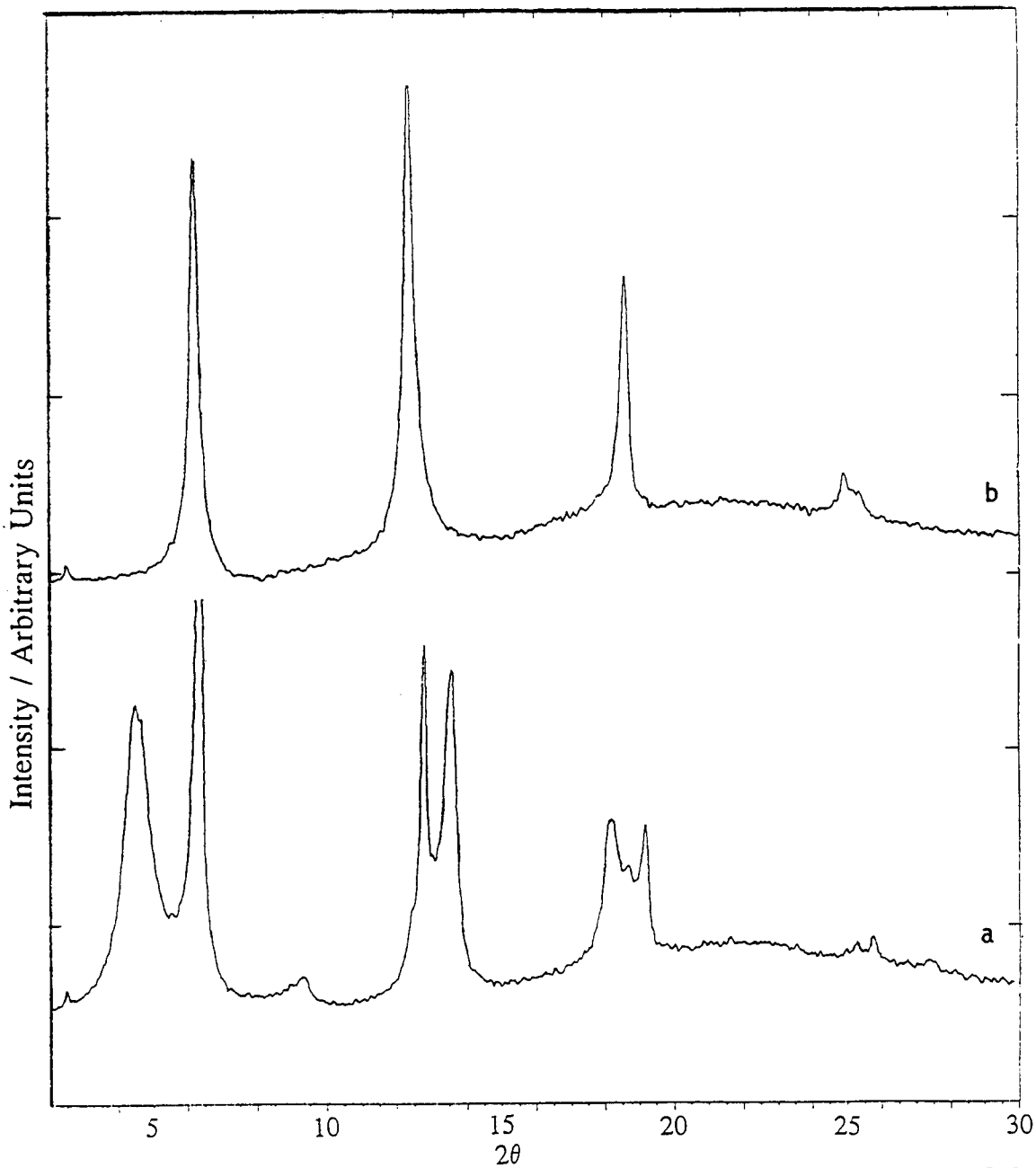

Figure 6.2 Diffraction patterns of products obtained with TiS_2 and PEO from NMF under (a) acidic and (b) basic conditions. The peaks in (b) are (00*l*) reflections related to a 14.2 Å stacking repeat.

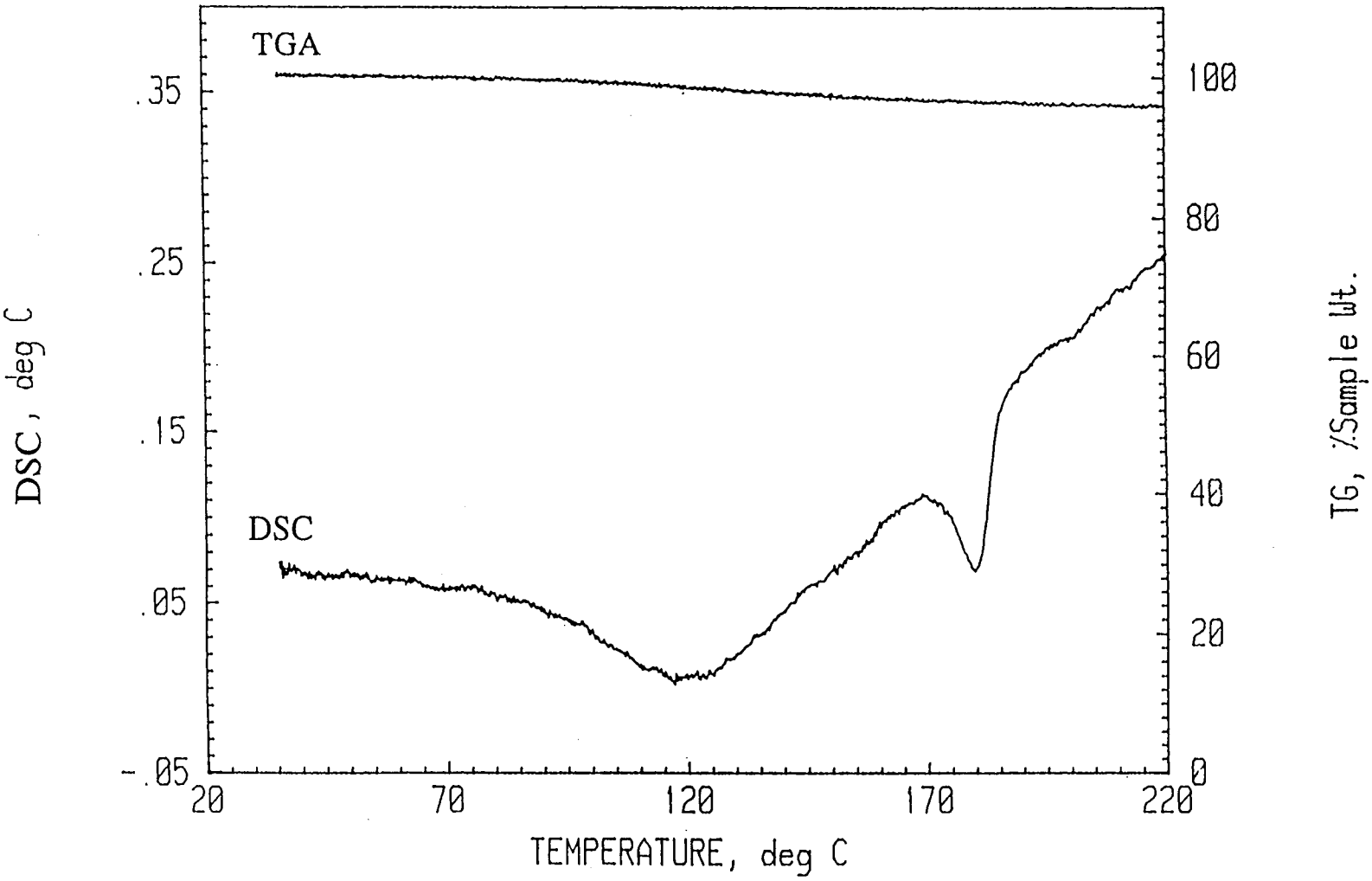

Figure 6.3 Simultaneous DSC and TGA scans of the $Li_{0.02}Na_{0.25}(PEO)_{0.8}TiS_2$ nanocomposite.

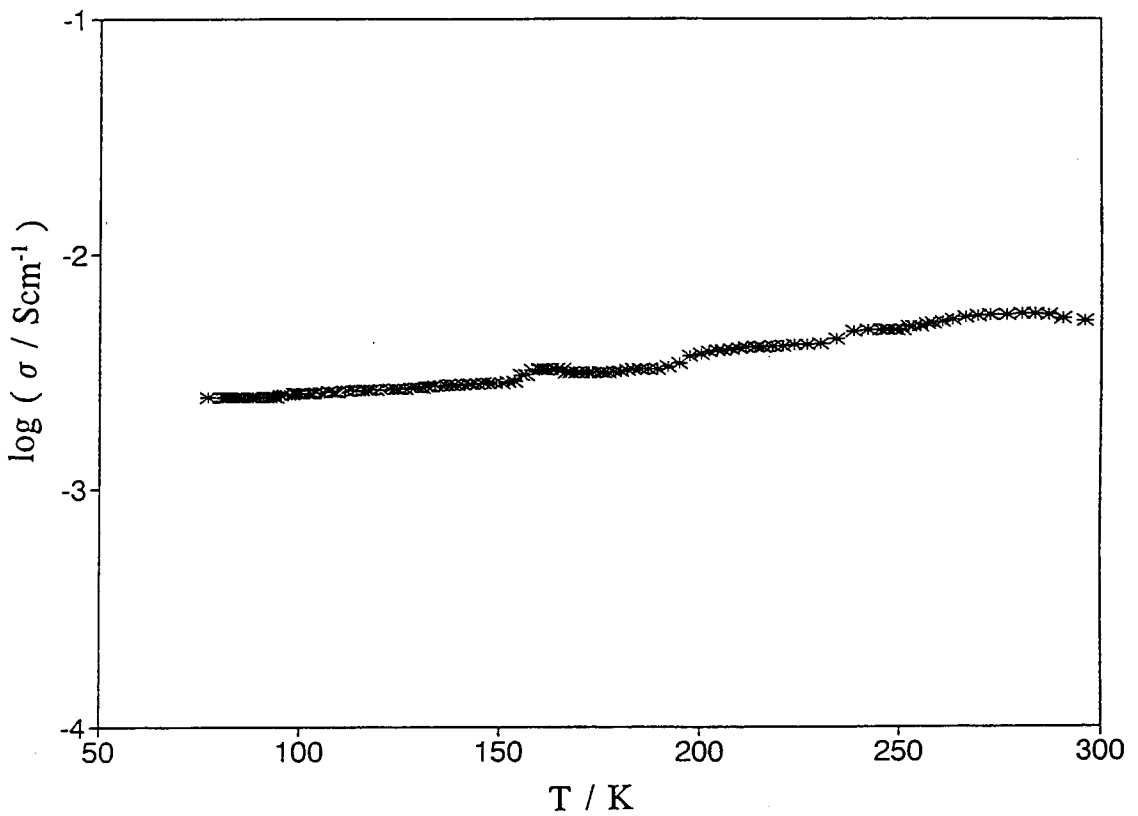

Figure 6.4 Four-probe electrical conductivity of the $Li_{0.02}Na_{0.25}(PEO)_{0.8}TiS_2$ nanocomposite.

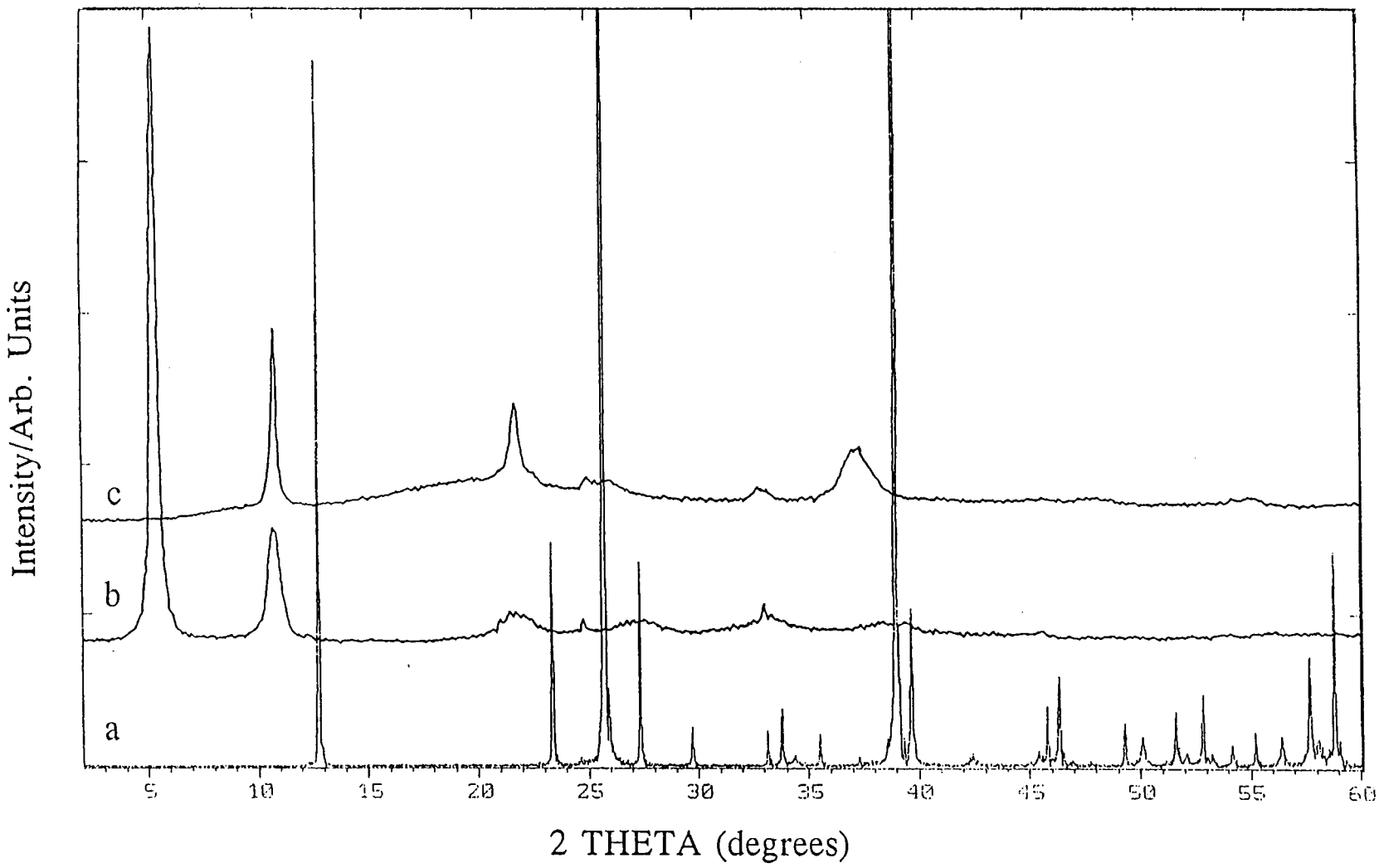

Figure 6.5 X-ray powder diffraction patterns of (a) MoO_3, (b) $Li_{0.25}(PEO)_{1.6}MoO_3$ nanocomposite, and (c) Li_xMoO_3.

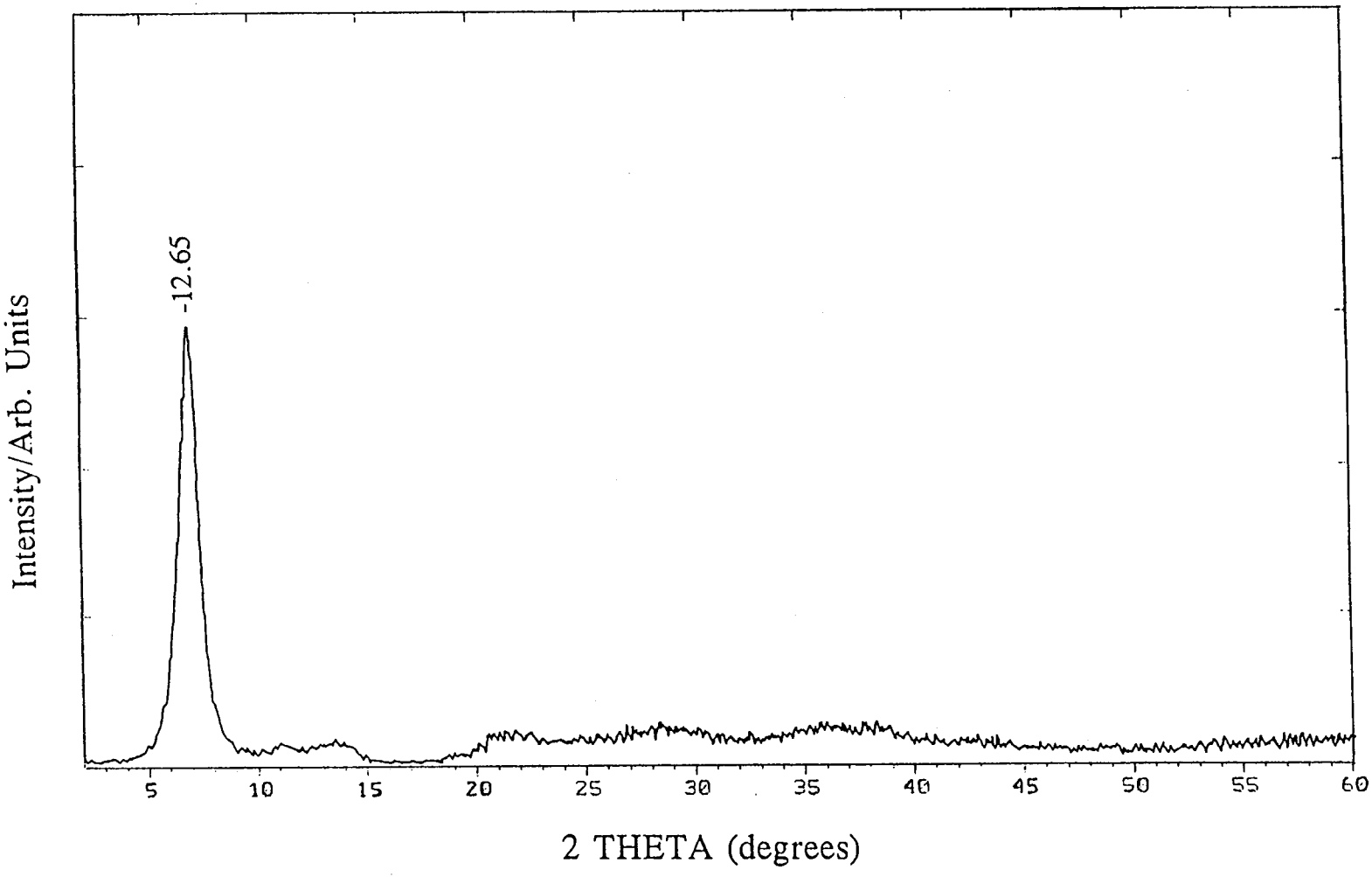

Figure 6.6 Diffraction pattern of $Li_x(PEO)_yMoO_3$ containing a single layer of polymer.

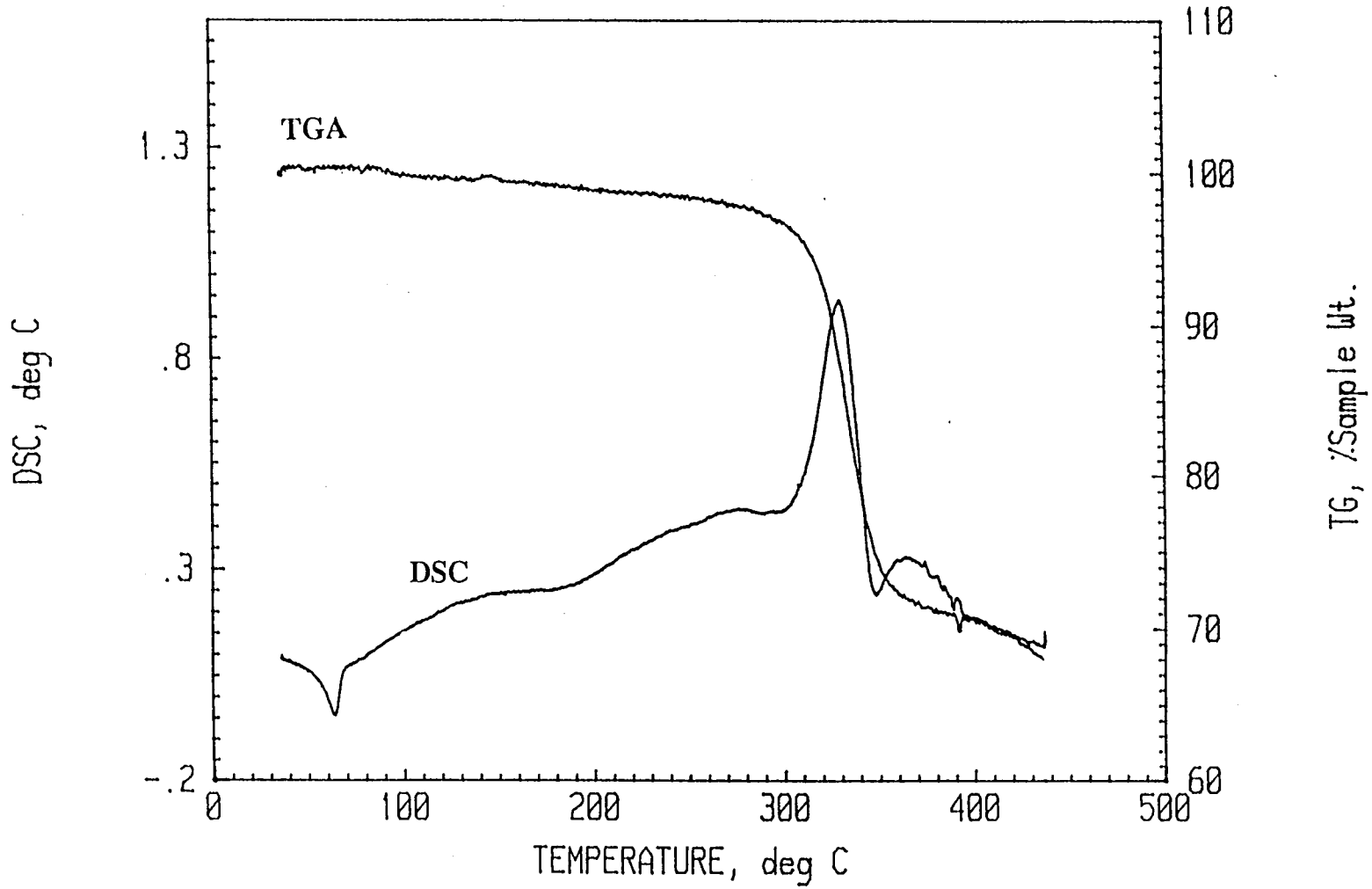

Figure 6.7 Simultaneous DSC and TGA scans of a PEO/MoO_3. The endotherm at 65 °C indicates the presence of bulk PEO.

BIBLIOGRAPHY

Abraham, K. M. *Applications of Electroactive Polymers,* Scrosati, B., Ed.; Chapman and Hall: New York, 1993.

Adamic, K.; Greenbaum, S.; Wintersgill, M.; Fontanella, J. *J. Appl. Phys.* **1986**, *60*, 1342.

Aranda, P.; Riuz-Hitsky, E. *Chem. Mater.* **1992**,*4*, 1395.

Armand, M. B. *Polymer Electrolyte Reviews - 1*; MacCallum, J. R., Vincent, C. A., Eds.; Elsevier: New York, 1987; and references contained therein.

Armand, M. B.; Duclot, M.; *Fast Ion Conduction in Solids*, Mundy, J. N.; Shenoy, G. K., Eds., New York, 1979.

Bartlett, N. private communication, University of California at Berkeley **1992**.

Bartlett, N.; Mc Quillan, B. W. In *Intercalation Chemistry*; Whittingham M. S.; Jacobson, A. J., Eds; Academic Press: New York, 1982a.

Behrens, P. *Adv. Mater.* **1993,** *5,* 127.

Berthier, C.; Gorecki, W.; Minier, M. *Solid State Ionics* **1983**, *11*, 91.

Bissessur, R.; DeGroot, D. C.; Schindler, J. L.; Kannewurf, C. R.; Kanatzidis, M. G. *J. Chem. Soc. Chem. Comm.* **1993**, 687.

Bissessur, R.; DeGroot, D. C.; Schindler. J. L.; Kannewurf, C. R.; Kanatzidis, M. G. *J. Chem. Soc., Chem. Commun.* **1988**, 223.

Bissessur, R.; Kanatzidis, M. G.; Schindler, J. L.; Kannewurf, C. R. *J. Chem. Soc., Chem. Commun.* **1993**, 1582.

Blonsky, P. M.; Shriver, D. F.; Austin, P.; Allcock, H. R. *J. Am. Chem. Soc.* **1984**, *106*, 6854.

Bode, H.; Jenssen, H.; Bandte, F. *Angew. Chem.* **1953**, *65*, 304.

Booth, C.; Nicholas, C. V.; Wilson, D. J. In *Polymer Electrolyte Reviews - 2;* MacCallulm, J. R., Vincent, C. A., Eds.; Elsevier: New York, 1989, and references contained therein.

Chang, T. C.; Ho, S. Y.; Chao, K. J.; *J. Chin. Chem. Soc.* **1992**, *39*, 209.

Court, T.; Dove, M. *J. Chem. Soc., Chem. Comm.* **1971**, 726.

Dahn, J. R.; Von Sachen, U.; Juzkow, M. W.; Al-Janaby, H. *J. Electrochem. Soc.* **1991**, *138*, 2207.

Divigalpitiya, W. M. R.; Frindt, R. F.; Morrison, S. R. *J. Mater. Res.* **1991**, *6*, 1103.

Divigalpitiya, W. M. R.; Frindt, R. F.; Morrison, S. R. *Science* **1989**, *246*, 369.

Doan, K. E.; Heyen, B. J.; Ratner, M. A.; Shriver, D. F. *Chem. Mater.* **1990**, *2*, 539.

Doscher, T. M.; Myers, G. C.; Atkins, D. C. *J. Colloid Sci.* **1951**, *6*, 223.

Fenton, B. E.; Parker, J. M.; Wright, P. V. *Polymer* **1973**, *14*, 589.

Flandrois, S.; Hun, B.; Grannec, J.; Tressaud, A.; Hauw, C. *Synth. Met.* **1988**, *23*, 435.

Gamble, F. R.; DiSalvo, F. J.; Klemn, R. A.; Geballe, T. H. *Science* **1970**, *168*, 568.

Gamble, F. R.; Osiecki, J. H.; DiSalvo, F. J. *J. Chem. Phys.* **1971**, *55*, 3525.

Gee, M. A.; Frindt, R. F.; Joensen, P.; Morrison, S. R. *Mater. Res. Bull.* **1986**, *21*, 543.

Gorecki, W.; Belorizky, E.; Berthier, C.; Donoso, P.; Armand, M. *Electrochim. Acta* **1992**, *37* (9), 1685.

Gray, F. M. *Solid State Ionics* **1990**, *40/41*, 637.

Greenbaum, S.; Pak, Y.; Wintersgill, M.; Fontanella, J.; Schultz J. *J. Electrochem. Soc.* **1988**, *135* (1), 235.

Greenbaum, S.; Pak, Y.; Adamic, K.; Wintersgill, M.; Fontanella, J. *Mater. Res. Symp. Proc.***1991**, *210*, 237.

Greenbaum, S.; Pak, Y.; Wintersgill, M.; Fontanella, J. *Solid State Ionics* **1988**, *31*, 241.

Grey, F. M. *Solid Polymer Electrolytes, Fundamentals and Technological Applications*, VCH: New York, 1991.

Guyomard, D.; Tarason, J. *Adv. Mater.* **1994**, *6*, 408.

Hagiwara, R.; Lerner, M.; Barlett, N. *J. Chem. Soc., Chem. Comm.* **1989**, 573.

Hagiwara, R.; Lerner, M.; Barlett, N. J. *Electrochem Soc.* **1988**, *135*, 2393.

Hagiwara, R.; Lerner, M.; Barteltt, N. *J. Electrochem. Soc.* **1988**, *35*, 2393.

Hamwi, A.; Daoud, M.; Cousseins, J. *Synth. Met.* **1989**, *30*, 23.

Hamwi, A.; Daoud, M.; Cousseins, J. *Synth. Met.* **1988**, *28/30*, 1756.

Hooper, A.; Gauthier, M.; Belanger, A. In *Electrochemical Science and Technology of Polymers Vol. 2*, Linford, R. G. Ed.; Elsevier, **1990**.

Hoppe, R. *Rec. Trav. Chim.* **1956**, *75*, 569.

Intercalated Layered Materials, Levy, F. Ed. D. Reidel: Boston, 1979.

Johansson, A.; Wendsjo, A.; Tegenfeldt, J. *Electrochim. Acta* **1992**, *37* (9), 1487.

Kanatzidis, M. G.; Wu, C.; Marcy, H. O.; De Groot, D. C.; Kannewurf, C. R. *Chem. Mater.* **1990**, *2*, 222.

Kanatzidis, M. G.; Wu, C.; Marcy, H. O.; Kannewurf, C. R. *J. Am. Chem. Soc.* **1989**, *111*, 4139.

Kanatzidis, M. G.; Bissessur, R.; DeGroot, D. C.; Schindler, J. L.; Kannewurf, C. R. *Chem. Mater.* **1993**, *5*, 595.

Kim, D.; Ryoo, B.; Park, J.; Maeng, K.; Hwang, T. *Polym. J.* **1992**, *24*, 509.

Kita, Y.; Watanabe, N.; Fujii, Y. *J. Am. Chem. Soc.* **1979**, *101*, 3832.

Kita, Y.; Kadono, K.; Fujii, Y.; Watanabe, N. *Z. Anorg. Allg. Chem.* **1987**, *544*, 7 and referneces contained therein.

Komarneni, S. *J. Mater. Chem.* **1992**, *2*, 1219.

Kuhlmann, R.; Schöllhorn, R. *Mat. Res. Bull.* **1976**, *11*, 83.

Lagadic, I.; Léaustic, A.; Clément R. *J. Chem. Soc., Chem. Commun.* **1992**, 1396.

Lemmon, J.; Lerner, M. *Proc. Oregon Acad. Sci.* **1991**, Salem, OR.

Lemmon, J. P.; Lerner, M. M. *Chem. Mater.* **1994**, *6*, 207.

Lemmon, J. P.; Lerner, M. M. *Macromolecules* **1992**, *25*, 2907.

Lemmon, J. P.; Sloop, S. E.; Lerner. M. M. *Proc. Am. Chem. Soc., Inorg. Chem. Soc., Inorg. Chem.* **1993**, Abstract No. 355.

Lerf, A.; Schöllhorn, R. *Inorg. Chem.* **1977**, *11*, 2950.

Lerner, M. Ph.D. Thesis, University of California at Berkeley **1988**.

Lerner, M.; Hagiwara, R.; Bartlett, N. *J. Fluor. Chem.* (in press).

Linden, D. *Handbook of Batteries and Fuel Cells*; Linden, D., Ed.; Mc Graw Hill: New York, 1984.

Lithium Batteries, New Developments and Perspectives, Industrial Chemistry Library; Pistoia G., Ed.; Elsevier: Netherlands, 1994.

Liu, Y.; DeGroot, D.; Schindler, J.; Kannewurf, C.; Kanatzidis, M. *Chem. Mater.* **1991**, *3*, 992.

Liu, Y. J.; DeGroot, D. C.; Schindler, J. L.; Kannewurf, C. R.; Kanatzidis, M. G. *J. Chem. Soc., Chem. Commun.* **1993**, 593.

Malachesky P. A. *Handbook of Batteries and Fuel Cells*; Linden, D., Ed.; Mc Graw Hill: New York, 1984.

Mallouk, T.; Bartlett, N.; *J. Chem. Soc., Chem. Comm.* **1983**, *103*.

Mallouk, T.; Hawkins, B.; Conrad, M.; Zilm, K.; Maciel, G.; Bartlett, N. *Phil. Trans. R. Soc. Lond.* **1985**, *A314*, 179.

Matsuura, H.; Fukuhara, K. *J. Polym. Sci., Part B* **1986**, *24*, 1383.

Mehrota, V.; Giannelis, E. P. *Solid State Comm.* **1991**, *77*, 155.

Miremadi, B. K.; Cowan, T.; Morrison, S. R. *J. Appl. Phys.* **1991**, *69*, 6373.

Murphy, D. W.; DiSalvo, F. J.; Hull, G. W.; Waszczak, J. V. *Inorg. Chem.* **1976**, *15*, 17.

Murphy, D. W.; Hull, G. W. *J. Chem. Phys.* **1975**, *62*, 973.

Murugesamoorthi, K. A.; Owen, J. R. *Br. Polym. J.* **1988**, *20*, 227.

Nagaoka, K.; Naruse, H.; Shinohara, I.; Watanabe, M. *J. Poly. Sci. Poly. Lett.* **1984**, *22*, 659.

Nakajima, T.; Molinier, M.; Motoyama, M. *Carbon*, **1991**, *29*, 429.

Nakajima, T.; Ino, T.; Watanabe, N.; Takenaka, H. *Carbon* **1988**, *26*, 397.

Nazar, L. F.; Liblong, S. W.; Yin, X. T. *J. Am. Chem. Soc.* **1991**, *113*, 5889.

Nazar, L. F.; Jacobson, A. J. *J. Chem. Soc., Chem. Commun.* **1986**, 570.

Nazar, L.; Zhang, Z.; Zinkweg, D. *J. Am. Chem. Soc.* **1992**, *114*, 6239.

Nazri, G. A.; MacArthur, D. M.; O'Gara, Aroca, R. J. F. *Mater. Res. Soc. Symp. Proc.* **1991**, *210*, 163.

Nekoomanesh, M.; Nagae, S.; Booth, C.; Owen, J. *J. Electrochem. Soc.* **1992**, *139*, 3046.

Nicholas, C. V.; Wilson, D. J.; Booth, C.; Giles, J. R. M. *Br. Polym. J.* **1988**, *20*, 289.

Nikolaev, A.; Nazarov, A.; Yudanov, N.; Ikorsky, V. *Izv. Sib. Otd. Akad. Nauk SSSR* **1972**, *7*, 1366.

Owens, B. B.; Skarstad, P. M.; Unterker, D. F. *Handbook of Batteries and Fuel Cells*; Linden, D., Ed.; Mc Graw Hill: New York, 1984.

Ozin, G. A. *Adv. Mater.* **1992**, *4*, 613.

Panero, S.; Scrosati, B.; Greenbaum, S. *Electrochim. Acta* **1992**, *37* (9), 1535.

Ratner, M.; Shriver, D. F. *Chem. Rev.* **1988**, *88*, 109.

Ratner, M. *Polymer Electrolyte Reviews - 1*; MacCallum, J. R., Vincent, C. A., Eds.; Elsevier: New York, 1987.

Reports (Wypych. F. and Schöllhorn) have indicated the metallic nature of 1T-MoS_2, which can be prepared from single-sheet MoS_2. The uncharged sheets, however, are prepared only when an oxidant such as $K_2Cr_2O_7$ or I_2 was added to the suspension.

Rüdorff, W.; Rüdorff, G. *Anorg. Allg. Chem.* **1947**, *253*, 281.

Ruff, O.; Bretschneider, O.; Ebert, F. *Z. Anorg. Allg. Chem.* **1934**, *217*, 1.

Ruiz-Hitzky, E.; Jimenez, R.; Casal, B.; Manriquez, V.; Santa Ana, A.; Gonzalez, G. *Adv. Mater.* **1993**, *5*, 738.

Schöllhorn, R. *Angew. Chem., Int. Engl. Ed.* **1980**, *19*, 983.

Schüth, F.; Stucky, G.; *et al. Nature* **1994**, *368*, 317.

Shriver D. F. *The Manipulation of Air-Sensitive Compounds*; Mc Graw Hill: New York, 1969.

Standard Potentials in Aqueous Solution, Bard, A., Parsons, R., Jordan, J. Eds.; Marcel Dekker: New York, **1985**.

Stein, A.; Keller, S. W.; Mallouk, T. E. *Science* **1993**, *259*, 1558.

Stucky, G. D. In *Progress in Inorganic Chemistry Vol, 40*, Lippert, S. J., Ed,; Wiley & Sons Inc., **1992**.

Stucky, G. D. *Prog. Inorg. Chem.* **1992**, *40*, 99-177.

Subba Rao, G. V.; Shafer, M. W. *Intercalated Layered Materials*; Levy, F., Ed.; D. Reidel: Holland, 1979; Vol. 6.

Tagaya, H.; Hashimoto, T.; Karasu, M.; Izumi, T.; Chiba, K. *Chem. Soc. Jpn., Chem. Lett.* **1991**, 2113.

Takehara Z. Seventh International Meeting on Lithium Batteries, Extended Abstracts. Boston, 1994.

Takenaka, H.; Kawaguchi, M.; Lerner, M.; Bartlett, N. *J. Chem. Soc., Chem. Comm.* **1987**, 1431.

Thomas, D.; McCarron, E. *Mat. Res. Bull.* **1986**, *21*, 945.

Uchida, T.; Kohiro, K.; Hinode, H.; Wakihara, M.; Taniguchi, M. *Mat. Res. Bull.* **1987**, *22*, 935.

Watanabe, N.; Touhara, H.; Nakajima T.; Bartlett, N.; Mallouk, T.; Selig, H In *Inorganic Solid Fluorides*, Hagenmuller, P. Ed.; Academic Press: New York, 1985, (pp 331-369) and references contained therein.

Whittingham, M. S. *Prog. Solid State Chem.* **1978**, *12*, 41.

Whittingham, M. S.; Huggins, R. A. J. *Chem. Phys.* **1971**, *54*, 414.

Whittingham, M. S. *Mater. Res. Bull.* **1974**, *9*, 1681.

Wilson, W.; Christe, K. *Inorg. Chem.* **1989**, *28*, 4172.

Wintersgill, M. C.; Fontanella, J. J.; Pak, Y. S.; Greenbaum, S. G.; Al-Mudaris, A.; Chadwick, A. V. *Polymer* **1989**, *30*, 1123.

Wintersgill, M.; Fontanella, J.; Smith, M.; Greenbaum, S.; Adamic, K.; Andeen, C. *Polymer* **1987**, *28*, 633.

Wu, J.; Lerner, M. M. *Chem.Mater* **1993**, *5*, 835

Wypych. F.; Schöllhorn, R. *J. Chem. Soc., Chem. Commun.* **1992**, 1386.

Yazami, R.; Hamwi, A. *Solid State Ionics* **1990**, *40/41*, 982.

Zemva, B. private communication, University of California at Berkeley **1992**.